
Enclosure 13 to L-MT-08-052

Steam Dryer Dynamic Stress Evaluation

(Non-Proprietary)

Table of Contents

1. Summary.....	1
1.1. Evaluations	1
1.2. Results	2
2. Screening Process.....	3
2.1. Analytical Method	3
2.1.1. CDI analysis.....	3
2.1.2. NSPM analysis	3
2.2. Subscale Test Method	5
2.2.1. Test Configuration.....	5
2.2.2. Test Results	6
3. Generation of Load Definition.....	9
3.1. Strain Gage Locations and Configuration	9
3.2. Raw Data Reduction.....	12
3.3. Acoustic Circuit Model Load Definition.....	14
3.4. ACM Input Processing.....	15
3.5. Uncertainty and Bias in the Acoustic Circuit Model	17
3.6. Bias and Uncertainty in the Finite Element Model	17
4. Dryer Stress Calculations.....	18
4.1. USAR Licensing Basis Stress Evaluation	18
4.2. Dynamic Stress Calculation.....	18
4.2.1. Model Description.....	19
4.3. Nominal and Frequency Shifted Results	21
5. Power Ascension Testing.....	22
5.1. Limit Curves.....	22
5.2. [[Quasi Real-time Stress Evaluation ⁽³⁾]]	23
6. References	24

Table of Figures

Figure 2-1:	Normalized RMS pressure.	7
Figure 3-1	MSL Strain Gage Installation (typical).....	10
Figure 3-2:	Channel 01 with a single operational strain gage.	11
Figure 3-3:	Channel 02 with a pair of operational strain gages	11
Figure 3-4:	Wheatstone Bridge and Strain Gage Electrical Schematic	12

Table of Tables

Table 2-1: Resonant properties of MNGP Main Steam Branch Lines.....4

Table 2-2: Comparison between predicted and measured excitation frequencies for Monticello.6

Table 2-3: Comparison between predicted and measured onset velocities for Monticello.....8

Table 3-1: Strain Gage to Dynamic Pressure Conversion Factors (PCF).....13

Table 3-2: Exclusion Frequencies15

1. Summary

1.1. Evaluations

An evaluation of the Monticello Nuclear Generating Plant (MNGP) Steam Dryer capability to operate satisfactorily at Extended Power Uprate (EPU) conditions was performed. This evaluation considered the effects of flow induced vibration on the dryer. The evaluation concentrated on the possibility of flow induced acoustic resonance. The evaluations analyzed the possibility that flow past the Safety Relief Valve (SRV) standpipes might induce a resonance that would be transmitted back to the steam dryer. Other possible contributors to acoustic resonance were also considered.

MNGP performed a series of evaluations to determine and characterize the loads upon the steam dryer. These evaluations were conducted at Current Licensed Thermal Power (CLTP) and at various other power levels or simulated power levels, including EPU conditions, to analyze the stresses these loads induce.

1. Screening calculations were performed to determine if the MNGP was susceptible to flow induced acoustic resonance that would be detrimental to the steam dryer.
2. Subscale testing was performed to validate the screening calculations and to provide a model of the behavior of the plant at various steam flow conditions.
3. The plant was instrumented to obtain baseline information as to the behavior of the plant at various steam flow conditions.
4. An Acoustic Circuit Model (ACM) was prepared to translate conditions observed in the main steam lines to the surface of the steam dryer in order to generate a conservative set of loads.
5. A Finite Element Analysis was performed to identify the stress levels of the steam dryer when various loads are applied.
6. Limit curves were generated to provide assurance during initial power ascension to EPU power levels that the dryer will not experience unusual or unexpected loading.

1.2. Results

A summary of results follows.

1. Monticello SRV standpipe resonant frequency is approximately 162 Hz at normal operating conditions of pressure and temperature.
2. The EPU steam flow velocity of 179 ft/sec is below the lowest conservatively calculated acoustic resonance onset velocity of 185 ft/sec.
3. The EPU steam flow velocity of 179 ft/sec is significantly below the empirically derived (scale model test) acoustic resonance onset velocity of 201 ft/sec.
4. The Monticello steam dryer stress results at CLTP conditions yield a lowest alternating stress ratio of 3.02.
5. The Monticello steam dryer stress results at EPU conditions yield a lowest alternating stress ratio of 2.28.

The conclusion of the analyses is that the steam dryer at Monticello Nuclear Generating Station is structurally adequate for operation at EPU conditions.

2. Screening Process

2.1. Analytical Method

Analyses were performed by Continuum Dynamics Incorporated (CDI) and by Northern States Power Company, a Minnesota corporation (NSPM). CDI analyses concentrated on the behavior of SRV standpipes in support of experimental analyses such as the subscale tests and empirical analyses such as the acoustic circuit model. NSPM performed an evaluation of the primary branch lines off of the main steam lines to determine resonant frequencies and to calculate Strouhal values (Reference 6.3) at CLTP and EPU conditions. Slight differences between the CDI methodology and the NSPM methodology result in approximately a two percent difference in results.

2.1.1. CDI analysis

CDI calculated excitation frequency of the SRV standpipes is documented in Reference 6.1. [[

^{(3)]]} The results were used in determining strain gage spacing for the acoustic circuit model. The results were validated in Reference 6.1. The CDI methodology resulted in a calculated excitation frequency for the Monticello standpipes of 160.2 Hz. Strouhal calculations based upon this excitation frequency yield an onset velocity for standpipe excitation of 193.8 ft/sec.

2.1.2. NSPM analysis

A simpler method was used by NSPM to calculate a series of excitation frequencies for various branches off of the main steam lines. The NSPM method utilized the $\frac{1}{4}$ wavelength distance from a branch opening to the reflection point for calculating excitation frequency. Velocity of sound was obtained from Reference 6.2.

Although different, this method yields results that compare favorably with the experimental results from the subscale tests. The calculated standpipe excitation frequency utilizing the NSPM methodology is 163.6 Hz. Strouhal calculations based upon this excitation frequency yield a very conservative onset velocity for standpipe excitation of 185.4 ft/sec.

It should be noted that this onset velocity is lower than that calculated by CDI. This is due to several conservatisms included in the NSPM calculation; for example, NSPM used a very conservative polynomial interpolation of the

Enclosure 13 to L-MT-08-052 NON-PROPRIETARY

d/D value from Reference 6.3. A logarithmic interpolation of d/D values yields an onset velocity of approximately 192 ft/sec and a linear interpolation yields 195 ft/sec. Nonetheless, these calculations continue to show significant margin to onset of acoustic resonance.

NSPM also performed screening calculations for branch lines other than the SRV standpipes. Branch lines larger than 2 inch nominal were evaluated. The results of these calculations are presented in Table 2-1.

Table 2-1: Resonant properties of MNGP Main Steam Branch Lines at EPU Conditions

Component/Line	HPCI	RCIC	Blank Flanges	SRV Stand Pipes	Drip Legs (drains downstream of MSIVs)
Branch Dia (ft)	0.635	0.242	0.480	0.568	0.797
Line Length (ft)	206.000	160.000	0.875	2.453	0.870
Steam Pressure (psia)	1015	1015	1015	1015	980
V_{sound} (ft/sec)	1605.3	1605.3	1605.3	1605.3	1609.2
Natural Frequency (Hz) $v/4l$	1.95	2.51	459	164	463
3v/4l (Hz)	5.84	7.52	1375.90	490.74	1387.50
5v/4l (Hz)	9.74	12.54	2293.16	817.90	2312.50
Steam Velocity (ft/sec)	179	179	179	179	186
Mach Number	0.112	0.112	0.112	0.112	0.116
Strouhal Number	0.0091	0.0050	1.336	0.557	1.979
S 3v/4l	0.027	0.015	4.009	1.670	5.937
S 5v/4l	0.046	0.025	6.681	2.783	9.895

Note that not only were the primary (v/4l) frequencies identified and evaluated, but the secondary and tertiary frequencies (odd number multiples of the natural frequency) were evaluated. In the case of intermediate length lines, an excitation might not occur for the primary frequency but might for one of the next higher multiples. None of the lines evaluated fall into the

Enclosure 13 to L-MT-08-052 NON-PROPRIETARY

category of intermediate length. None of the lines evaluated reach the associated onset Strouhal number for its particular geometry considering primary, secondary or tertiary resonant frequencies.

2.2. Subscale Test Method

Reference 6.1, CDI Report No. 07-23P describes the subscale testing performed to evaluate the MNGP steam system susceptibility to excitation of acoustic resonance at EPU conditions. Additionally, this subscale test quantifies the ratio of acoustic loads to be expected at Monticello at EPU conditions compared to CLTP. This ratio can be used to develop bump-up factors. Bump-up factors are used to scale CLTP in-plant data to EPU conditions.

The purpose of the testing effort was to measure the excitation frequency and amplitudes of the as-built standpipe/valve configuration, and determine its behavior at CLTP and EPU conditions. To do so, a one-eighth scale test facility was constructed that represents the Monticello steam delivery system.

[[

.⁽³⁾]]

2.2.1. Test Configuration

[[

⁽³⁾]]

2.2.2. Test Results

The purpose of the subscale test program was to characterize the behavior of the standpipe/valves currently at Monticello. The results of the test program (38 tests) may be examined with regard to excitation frequency and Root-Mean-Square (RMS) pressure as a function of power level, comparison of Power Spectral Densities (PSDs), and predicted peak pressures on the steam dryer. Of these, the change in peak pressures on the steam dryer provides the best extrapolation of the potential impact on steam dryer stresses.

[[

⁽³⁾]]

Table 2-2: Comparison between predicted and measured excitation frequencies for Monticello. [[

⁽³⁾]]

[[

⁽³⁾]]

Figure 2-1: Normalized RMS pressure for the pressure transducers at the ends of the standpipe/valves on main steam line C (top) and D (bottom). Polynomial curve fits to all data (black dots) are shown by the black curves.

[[

³⁾]]

Table 2-3: Comparison between predicted and measured onset velocities for Monticello. [[

³⁾]]

3. Generation of Load Definition

Measured strain gage time-history data in the four main steam lines at the Monticello Nuclear Generating Plant were processed by a dynamic model of the steam delivery system to predict loads on the full-scale steam dryer. These measured data were first converted to pressures, then positioned on the four main steam lines and used to extract acoustic sources in the system. A validated acoustic circuit methodology was used to predict the fluctuating pressures anticipated across components of the steam dryer in the reactor vessel. The acoustic circuit methodology included a low frequency hydrodynamic contribution, in addition to an acoustic contribution at all frequencies. This pressure loading was then provided for structural analysis to assess the structural adequacy of the steam dryer in Monticello.

3.1. Strain Gage Locations and Configuration

Strain gage (SG) locations were determined by CDI. The locations were selected to optimize the signal for the frequency of interest (162 Hz) and to minimize uncertainties associated with comparisons to the Quad Cities benchmark data Reference 6.4. The locations were selected so that no acoustic sources would be present between upper and lower strain gages.

Strain gages were installed during the Spring 2007 refueling outage. Figure 3-1 displays the general locations of the strain gages as installed at Monticello. The upper strain gages were located on the vertical pipe runs at the same location on each pipe; approximately 12 feet from the vessel steam outlets. The lower strain gages were located exactly 32 feet downstream of the upper gages on the diagonal runs of each line (not shown in the figure).

Each of the four main steam lines were instrumented with eight strain gages installed circumferentially and equally spaced for a total of 64 strain gages. In order to minimize the bending error, the strain gages that are diametrically opposite to each other are connected in a half-bridge "Wheatstone Bridge" configuration. Consequently, signals from the individual SGs are additive, resulting in the partial cancellation of the bending strain and enhancement of the hoop strain sensitivity. For every such location, the four signals are averaged to minimize the bending errors and improve the signal to noise ratio. Failure of individual strain gages can cause spurious signals as cancellation of bending strains is reduced. The effect of this is addressed in Section 3.3 and shown graphically in Figure 3-2 and Figure 3-3.

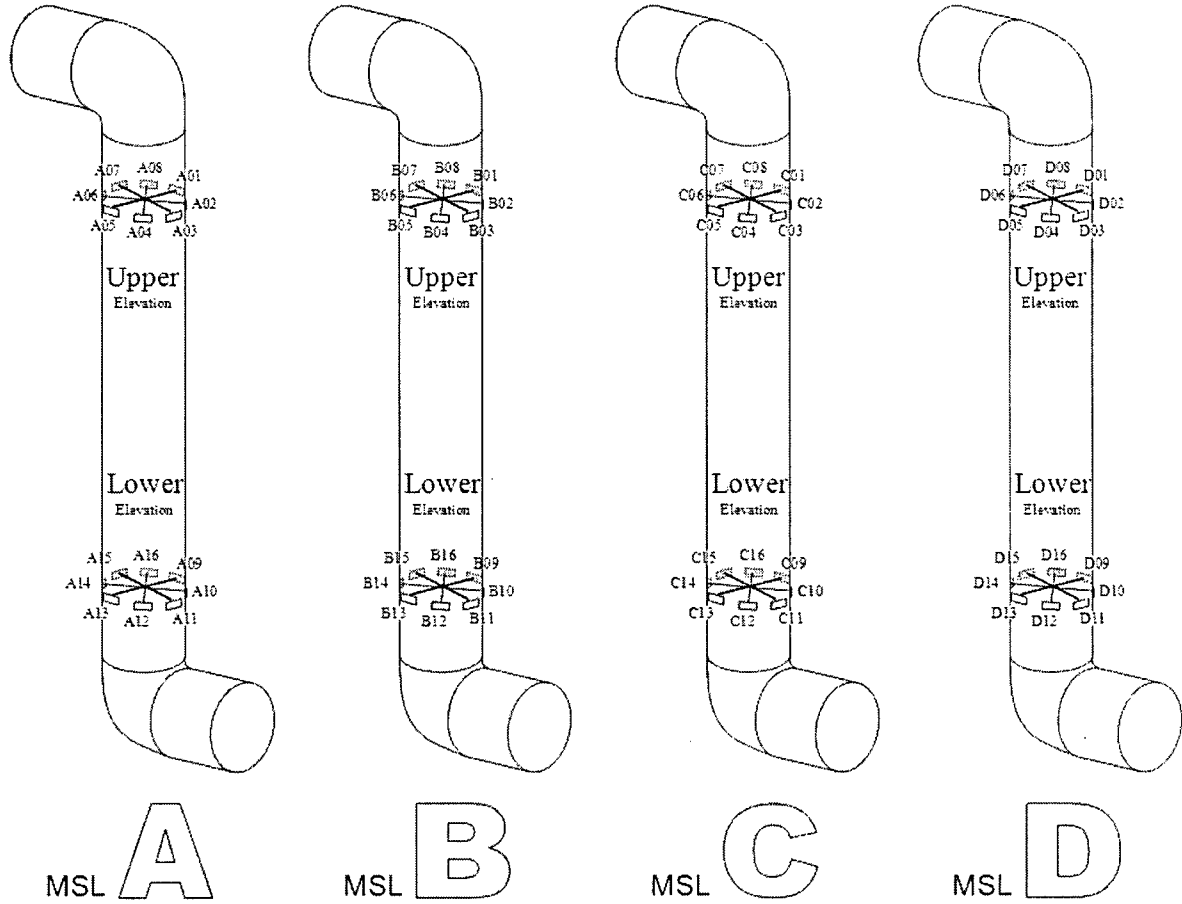


Figure 3-1 MSL Acoustic Pressure Vibration Monitoring Strain Gage Installation (typical)

Channels 01 and 02 are two of the 4 channels measuring hoop strain at the upper location on main steam line A. The strain gages that make up these two channels are mounted adjacent to each other as strain gage pairs A01-A05 (channel 01) and A02-A06 (channel 02) (Figure 3-1).

Figure 3-2 and Figure 3-3 demonstrate the effect of the loss of one strain gage from channel 01. Without an apposed strain gage to cancel the bending strain caused by a pipe vibration mode at approximately 22 Hz, an artificial peak is generated in the channel 01 data. This effect is repeated in the data each time a single strain gage is lost from a channel. How these artificial peaks are treated in the load definition is addressed in Section 3.4.

Enclosure 13 to L-MT-08-052 NON-PROPRIETARY

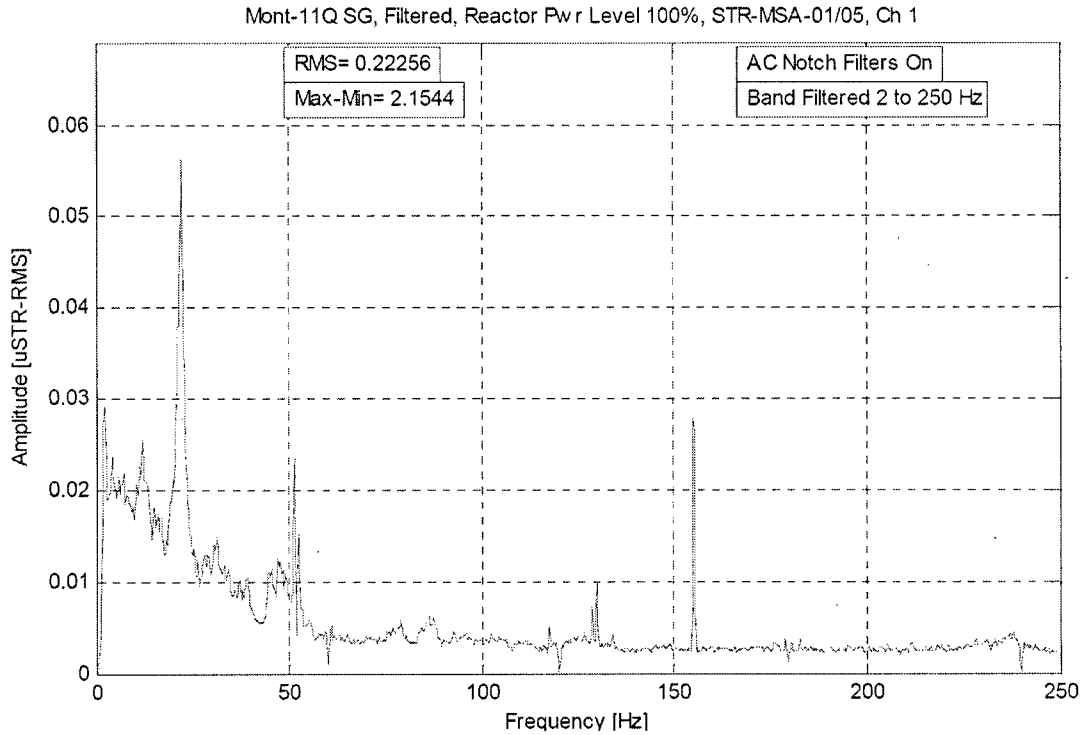


Figure 3-2: Channel 01 with a single operational strain gage. Note the peak at approximately 22 Hz.

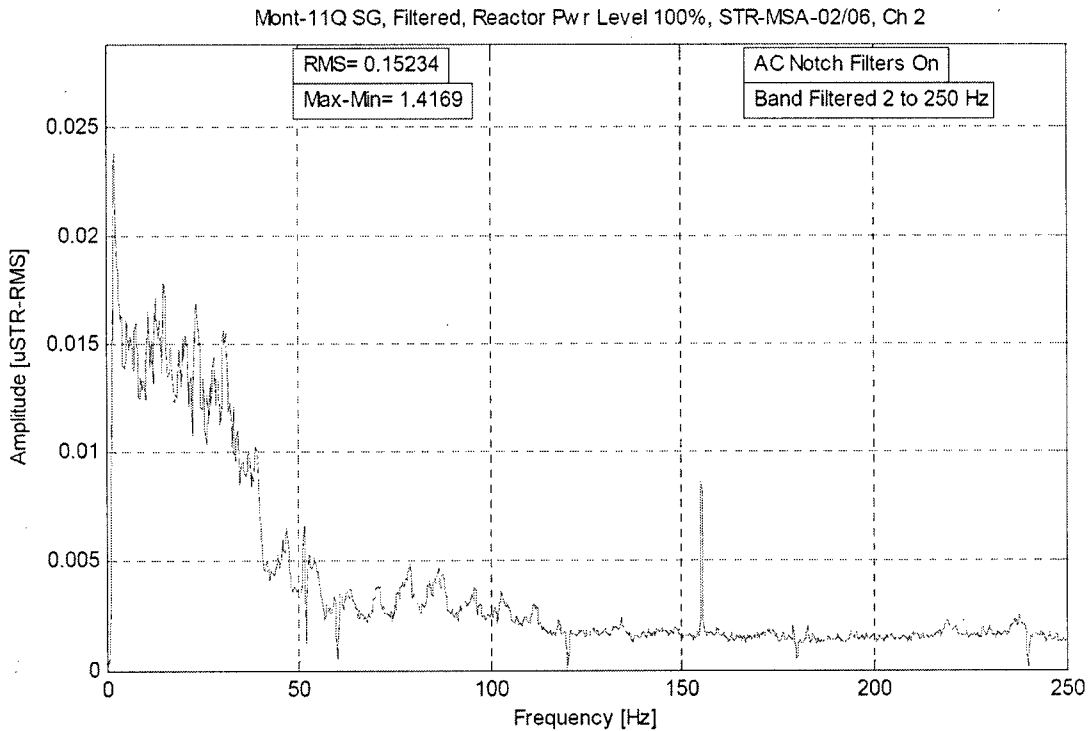
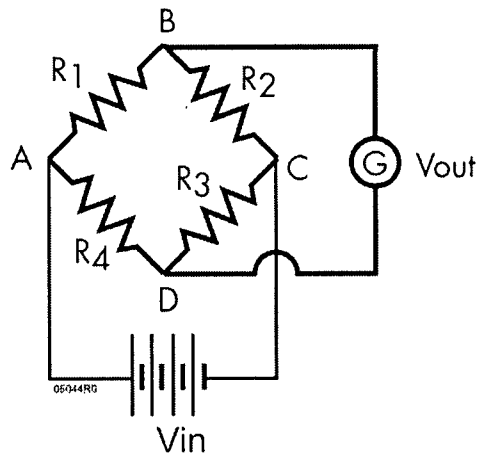


Figure 3-3: Channel 02 with a pair of operational strain gages. Note the absence of the peak at approximately 22 Hz.

Enclosure 13 to L-MT-08-052 NON-PROPRIETARY

A typical strain gage system is comprised of a Wheatstone Bridge (WB) as shown in Figure 3-4. In Figure 3-4, V_{in} is the DC voltage supplied to the WB circuit, V_{out} is the output voltage measured. R_1 to R_4 are the four resistances on the four arms of the WB circuit. In order to minimize the bending strain error, at each SG location the WB circuit was wired in a half bridge configuration. This means that one of the two diametrically attached SG's occupied the position of R_1 and the other SG, that is 180° apart, occupied the R_3 position. The WB circuit analysis will show that the active resistances R_1 and R_3 in this case will be additive. Before the start of the measurements and with no applied strain on the active gages, the compensating resistors R_2 and R_4 will be adjusted such that the output voltage V_{out} is zero, which means that the WB circuit is balanced. In the presence of applied strain the resistances R_1 and R_3 will vary and the output voltage consequently will change and be proportional to the applied strain.



R_1, R_3 - Active Gage Resistors (Half-Bridge)
 R_2, R_4 - Compensating Gage Resistors

Figure 3-4: Wheatstone Bridge and Strain Gage Electrical Schematic

3.2. Raw Data Reduction

Since the relationship between SG and pressure is governed by the geometry of the piping, thickness and OD measurements of the piping are performed at all the instrumented locations. Average SG to dynamic pressure conversion factors (PCFs)

Enclosure 13 to L-MT-08-052 NON-PROPRIETARY

are computed for each location and are provided in Table 3-1. The uncertainties of the various quantities in the SG to pressure relationship were considered when computing the uncertainty in the indirect pressure measurement.

Table 3-1: Strain Gage to Dynamic Pressure Conversion Factors (PCF)

DAS Channel No	SG PAIRS	Circumference (in)	OD (in)	Wall Thickness at LOC.1 (in)	Wall Thickness at LOC.2 (in)	ID (in)	Scale Factor (psi/με)	Averaged SF (psi/με)	Thick/ ID
1	MSA 1&5	57.0	18.144	0.949	0.944	16.251	3.756	3.733	0.058
2	MSA 2&6	57.0	18.144	0.928	0.938	16.278	3.693		0.057
3	MSA 3&7	57.0	18.144	0.945	0.938	16.261	3.733		0.058
4	MSA 4&8	57.0	18.144	0.938	0.952	16.254	3.749		0.058
5	MSA 9&13	56.875	18.104	0.883	0.932	16.289	3.584	3.603	0.056
6	MSA 10&14	56.875	18.104	0.893	0.929	16.282	3.600		0.056
7	MSA 11&15	56.875	18.104	0.915	0.914	16.275	3.617		0.056
8	MSA 12&16	56.875	18.104	0.927	0.900	16.277	3.612		0.056
9	MSB 1&5	57.0	18.144	0.915	0.910	16.319	3.598	3.604	0.056
10	MSB 2&6	57.0	18.144	0.922	0.905	16.317	3.603		0.056
11	MSB 3&7	57.0	18.144	0.922	0.915	16.307	3.626		0.056
12	MSB 4&8	57.0	18.144	0.921	0.901	16.322	3.591		0.056
13	MSB 9&13	56.875	18.104	0.911	0.910	16.283	3.598	3.616	0.056
14	MSB 10&14	56.875	18.104	0.918	0.920	16.266	3.637		0.056
15	MSB 11&15	56.875	18.104	0.914	0.917	16.273	3.621		0.056
16	MSB 12&16	56.875	18.104	0.914	0.911	16.279	3.607		0.056
17	MSC 1&5	56.75	18.064	0.896	0.874	16.294	3.490	3.485	0.054
18	MSC 2&6	56.75	18.064	0.885	0.871	16.308	3.457		0.054
19	MSC 3&7	56.75	18.064	0.890	0.884	16.290	3.499		0.054
20	MSC 4&8	56.75	18.064	0.880	0.892	16.292	3.494		0.054
21	MSC 9&13	56.875	18.104	0.927	0.890	16.287	3.589	3.581	0.056
22	MSC 10&14	56.875	18.104	0.922	0.879	16.303	3.552		0.055
23	MSC 11&15	56.875	18.104	0.932	0.887	16.285	3.593		0.056
24	MSC 12&16	56.875	18.104	0.910	0.907	16.287	3.589		0.056
25	MSD 1&5	56.875	18.104	0.904	0.896	16.304	3.550	3.541	0.055
26	MSD 2&6	56.875	18.104	0.908	0.892	16.304	3.550		0.055
27	MSD 3&7	56.875	18.104	0.903	0.902	16.299	3.561		0.055
28	MSD 4&8	56.875	18.104	0.882	0.898	16.324	3.504		0.055
29	MSD 9&13	57.0	18.144	0.896	0.900	16.348	3.531	3.538	0.055
30	MSD 10&14	57.0	18.144	0.923	0.869	16.352	3.522		0.055
31	MSD 11&15	57.0	18.144	0.935	0.868	16.341	3.547		0.055
32	MSD 12&16	57.0	18.144	0.933	0.871	16.340	3.550		0.055

The raw data is independently processed twice. The raw data for the analyses was first transmitted to Structural Integrity Associates (SIA). SIA processed the data as described below to generate frequency versus amplitude (microstrain) plots for each channel. The raw data was also transmitted to CDI. CDI performs a similar processing of the data as described in Section 3.4

The strain gage time histories were first filtered using a Chebychev type bandpass filter (data from 2- 250 Hertz was allowed to pass). Since the data had electrical noise, digital notch filters were applied to the time histories at 60, 120, 180, and 240 Hz. Also, digital notch filters were used to exclude the electrical excitation from a recirculation pump drive. Once the signal was bandpass and notch filtered, each

Enclosure 13 to L-MT-08-052 NON-PROPRIETARY

time history was converted from the time domain to the frequency domain (frequency spectra) using a Fast Fourier Transform (FFT) algorithm. Each time signal was averaged over the recording length in groups of 2500/.25 samples (the block size); that is, the time history was grouped into 50 percent overlapping groups of 2500/.25 samples. Due to the digital filter imperfections, first few seconds of processed strain data were artificially amplified causing erroneously high readings. To overcome this phenomenon, the first 2 to 5 seconds of processed data were removed before the frequency spectrum was calculated. An FFT was generated for each group and then all FFT groups were summed together, and divided by the number of groups to provide linearly averaged frequency spectra. Plots for each averaged frequency spectrum (amplitude, $\mu\epsilon$ versus frequency, Hz) were generated for each channel. Figure 3-2 and Figure 3-3 are representative of the post-processed data.

3.3. Acoustic Circuit Model Load Definition

In Spring 2005 Exelon installed new stream dryers into Quad Cities Unit 2 (QC2) and Quad Cities Unit 1 (QC1). This replacement design, developed by General Electric, sought to improve dryer performance and overcome structural inadequacies identified on the original dryers, which had been in place for the last 30 years. As a means for confirming the adequacy of the steam dryer, the QC2 replacement dryer was instrumented with pressure sensors at 27 locations. These pressures formed the set of data used to validate the predictions of an acoustic circuit methodology under development by CDI for several years. One of the results of this benchmark exercise confirmed the predictive ability of the acoustic circuit methodology for pressure loading across the dryer, with the inclusion of a low frequency hydrodynamic load. This methodology, validated against the Exelon full-scale data and identified as the Modified Bounding Pressure model, is used in the effort discussed herein.

Reference 6.4 applies this validated methodology to the Monticello Nuclear Generating Plant steam dryer and main steam line geometry. Strain gage data obtained from the four main steam lines were used to predict pressure levels on the Monticello full-scale dryer at Current Licensed Thermal Power.

The acoustic circuit analysis of the Monticello steam supply system is broken into two distinct analyses: a Helmholtz solution within the steam dome and an acoustic circuit analysis in the main steam lines. These analyses are then coupled for an integrated solution. Additional discussion of this analytical technique is provided in Attachment II to this enclosure.

3.4. ACM Input Processing

Two strain gage data sets were examined in this analysis. The first data set recorded the strain at Current Licensed Thermal Power (100 percent power level or CLTP), while the second data set recorded the strain at 28 percent power level. The strain gage signals were converted to pressures by the use of the conversion factors provided by Structural Integrity Associates and summarized in Table 3-1. Exclusion frequencies were used to remove extraneous signals, as summarized in Table 3-2. These signals were further processed by the coherence factor and mean filtering as described in Reference 6.4.

MNGP had an opportunity to obtain additional data following a forced outage in 2008. These data were used to verify and supplement the original data taken in 2007. In addition to taking strain gage measurements at multiple power levels, an electrical interference check was performed at each power level where data was taken. These data are discussed in Attachment II to this enclosure.

Table 3-2: Exclusion Frequencies

Frequency Range (Hz)	Exclusion Cause
0 – 2	Mean
14 - 34	Pipe Vibration
58.5 – 61.5	Line Noise
119.7 – 120.3	Line Noise
179.6 – 180.4	Line Noise
51.2 – 52.3	Recirc Pump B Electrical (1P)
128.6 – 130.2	Recirc Pump B VPF (5x)
133.8 – 134.2	Recirc Pump A VPF (5x)
154.9 – 155.4	Recirc Pump B Electrical (3P)

The measured CLTP strain gage signals contain significant contributions from non-acoustic sources such as sensor noise, Main Steam Line (MSL) turbulence and pipe bending vibration that contribute to the hoop strain measurements. The ACM analysis does not distinguish between the acoustic and non-acoustic fluctuations in the MSL signals that could lead to sizeable, but fictitious acoustic loads and resulting

Enclosure 13 to L-MT-08-052 NON-PROPRIETARY

stresses on the dryer. One way to remove these fictitious loads is to collect data with the system at low (less than 30 percent of CLTP) flow. By operating the recirculation pumps at this condition, much of the background plant noise and vibrations remain present. At these conditions the acoustic loads are known to be negligible so that collected data, referred to as the low power data, originate entirely from non-acoustic sources such as sensor noise and mechanical vibrations. This information is valuable since it allows one to now distinguish between the acoustic and non-acoustic content in the CLTP signal and therefore modify the CLTP loads so that only the acoustic component is retained. For consistency, the low power strain gage signals are filtered in the same manner as the CLTP data and are fed into the ACM model to obtain the monopole and dipole signals at the MSL inlets. Since there is negligible flow, these signals are fictitious, i.e., the hoop strains measured by the strain gages are not due to pressure fluctuations, but rather due to noise. However, under the supposition that these signals are acoustic in origin, the hypothetical stresses due to these signals can nevertheless be computed. The contribution of background noise in the Monticello steam dryer was quantified by taking strain gage measurements at 28 percent power.

As shown in Figure 3-2 and Figure 3-3, spurious peaks occur due to loss of one strain gage in a pair. Peaks attributable to this phenomenon in the range of 15 Hz to 25 Hz were filtered back to background noise. To do this, the magnitudes of the affected signals were determined at 15 Hz, then these magnitudes were imposed on the strain gage signals up to 25 Hz. Phasing of the original signals was preserved by the formula:

$$SG_{MOD}(\omega) = SG(\omega) \left| \frac{SG(\omega_{15HZ})}{SG(\omega)} \right|$$

where $SG_{MOD}(\omega)$ is the modified strain gage signal at the strain gage, $SG(\omega)$ is the original strain gage signal at the strain gage, ω is frequency between 15 and 25 Hz, and $\omega_{15HZ} = 15$ Hz.

The resulting main steam line pressure signals may be represented in two ways: by the minimum and maximum pressure levels, and by PSDs. These results are presented in Attachment II to this enclosure. The measured main steam line pressure data were used to drive the validated acoustic circuit methodology for the Monticello steam dome coupled to the main steam lines to make a pressure load prediction on the Monticello dryer. A low resolution load produces the maximum

differential and RMS pressure levels across the dryer as demonstrated in Attachment II to this enclosure. PSDs of the peak loads on either side of the dryer are also shown in Attachment II to this enclosure.

3.5. Uncertainty and Bias in the Acoustic Circuit Model

The analysis of potential uncertainty occurring at Monticello consists of several contributions, including the uncertainty from collecting data on the main steam lines at locations other than the locations on QC2 and the uncertainty in the Modified Bounding Pressure model. QC2 dryer data at Original Licensed Thermal Power (OLTP) conditions were used to generate an uncertainty analysis of the Acoustic Circuit Methodology for Monticello.

The approach taken for bias and uncertainty is similar to that used by Vermont Yankee for power uprate and is discussed in Attachment II to this enclosure

3.6. Bias and Uncertainty in the Finite Element Model

The applied load includes all biases and uncertainties for both the ACM and the Finite Element Model (FEM). For the latter there are three main contributors to the bias and uncertainty. The first is an uncertainty that accounts for modeling idealizations (e.g., vane bank mass model), geometrical approximations and other discrepancies between the modeled and actual dryer such as neglecting of weld mass and stiffness in the Finite Element Analysis (FEA). The second contributor is a bias accounting for discretization errors associated with using a finite size mesh, upon computed stresses. The third contributor is also a bias and compensates for the use of a finite discretization schedule in the construction of the unit solutions. Bias and uncertainty is discussed in more detail in Attachment II to this enclosure.

4. Dryer Stress Calculations

4.1. USAR Licensing Basis Stress Evaluation

The MNGP licensing basis dryer analysis is a static calculation that only considers faulted loads created by the guillotine rupture of a main steam line outside of containment. The limiting structures on the MNGP dryer for this analysis are the lifting rods. The lifting rods also restrain the dryer during this event by limiting upward movement of the dryer.

Per Section 3.6.3.3 of the MNGP USAR:

“During the steam line rupture DBA, the sensitive component is the steam dryer assembly. The design criteria for the steam dryer requires that the structural integrity of the dryer be maintained for a steam line break which occurs beyond the main isolation valves so as to assure that no part of the dryer can become lodged in the valve and prevent its proper closure. The sensitive components in the dryer are the dryer lifting rods. The calculated differential pressure which is likely to cause buckling of the dryer lifting rods is 12 psi. This represents a margin of safety above the 9.0 psi differential pressure for the limiting faulted Condition...”

The 9.0 psi differential pressure is a very conservative value. Current methodology for calculating the faulted differential pressure (Section 2.2.3 of Enclosure 5) yields a substantially lower value. Nonetheless, this value is calculated at an off-rated plant condition (hot standby), which does not change due to EPU. This differential pressure remains the bounding condition for the MNGP dryer under EPU conditions. Therefore, the limiting static dryer stress for the MNGP dryer is unaffected by EPU.

4.2. Dynamic Stress Calculation

A harmonic finite element stress analysis method is used to assess stresses on the Monticello steam dryer resulting from acoustic and hydrodynamic loads. The harmonic stress analysis confers a number of useful computational advantages over a time-domain method including the ability to assess the effects of frequency scaling in the loads without the need for additional finite element calculations. [[

⁽³⁾]]

The analysis first develops a series of unit stress solutions corresponding to the application of a unit pressure at a MSL at specified frequency, f . Each unit solution is obtained by calculating the associated acoustic pressure field using a separate

Enclosure 13 to L-MT-08-052 NON-PROPRIETARY

analysis that solves the damped Helmholtz equation within the steam dryer. This pressure field is then applied to a finite element structural model of the steam dryer and the stress response at frequency, f , calculated using the commercial ANSYS 10.0 finite element analysis software. This stress response constitutes the unit solution stress and is stored as a file for subsequent processing. Once all unit solutions have been computed, the stress response for any combination of MSL pressure spectrums (obtained by Fast Fourier Transform of the pressure histories in the MSLs) is determined by a simple matrix multiplication of these spectrums with the unit solutions.

Reference 6.6 provides details of the ANSYS 10.0 finite element structural model of the Monticello steam dryer and reviews pertinent modeling considerations. It also summarizes the framework underlying the development and application of unit solutions in the frequency domain and shows how these solutions are used to develop stress histories for general load conditions. Next, it reviews the assessment of these stresses for compliance with the ASME B&PV Code, Section III, subsection NG, for the load combination corresponding to normal operation (the Level A Service Condition).

4.2.1. Model Description

Details regarding the ANSYS 10.0 finite element model are provided in Reference 6.6. The solution is decomposed into static and harmonic parts, where the static solution produces the stress field induced by the supported structure subjected to its own weight and the harmonic solution accounts for the harmonic stress field due to the unit pressure of given frequency in one of the main steam lines. All solutions are linearly combined, with amplitudes provided by signal measurements in each steam line, to obtain the final displacement and stress time histories. This decomposition facilitates the prescription of the added mass model accounting for hydrodynamic interaction and allows one to compare the stress contributions arising from static and harmonic loads separately. Proper evaluation of the maximum membrane and membrane+bending stresses requires that the static loads due to weight be accounted for. Hence both static and harmonic analyses are carried out.

4.2.1.1. Static Analysis

The results of the static analysis are shown in Reference 6.6. Only a few locations exhibited high stress intensity levels. These locations include the top cover plate/end plate connection with stress intensity 3,510 psi. High stress locations are also near the steam dryer support brackets and on tie bars. Note

that these locations have high stress intensity also when static and transient runs are combined, primarily due to static loading.

4.2.1.2. Harmonic Analysis

The harmonic pressure loads were applied to the structural model at all surface nodes. Stresses were calculated for each frequency, and results from static and harmonic calculations were combined.

To evaluate maximum stresses, the stress harmonics including the static component are transformed into a time history using FFT, and the maximum and alternating stress intensities for the response, evaluated. According to ASME B&PV Code, Section III, Subsection NG-321, the following procedure was established to calculate alternating stresses. For every node, the stress difference tensors, $\sigma'_{nm} = \sigma_n - \sigma_m$, are considered for all possible pairs of the stresses s_n and s_m at different time levels, t_n and t_m . Note that all possible pairs require consideration, since there are no "obvious" extrema in the stress responses. However, in order to contain computational cost, extensive screening of the pairs takes place, so that pairs known to produce alternating stress intensities less than 500 psi are rejected. For each remaining stress difference tensor, the principal stresses S_1, S_2, S_3 are computed and the maximum absolute value among principal stress differences, $S_{nm} = \max\{|S_1 - S_2|, |S_1 - S_3|, |S_2 - S_3|\}$, obtained. The alternating stress at the node is then one-half the maximum value of S_{nm} taken over all combinations (n,m), i.e., $S_{alt} = \frac{1}{2} \max_{n,m} \{S_{nm}\}$. This alternating stress is compared against allowable values, depending on the node location with respect to welds.

4.2.1.3. Post-Processing

The static and unsteady stresses computed at every node with ANSYS were exported into files for subsequent post-processing. These files were then read into separate customized software to compute the maximum and alternating stresses at every node. The maximum stress was defined for each node as the largest stress intensity occurring during the time history. Alternating stresses were calculated according to the ASME standard described above. For shell elements, the maximum stresses were calculated separately at the mid-plane, where only membrane stress is present, and at top/bottom of the shell, where bending stresses are also present.

For nodes that are shared between several structural components or lie on junctions, the maximum and alternating stress intensities are calculated as follows. First, the nodal stress tensor is computed separately for each individual component by averaging over all finite elements meeting at the

Enclosure 13 to L-MT-08-052 NON-PROPRIETARY

node and belonging to the same structural component. The time histories of these stress tensors are then processed to deduce the maximum and alternating stress intensities for each structural component. Finally, for nodes shared across multiple components, the highest of the component-wise maximum and alternating stresses is recorded as the "nodal" stress. This approach prevents averaging of stresses across components and thus yields conservative estimates for nodal stresses at the weld locations where several components are joined together.

The maximum stresses are compared against allowable values which depend upon the stress type (membrane, membrane+bending, alternating – P_m , P_m+P_b , S_{alt}) and location (at a weld or away from welds). These allowables are specified in Reference 6.6. For solid elements the most conservative allowable for membrane stress, P_m , is used, although bending stresses are nearly always present also. The structure is then assessed in terms of stress ratios formed by dividing allowables by the computed stresses at every node. Stress ratios less than unity imply that the associated maximum and/or alternating stress intensities exceed the allowable levels. Post-processing tools calculate the stress ratios, identifying the nodes with low stress ratios and generating files formatted for input to the 3D graphics program, TecPlot, which provides more general and sophisticated plotting options than currently available in ANSYS.

4.3. Nominal and Frequency Shifted Results

Results obtained from application of the harmonic FEM to the Monticello steam dryer using the Rev. 4 acoustic/hydrodynamic loads show that at nominal CLTP operation the minimum stress ratio (SR) anywhere on the steam dryer, at any frequency shift is $SR=3.02$ and corresponds to an alternating maximum stress intensity at a weld (where the outer hood and outer cover plates meet). These results account for all the end-to-end biases and uncertainties in the loads model.

At EPU conditions, the limiting stress ratio without frequency shifting is $SR-a=2.81$ and corresponds to an alternating stress. When frequency shifting is included the stress ratio reduces to 2.28. Both a maximum stress intensity and an alternating stress intensity (obtained at different nodes) reduce to this same stress ratio.

5. Power Ascension Testing

Power ascension at Monticello will be accomplished over two fuel cycles. During the first cycle, power increases will be limited to approximately 5 percent above the current level of 1775 MWt. The remainder of the power ascension to approximately 2004 MWt will be performed following the 2011 refueling outage when balance of plant modifications will be performed to make the higher power levels possible.

During each power ascension, the dryer stress levels will be evaluated at approximately 2.5 percent intervals beyond the current licensed power level. Limit curves and [()⁽³⁾] will be utilized to assure MNGP steam dryer stress levels remain acceptable. These two methods are described below.

5.1. Limit Curves

During power ascension of Monticello Nuclear Generating Plant, from CLTP to EPU conditions, NSPM intends to monitor the dryer stresses at plant power levels that have not yet been achieved. Limit curves provide an upper bound safeguard against the potential for dryer stresses becoming higher than allowable, by estimating the not-to-be-exceeded main steam line pressure levels. In the case of MNGP, in plant main steam line data have been analyzed at CLTP conditions to provide steam dryer hydrodynamic loads. A finite element model stress analysis has been undertaken on the CLTP loads. These loads provide the basis for generation of the limit curves to be used during MNGP power ascension.

To develop the limit curves for MNGP, the stress levels in the dryer were calculated for the current plant acoustic signature, at CLTP conditions, and then used to determine how much the acoustic signature could be increased while maintaining stress levels below the stress fatigue limit. During power ascension, strain gage data will be converted to pressure in PSD format at each of the eight main steam line locations, for comparison with the limit curves. The strain gage data will be monitored throughout power ascension to observe the onset of discrete peaks, if they occur.

Limit curves were generated from the in-plant CLTP strain gage data reported in Reference 6.4. These data were filtered across the frequency ranges shown in Table 3-2 to remove noise and extraneous signal content. The resulting PSD curves for each of the eight strain gage locations were used to develop the limit curves (Reference 6.7). Level 1 limit curves are found by multiplying the main steam line pressure PSD base traces by the square of the corrected limiting stress ratio ($3.02^2 = 9.12$), while the Level 2 limit curves are found by multiplying the PSD base traces by

Enclosure 13 to L-MT-08-052 NON-PROPRIETARY

0.64 of the square of the corrected limiting stress ratio (recovering 80 percent of the limiting stress ratio, or $0.80^2 \times 3.02^2 = 0.64 \times 9.12 = 5.84$), as PSD is related to the square of the pressure. The resulting limit curves for MNGP EPU power ascension are provided in Attachment IV to this enclosure.

[[

[[

(3)]]

(3)]]

6. References

- 6.1. **C.D.I. Report No. 07-23P:** Flow-Induced Vibration in the Main Steam Lines at Monticello and Resulting Steam Dryer Loads, Revision 0, February 2008 (Proprietary, Attached)
- 6.2. **ASME Steam Tables (1998):** Properties based upon IAPWS-IF97
- 6.3. **STROUHAL NUMBERS OF FLOW-EXCITED ACOUSTIC RESONANCE OF CLOSED SIDE BRANCHES:** Ziada and Shine, Journal of Fluids and Structures (1999) 13, 127-142
- 6.4. **C.D.I. Report No. 07-25P:** Acoustic and Low Frequency Hydrodynamic Loads at CLTP Power Level on Monticello Steam Dryer to 200 Hz, Revision 4, November 2008 (Proprietary, Attached)
- 6.5. **NRC Request for Additional Information on the Hope Creek Generating Station, Extended Power Uprate.** 2007. TAC No. MD3002. RAI No. 14.67.
- 6.6. **CDI Report No. 07-26P:** Stress Assessment of Monticello Steam Dryer, Revision 2, November 2008 (Proprietary, Attached)
- 6.7. **C.D.I. Technical Note No. 08-12P,** Limit Curve Analysis with ACM Rev. 4 for Power Ascension at Monticello, Revision 2, November 2008 (Proprietary, Attached)
- 6.8. **Safety Analysis Report for Monticello Constant Pressure Power Uprate,** Docket No. 050-263, enclosure 5, November 2008

**Attachment I of
Enclosure 13 to L-MT-08-052**

C.D.I. Report No. 07-23NP:
Flow-Induced Vibration in the Main Steam Lines
at Monticello and Resulting Steam Dryer Loads,
Revision 0, February 2008

(Non-Proprietary)

Flow-Induced Vibration in the Main Steam Lines at Monticello
and Resulting Steam Dryer Loads

Revision 0

Prepared by

Continuum Dynamics, Inc.
34 Lexington Avenue
Ewing, NJ 08618

Prepared under Purchase Order No. 13758 for

Nuclear Management Company, LLC
Monticello Nuclear Generating Plant
2807 W. County Road 75
Monticello, MN 55362-9637

Approved by



Alan J. Bilanin

Reviewed by



Milton E. Teske
February 2008

Executive Summary

As part of the engineering effort in support of power uprate at Monticello Nuclear Generating Plant, Continuum Dynamics, Inc. (C.D.I.) first analyzed the standpipe/valves based on engineering drawings supplied by Nuclear Management Company LLC (NMC). This analysis suggested that the excitation frequency of the standpipe/valves at Monticello would begin at a power level just above that of EPU conditions. To support these calculations, C.D.I. then constructed a nominal one-eighth scale model of the complete steam line system at Monticello, from the steam dome to the turbine. The subscale tests described herein (1) confirm that the existing standpipes have little excitation up to EPU conditions and (2) determine steam dryer loads in the frequency range 0 to 200 Hz. This effort provides NMC with a subscale test that quantifies the level of excitation to be expected at Monticello at EPU conditions and can be used to develop bump-up factors to scale CLTP in-plant data to EPU conditions.

Table of Contents

Section	Page
Executive Summary	i
Table of Contents	ii
1. Introduction	1
2. Objectives	2
3. Theoretical Approach	3
3.1 Side Branch Excitation Mechanism	3
3.2 Scaling Laws	4
4. Test Approach	7
5. Test Apparatus and Instrumentation	19
5.1 Experimental Facility	19
5.2 Evaluation of Mach Number at the Standpipes	19
5.3 Instrumentation and Data Acquisition	21
6. Test Matrix	24
7. Test Procedure	25
7.1 Data Collection	25
7.2 Data Reduction	25
8. Results and Discussion	27
8.1 Excitation Frequency	27
8.2 Mach Number	27
8.3 Comparison of PDSs	28
8.4 Main Steam Line / Steam Dryer	28
9. Bump-Up Factor	36
10. Conclusions	37
11. References	38
Appendix: PSD Results	40

1. Introduction

As part of its effort in support of power uprate at Monticello Nuclear Generating Plant, Nuclear Management Company LLC (NMC) contracted with Continuum Dynamics, Inc. (C.D.I.) to construct a nominal one-eighth scale model of their main steam lines, to evaluate the potential for flow induced vibration (FIV) in the main steam lines as a result of resonance of the as-built standpipe/valve combination. These results, described herein, would confirm that the current steam dryer would not be subjected to pressure loadings that exceed its stress limit. Similar studies conducted by Exelon for Quad Cities Units 1 and 2 suggested that excitation of the standpipe/valves should be explored, as this mechanism was most responsible for the pressure loading experienced on the Quad Cities steam dryers [1]. Such a study has also been undertaken for Hope Creek [2].

The frequencies associated with FIV are known to correspond to a resonance associated with the inlet standpipes connected to safety valves, and have been the source of problems in several power plants in recent years [3–6]. Specifically, in [6], C.D.I. conducted a series of tests in support of damage observed on Columbia's main steam line safety valves. These tests concluded that the geometry of the Columbia standpipes and safety valve inlets, with flow conditions of approximately 60% to 70% of licensed power, resulted in a resonance at approximately 1050 Hz in a scaled facility (corresponding to approximately 204 Hz in the plant). The observation was made that properly scaled tests could provide data that could be used for design.

At the request of NMC, C.D.I. applied the insights gained from the study on Columbia, and previous work for Exelon and Hope Creek, to the Monticello standpipe/valve configuration. This report summarizes the test results on a scale model of the Monticello plant with four main steam lines.

2. Objectives

Construction of a high Reynolds number subscale test facility, simulating the Monticello steam delivery system, was done so as to achieve the following goals:

1. Measure the excitation frequency and amplitudes of the as-built standpipe/valve configuration (encompassing all four main steam lines) at Monticello, determine the behavior of the system from below CLTP conditions to above EPU conditions, and identify the Mach number at which excitation onset of the standpipe/valves begins.
2. Provide main steam line pressure data to be used with the acoustic circuit model to develop a bump-up factor relating unsteady steam dryer loads at CLTP conditions to those anticipated at EPU conditions. The bump-up factor would then be applied to the full-scale CLTP strain gage data collected on the Monticello main steam lines to obtain an estimate of the full-scale EPU strain gage data. The EPU strain gage data would then be used to estimate steam dryer stresses at full power.

3. Theoretical Approach

A one-eighth test facility is proposed as a means of measuring the effect of standpipes on the anticipated acoustic signal to the steam dome. A description of the phenomenon at work, analytical tools used, and scaling laws justifying the subscale tests are given here.

3.1 Side Branch Excitation Mechanism

The phenomenon of flow-excited acoustic resonance of closed side branches has been examined for many years (see as early as [7] and [8]). In this situation acoustic resonance of the side branch is caused by feedback from the acoustic velocity of the resonant standing wave in the side branch itself. Figure 3.1 illustrates the typical geometry used here and in the standpipes at Monticello. The main steam line flow velocity U approaches an open side branch of diameter d and length L . Pressure p as a function of time t can be measured at the closed end of the pipe. The flow velocity induces perturbations in the shear layer at the upstream separation location in the main steam line. As these perturbations are amplified and convected downstream, they interact with the acoustic field and produce acoustic energy which reinforces the resonance of the acoustic mode. Ziada has studied this effect extensively [9–11], and has shown that the flow velocity of first onset of instability U_{on} corresponds to a typical Strouhal number of $St = 0.55$, where St is defined as

$$St = \frac{f(d+r)}{U_{on}} \quad (3.1)$$

where d is the diameter of the standpipe, r is the radius of the inlet chamfer, and f is the first mode of acoustic oscillation in the pipe system. A design chart that more accurately infers St , based on d and the diameter D of the main steam line, may be found in [9].

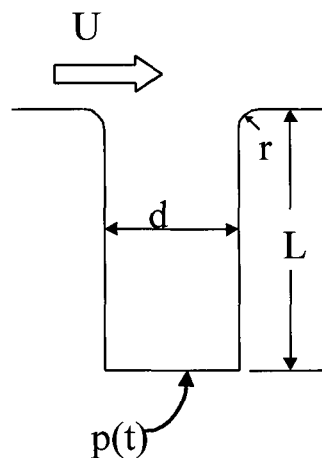


Figure 3.1. Schematic of the side branch geometry.

Solving for U_{on} in Equation 3.1, it may be seen that the onset velocity is linearly proportional to the standpipe diameter, so long as that diameter does not change the first acoustic mode frequency of the standpipe.

The implications of this side branch excitation frequency may be seen by examining the behavior of the pressure response as a function of Strouhal number St (Figure 3.2). For large Strouhal numbers (beginning on the right side of the figure), the RMS pressure p_{RMS} begins increasing (at a specific onset Strouhal number and flow velocity U_{on} , depending on acoustic speed a , pipe diameter d , and pipe length L), reaches a peak value, then decreases. Flow velocity increases from right to left in this figure, where it may then be seen that this phenomenon – if it occurs in a standpipe/valve configuration – will occur at a low power level, reach a peak effect, then diminish and disappear at sufficiently high power levels.

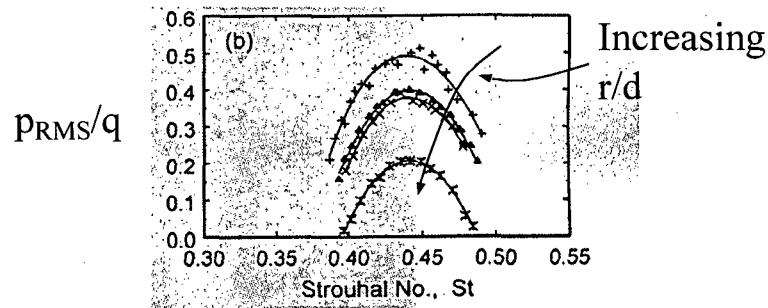


Figure 3.2. Strouhal number behavior, where q is the dynamic pressure ($\frac{1}{2}\rho U^2$) and ρ is the fluid density [12].

Initially, it may be anticipated that the first mode frequency f_1 can be approximated by the quarter-standing wave frequency of the standpipe/valve combination

$$f_1 = \frac{a}{4L} \tag{3.2}$$

where a is the acoustic speed. Since the standpipe/valve combination changes area as a function of distance from the main steam line to the valve disk, a more accurate estimate of f_1 may be generated by including these area change effects. The combination of an accurate excitation frequency f_1 and subsequent calculation of onset velocity U_{on} with the appropriate Strouhal number then characterizes the behavior of the standpipe/valve combination considered.

3.2 Scaling Laws

[[

(3)]]

[[

⁽³⁾]]

[[

⁽³⁾]]

4. Test Approach

The purpose of the testing effort is to measure the excitation frequency and amplitudes of the as-built standpipe/valve configuration, and determine its behavior at CLTP and EPU conditions. To do so, a one-eighth scale test facility was constructed that represents the Monticello steam delivery system.

[[

⁽³⁾]]

[[

(3)]]

Table 4.1. Standpipe location summary at Monticello.

Main Steam Line	Valve Type	Distance From Upstream Elbow (ft)
A and D	Target Rock	6.91
A and D	Blank	9.79
A and D	Target Rock	12.67
A and D	Blank	18.43
A and D	Blank	21.31
A and D	Blank	24.19
B and C	Target Rock	3.18
B and C	Blank	5.73
B and C	Target Rock	8.60

From drawings, pictures, and additional information supplied by NMC [14], approximate cross-sectional areas of the two standpipe/valve configurations – as a function of distance from the main steam line – were generated. Blank standpipes end at blank flanges. These cross-sectional areas include the standpipe length and diameter, mating flange to the valve, and internal valve geometries to the closed end of the valve. The two standpipe configurations are shown in Figures 4.8 and 4.9.

[[

⁽³⁾]]

Figure 4.2. Monticello subscale dryer schematic.

[[

Figure 4.3. Schematic of Monticello main steam line A. Tables 4.2 and 4.3 summarize the piping connections.

⁽³⁾]]

[[

Figure 4.4. Schematic of Monticello main steam line B. Tables 4.2 and 4.3 summarize the piping connections.

⁽³⁾]]

[[

Figure 4.5. Schematic of Monticello main steam line C. Tables 4.2 and 4.3 summarize the piping connections.

⁽³⁾]]

[[

⁽³⁾]]

Figure 4.6. Schematic of Monticello main steam line D. Tables 4.2 and 4.3 summarize the piping connections.

Table 4.2. Summary of subscale main steam line piping lengths. Segments are identified in Figures 4.3 through 4.6. Elbows are identified in Table 4.3.

[[

⁽³⁾]]

Table 4.3. Summary of subscale main steam line piping fittings. Connections are identified in Figures 4.3 through 4.6. Segments are identified in Table 4.2.

[[

⁽³⁾]]

[[

Figure 4.7. Photographs of the Monticello steam delivery system at nominal one-eighth scale.⁽³⁾]]

[[

⁽³⁾]]

[[

Figure 4.9. Scale drawing of the ten blank standpipe models at Monticello.

⁽³⁾]]

5. Test Apparatus and Instrumentation

Test apparatus for the Monticello one-eighth scale test program consists of a pressure tank, a system of PVC piping to model full-scale steam lines, two sets of interchangeable model pressure relief valves, four ball valves, and a set of interchangeable orifices.

5.1 Experimental Facility

[[

⁽³⁾]]

[[

⁽³⁾]]

This Document Does Not Contain Continuum Dynamics, Inc. Proprietary Information

Table 5.1. Plant power and average inlet Mach numbers, where the CLTP Mach number = 0.0975 and the EPU ($1.16 \times$ CLTP) Mach number = 0.1131.

[[

⁽³⁾]]

[[

⁽³⁾]]

[[

Figure 5.2. Schematic of data acquisition system with fourteen DP transducers. ⁽³⁾]]

6. Test Matrix

Table 6.1. Monticello Four-Line Test Matrix.

[[

⁽³⁾]]

7. Test Procedure

7.1 Data Collection

[[

7.2 Data Reduction

[[

⁽³⁾]]

⁽³⁾]]

[[

Figure 7.1. Typical stagnation pressure time history.

⁽³⁾]]

8. Results and Discussion

The purpose of the subscale test program was to characterize the behavior of the standpipe/valves currently at Monticello. The results of the test program (38 tests) may be examined with regard to excitation frequency and RMS pressure as a function of power level, comparison of PSDs, and predicted peak pressures on the steam dryer. Of these, the change in peak pressures on the steam dryer provides the best extrapolation of the potential impact on steam dryer stresses.

8.1 Excitation Frequency

[[

(3)]]

8.2 Mach Number

The PSD results shown in the Appendix provide a good indication of peak response for standpipe/valve behavior at specific Mach numbers. However, a better metric is the root mean square (RMS) of the recorded signal. This parameter was determined by integrating the PSD from 600 to 1000 Hz, then taking the square root to recover the RMS pressure level over this frequency range. These results will now be examined for the pressure transducer measurements at the ends of the standpipe/valves on main steam lines C and D.

[[

(3)]]

[[

8.3 Onset Velocity

⁽³⁾]]

[[

8.4 Main Steam Line / Steam Dryer

⁽³⁾]]

The effect of Mach number on normalized RMS pressure in the MSL and on the dryer may be seen in Figures 8.2 to 8.6. The largest contribution to the RMS is the discrete frequency peaks attributed to the standpipe/valve excitation, as previously seen in Figure 8.1. RMS pressures include the signal from 600 to 1000 Hz subscale.

[[

⁽³⁾]]

[[

Figure 8.1. Normalized RMS pressure for the pressure transducers at the ends of the standpipe/valves on main steam line C (top) and D (bottom). Polynomial curve fits to all data (black dots) are shown by the black curves. ⁽³⁾]]

[[

Figure 8.2. Normalized RMS pressure on main steam line A. PD1: upstream pressure transducer; PD2: downstream pressure transducer. Polynomial curve fits to all data (black dots) are shown by the black curves. ⁽³⁾]]

[[

Figure 8.3. Normalized RMS pressure on main steam line B. PD3: upstream pressure transducer; PD4: downstream pressure transducer. Polynomial curve fits to all data (black dots) are shown by the black curves. ⁽³⁾]]

[[

Figure 8.4. Normalized RMS pressure on main steam line C. PD5: upstream pressure transducer; PD6: downstream pressure transducer. Polynomial curve fits to all data (black dots) are shown by the black curves. ⁽³⁾]]

[[

Figure 8.5. Normalized RMS pressure on main steam line D. PD7: upstream pressure transducer; PD8: downstream pressure transducer. Polynomial curve fits to all data (black dots) are shown by the black curves. ⁽³⁾]]

[[

Figure 8.6. Normalized RMS pressure at the dryer pressure transducers. PD9: opposite main steam line A; PD10: opposite main steam line D. Polynomial curve fits to all data (black dots) are shown by the black curves. ⁽³⁾]]

Table 8.3. RMS pressure summary of the Monticello subscale tests (600 to 1000 Hz).

[[

⁽³⁾]]

9. Bump-Up Factor

One of the objectives of subscale testing is to develop a bump-up factor that relates unsteady steam dryer loads at CLTP conditions to those anticipated at EPU conditions. This bump-up factor would then be applied to full-scale CLTP strain gage data collected on the Monticello main steam lines to obtain an estimate of the full-scale EPU strain gage data. The EPU strain gage data would then be used to estimate steam dryer stresses at full power.

[[

Figure 9.1. Bump-up factor developed from Monticello subscale data. The eight locations are shown by the eight pressure transducer identifiers. ⁽³⁾]]

10. Conclusions

One-eighth scale tests measured the excitation frequency and amplitudes of the as-built steam delivery system (encompassing all four main steam lines) at Monticello, as a function of entrance Mach number, and determined the behavior of the system at CLTP and EPU conditions.

[[

⁽³⁾]]

11. References

1. Continuum Dynamics, Inc. 2006. Mitigation of Pressure Oscillations in the Quad Cities Unit 2 Steam Delivery System: A Subscale Four Main Steam Line Investigation of Standpipe Behavior. C.D.I. Report No. 06-08.
2. Continuum Dynamics, Inc. 2005. Onset of High Frequency Flow Induced Vibration in the Main Steam Lines at Hope Creek Unit 1: A Subscale Investigation of Standpipe Behavior. C.D.I. Report No. 05-31.
3. Webb, M. and P. Ellenberger. 1995. Piping Retrofit Reduces Valve-Damaging Flow Vibration. *Power Engineering* 99(1): 27-29.
4. Bernstein, M. D. and Bloomfield, W. J. 1989. Malfunction of Safety Valves Due to Flow Induced Vibration. *Flow-Induced Vibrations 1989* (ed: M. K. Au-Yang, S. S. Chen, S. Kaneko and R. Chilukuri) PVP 154: 155-164. New York: ASME.
5. Coffman, J. T. and Bernstein, M. D. 1980. Failure of Safety Valves Due to Flow-Induced Vibration. *Transactions of the ASME* 102(1): 112-118.
6. Continuum Dynamics, Inc. 2002. Mechanisms Resulting in Leakage from Main Steam Safety Valves. C.D.I. Technical Note No. 02-16.
7. Chen, Y. N. and D. Florjancic. 1975. Vortex-Induced Resonance in a Pipe System due to Branching. *Proceedings of International Conference on Vibration and Noise in Pump, Fan and Compressor Installations* 79-86. University of Southampton, England.
8. Baldwin, R. M. and H. R. Simmons. 1986. Flow-Induced Vibration in Safety Relief Valves. *ASME Journal of Pressure Vessel Technology* 108: 267-272.
9. Ziada, S. and Shine, S. 1999. Strouhal Numbers of Flow-Excited Acoustic Resonance of Closed Side Branches. *Journal of Fluids and Structures* 13: 127-142.
10. Ziada, S. 1994. A Flow Visualization Study of Flow Acoustic Coupling at the Mouth of a Resonant Side-Branch. *Journals of Fluids and Structures* 8: 391-416.
11. Graf, H. R. and S. Ziada. 1992. Flow-Induced Acoustic Resonance in Closed Side Branches: An Experimental Determination of the Excitation Source. *Proceedings of ASME International Symposium on Flow-Induced Vibration and Noise, Vol. 7: Fundamental Aspects of Fluid-Structure Interactions* (ed: M. P. Paidoussis, T. Akylas and P. B. Abraham). AMD 51: 63-80. New York: ASME.
12. Weaver, D. S. and MacLeod, G. O. 1999. Entrance Port Rounding Effects on Acoustic Resonance in Safety Relief Valves. Flow-Induced Vibration: The 1999 ASME Pressure Vessels and Piping Conference. 291-298.

13. Continuum Dynamics, Inc. 2004. Plant Unique Steam Dryer Loads to Support I&E Guidelines. C.D.I. Technical Memorandum No. 04-14.
14. Monticello Drawings No. NX-13142-33, NX-13142-34, NX-13142-35, NX-13142-36, NF-36271, NX-8435-183-1, and NX-7831-437. Email from J. Ferrante, "RE: Valve Placement in Monticello," dated 30 July 2007. Email from J. Ferrante, "SG Distance from the Vessel ID," dated 20 September 2007.
15. Shapiro, A. H. 1953. The Dynamics and Thermodynamics of Compressible Fluid Flow. Volume I. John Wiley and Sons: New York, NY. Chapter 4.
16. Kayser, J. C. and R. L. Shambaugh. 1991. Discharge Coefficients for Compressible Flow Through Small-Diameter Orifices and Convergent Nozzles. *Chemical Engineering Science* 46: 1697-1711.
17. Graf, H. R. and S. Ziada. 1992. Flow Induced Acoustic Resonance in Closed Side Branches: An Experimental Determination of the Excitation Source. AMD 151 / PVP 247. Symposium on Flow-Induced Vibration and Noise – Volume 7. ASME. 63-80.

Appendix: PSD Results

This Appendix provides the normalized PSDs for the main steam line and steam dryer pressure transducers in Figures A1 to A38. Here, normalized PSD is obtained by normalizing the pressure trace by the dynamic pressure at CLTP, then constructing the PSD from the Fast Fourier transform.

The test matrix is found in Table 6.1. The transducer designations are shown in Table A1 and include the four pressure transducers located on the ends of the standpipe/valves on main steam lines C and D.

Table A1. Pressure Transducer Designations

Pressure Transducer Number	Pressure Transducer Location
PD1	MSL A upstream strain gage location
PD2	MSL A downstream strain gage location
PD3	MSL B upstream strain gage location
PD4	MSL B downstream strain gage location
PD5	MSL C upstream strain gage location
PD6	MSL C downstream strain gage location
PD7	MSL D upstream strain gage location
PD8	MSL D downstream strain gage location
PD9	Steam dryer location opposite MSL A
PD10	Steam dryer location opposite MSL D
PD11	End of Standpipe C upstream location
PD12	End of Standpipe C downstream location
PD13	End of Standpipe D upstream location
PD14	End of Standpipe D downstream location

[[

⁽³⁾]]

[[

(3)]]

[[

⁽³⁾]]

[[

⁽³⁾]]

II

⁽³⁾II

[[

⁽³⁾]]

[[

⁽³⁾]]

[[

(3)]]

[[

⁽³⁾]]

[[

⁽³⁾]]

[[

⁽³⁾]]

[[

⁽³⁾]]

[[

⁽³⁾]]

[[

⁽³⁾]]

[[

.(³)]]

[[

⁽³⁾]]

This Document Does Not Contain Continuum Dynamics, Inc. Proprietary Information

[[

⁽³⁾]]

[[

-(³)]]

[[

⁽³⁾]]

This Document Does Not Contain Continuum Dynamics, Inc. Proprietary Information

[[

⁽³⁾]]

**Attachment II of
Enclosure 13 to L-MT-08-052**

C.D.I. Report No. 07-25NP:

Acoustic and Low Frequency Hydrodynamic
Loads at CLTP Power Level on Monticello Steam
Dryer to 200 Hz, Revision 4,
November, 2008

(Non-Proprietary)

Acoustic and Low Frequency Hydrodynamic Loads at CLTP Power Level on
Monticello Steam Dryer to 200 Hz

Revision 4

Prepared by

Continuum Dynamics, Inc.
34 Lexington Avenue
Ewing, NJ 08618

Prepared under Purchase Order No. 00013758 for

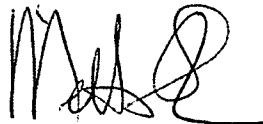
Northern States Power Company, a Minnesota Corporation (NSPM)
Monticello Nuclear Generating Plant
2807 W County Road 75
Monticello, MN 55362

Approved by



Alan J. Bilanin

Prepared by



Milton E. Teske

November 2008

Executive Summary

Measured strain gage time-history data in the four main steam lines at the Monticello Nuclear Generating Plant (MNGP) were processed by a dynamic model of the steam delivery system to predict loads on the full-scale steam dryer. These measured data were first converted to pressures, then positioned on the four main steam lines and used to extract acoustic sources in the system. A validated acoustic circuit methodology was used to predict the fluctuating pressures anticipated across components of the steam dryer in the reactor vessel. The acoustic circuit methodology included a low frequency hydrodynamic contribution, in addition to an acoustic contribution at all frequencies. This pressure loading was then provided for structural analysis to assess the structural adequacy of the steam dryer in Monticello.

The dryer pressure loading at CLTP conditions was computed using the methodology in BWRVIP-194 [1], with the exception that the EIC signal was not used.

This effort provides the Northern States Power Company, a Minnesota Corporation (NSPM), with a dryer dynamic load definition that comes directly from measured Monticello full-scale data and the application of a validated acoustic circuit methodology, at a power level where data were acquired.

Table of Contents

Section	Page
Executive Summary	i
Table of Contents	ii
1. Introduction	1
2. Modeling Considerations	2
2.1 Helmholtz Analysis	2
2.2 Acoustic Circuit Analysis	3
2.3 Low Frequency Contribution	4
3. Input Pressure Data	5
4. Results	17
5. Uncertainty Analysis	24
6. Conclusions	26
7. References	27

1. Introduction

In Spring 2005 Exelon installed new steam dryers into Quad Cities Unit 2 (QC2) and Quad Cities Unit 1. This replacement design, developed by General Electric, sought to improve dryer performance and overcome structural inadequacies identified on the original dryers, which had been in place for the last 30 years. As a means for confirming the adequacy of the steam dryer, the QC2 replacement dryer was instrumented with pressure sensors at 27 locations. These pressures formed the set of data used to validate the predictions of an acoustic circuit methodology under development by Continuum Dynamics, Inc. (C.D.I.) for several years [2]. One of the results of this benchmark exercise [3] confirmed the predictive ability of the acoustic circuit methodology for pressure loading across the dryer, with the inclusion of a low frequency hydrodynamic load. This methodology, validated against the Exelon full-scale data and identified as the Modified Bounding Pressure model, is used in the effort discussed herein.

This report applies this validated methodology to the Monticello Nuclear Generating Plant (MNGP) steam dryer and main steam line geometry. Strain gage data obtained from the four main steam lines were used to predict pressure levels on the Monticello full-scale dryer at Current Licensed Thermal Power (CLTP).

2. Modeling Considerations

The acoustic circuit analysis of the Monticello steam supply system is broken into two distinct analyses: a Helmholtz solution within the steam dome and an acoustic circuit analysis in the main steam lines. This section of the report highlights the two approaches taken here. These analyses are then coupled for an integrated solution.

2.1 Helmholtz Analysis

A cross-section of the steam dome (and steam dryer) is shown below in Figure 2.1, with Monticello dimensions as shown [4]. The complex three-dimensional geometry is rendered onto a uniformly-spaced rectangular grid (with mesh spacing of approximately 1.5 inches to accommodate frequency from 0 to 200 Hz in full scale), and a solution, over the frequency range of interest, is obtained for the Helmholtz equation

$$\frac{\partial^2 P}{\partial x^2} + \frac{\partial^2 P}{\partial y^2} + \frac{\partial^2 P}{\partial z^2} + \frac{\omega^2}{a^2} P = \nabla^2 P + \frac{\omega^2}{a^2} P = 0$$

where P is the pressure at a grid point, ω is frequency, and a is acoustic speed in steam.

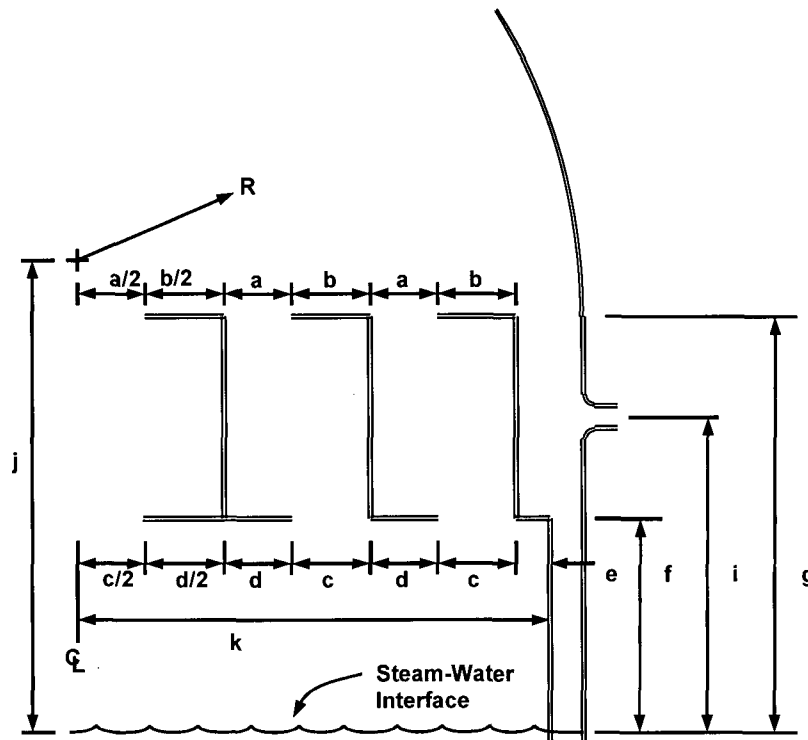


Figure 2.1. Cross-sectional description of the steam dome and dryer at Monticello, with the dimensions of $a = 6.5$ in, $b = 27.0$ in, $c = 18.5$ in, $d = 15.0$ in, $e = 16.75$ in, $f = 68.5$ in, $g = 130.5$ in, $i = 82.5$ in, $j = 142.5$ in, $k = 100.5$ in, and $R = 102.5$ in.

This equation is solved for incremental frequencies from 0 to 200 Hz (full scale), subject to the boundary conditions

$$\frac{dP}{dn} = 0$$

normal to all solid surfaces (the steam dome wall and interior and exterior surfaces of the dryer),

$$\frac{dP}{dn} \propto \frac{i\omega}{a} P$$

normal to the nominal water level surface, and unit pressure applied to one inlet to a main steam line and zero applied to the other three.

2.2 Acoustic Circuit Analysis

The Helmholtz solution within the steam dome is coupled to an acoustic circuit solution in the main steam lines. Pulsation in a single-phase compressible medium, where acoustic wavelengths are long compared to transverse dimensions (directions perpendicular to the primary flow directions), lend themselves to application of the acoustic circuit methodology. If the analysis is restricted to frequencies below 200 Hz, acoustic wavelengths are approximately 8 feet in length and wavelengths are therefore long compared to most components of interest, such as branch junctions.

Acoustic circuit analysis divides the main steam lines into elements which are each characterized, as sketched in Figure 2.2, by a length L , a cross-sectional area A , a fluid mean density $\bar{\rho}$, a fluid mean flow velocity \bar{U} , and a fluid mean acoustic speed \bar{a} .

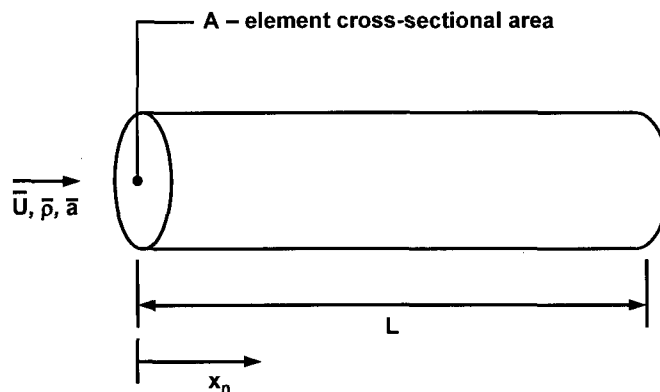


Figure 2.2. Schematic of an element in the acoustic circuit analysis, with length L and cross-sectional area A .

Application of acoustic circuit methodology generates solutions for the fluctuating pressure P_n and velocity u_n in the n^{th} element of the form

$$P_n = [A_n e^{ik_{1n}X_n} + B_n e^{ik_{2n}X_n}] e^{i\omega t}$$

$$u_n = -\frac{1}{\rho \bar{a}^2} \left[\frac{(\omega + \bar{U}_n k_{1n})}{k_{1n}} A_n e^{ik_{1n}X_n} + \frac{(\omega + \bar{U}_n k_{2n})}{k_{2n}} B_n e^{ik_{2n}X_n} \right] e^{i\omega t}$$

where harmonic time dependence of the form $e^{i\omega t}$ has been assumed. The wave numbers k_{1n} and k_{2n} are the two complex roots of the equation

$$k_n^2 + i \frac{f_n |\bar{U}_n|}{D_n a} (\omega + \bar{U}_n k_n) - \frac{1}{a} (\omega + \bar{U}_n k_n)^2 = 0$$

where f_n is the pipe friction factor for element n , D_n is the hydrodynamic diameter for element n , and $i = \sqrt{-1}$. A_n and B_n are complex constants which are a function of frequency and are determined by satisfying continuity of pressure and mass conservation at element junctions.

The solution for pressure and velocity in the main steam lines is coupled to the Helmholtz solution in the steam dome, to predict the pressure loading on the steam dryer.

The main steam line piping geometry is summarized in Table 2.1.

Table 2.1. Main steam line lengths at Monticello, measured from the inside wall of the steam dome down the centerline of the main steam lines. Main steam line diameter is 18 inch Schedule 80 (ID = 16.124 in).

Main Steam Line	Length to First Strain Gage Measurement (ft)	Length to Second Strain Gage Measurement (ft)
A	11.9	43.9
B	11.9	43.9
C	11.9	43.9
D	11.9	43.9

2.3 Low Frequency Contribution

[[

(3)]]

3. Input Pressure Data

Strain gages were mounted on the four main steam lines of Monticello. Two data sets were examined in this analysis. The first data set recorded the strain at Current Licensed Thermal Power (100% power level or CLTP), while the second data set recorded the strain at 28% power level. The strain gage signals were converted to pressures by the use of the conversion factors provided in [5] and summarized in Table 3.1. Exclusion frequencies were used to remove extraneous signals, as also identified in [5], and summarized in Table 3.2. In particular, signals attributed to main steam line pipe vibration were identified and removed [6]. These signals were further processed by the coherence factor and mean filtering as described in [3]. Coherence is shown in Figure 3.1.

The data were provided in the following files:

Data File Name	Power Level	Voltage
20070613105949	100%	10.0 V
20070429134325	28%	10.0 V

The upper and lower strain gages on main steam line C were not operable when the low power (28% power level) data were taken. As a consequence, the data from main steam line B were placed on main steam line C, and the phasing of the replaced data on main steam line C was varied until the minimum peak PSD on the dryer (from a low resolution load, at node 7) was determined. This process shifted the time signal on main steam line C by 64 time increments from the time signal on main steam line B.

EIC data (taken at 0.01 V) were not recorded when these data were taken; thus, the results shown here have not removed this particular noise component. However, at a later date, Monticello took additional data, including EIC data at comparable power levels:

Data File Name	Power Level	Voltage
20081001162826	100%	0.01 V (EIC)
20080928013040	23%	0.01 V (EIC)

Exclusion frequencies were used to remove extraneous signals from these data as well. The resulting EIC data are compared in Figure 3.2, where it may be seen that the two sets of data are similar at the two power levels examined. This observation is significant, since EIC data was not subtracted from the CLTP and low power data.

The resulting main steam line pressure signals (which do not include EIC subtraction, since EIC data were not taken during data acquisition of the CLTP data) may be represented in two ways, by their minimum and maximum pressure levels, and by their PSDs. Table 3.3 provides the pressure level information, while Figure 3.3 compares the CLTP frequency content at the eight measurement locations compared with the resulting main steam line signals when up to 80% of the low power data is removed from the CLTP data.

Table 3.1. Conversion factors from strain to pressure [5]. Channels are averaged to give the average strain; blank sensors indicate that the sensor was inoperative.

	Strain to Pressure (psid/ μ strain)	Channel Number	Channel Number	Channel Number	Channel Number
MSL A Upper	3.733	1	2	3	4
MSL A Lower	3.603	5	6	7	8
MSL B Upper	3.604	9	10	11	12
MSL B Lower	3.616	13	14	15	16
MSL C Upper	3.485	17	18	19	20
MSL C Lower	3.581	21	22	23	
MSL D Upper	3.541	25	26	27	28
MSL D Lower	3.538	29	30	31	32

Table 3.2. Exclusion frequencies for Monticello strain gage data recorded at 10.0 V, as suggested in [5]. Recirc Pump = recirculation pump.

Frequency Range (Hz)	Exclusion Cause
0.0 – 2.0	Mean
58.5 – 61.5	Line Noise
119.7 – 120.3	Line Noise
179.6 – 180.4	Line Noise
51.2 – 52.3	Recirc Pump B Electrical Single Phase
128.6 – 130.2	Recirc Pump B Speed (5x)
133.8 – 134.2	Recirc Pump A Speed (5x)
154.9 – 155.4	Recirc Pump B Electrical Three Phase
14.0 – 34.0	Pipe Vibration

Table 3.3. Main steam line (MSL) pressure levels in Monticello.

	CLTP Minimum Pressure (psid)	CLTP Maximum Pressure (psid)	CLTP RMS Pressure (psid)
MSL A Upper	-1.85	1.80	0.42
MSL A Lower	-2.27	2.24	0.53
MSL B Upper	-2.03	1.98	0.46
MSL B Lower	-2.60	2.17	0.52
MSL C Upper	-1.88	1.90	0.47
MSL C Lower	-2.42	2.14	0.56
MSL D Upper	-1.61	1.59	0.40
MSL D Lower	-2.46	2.24	0.55

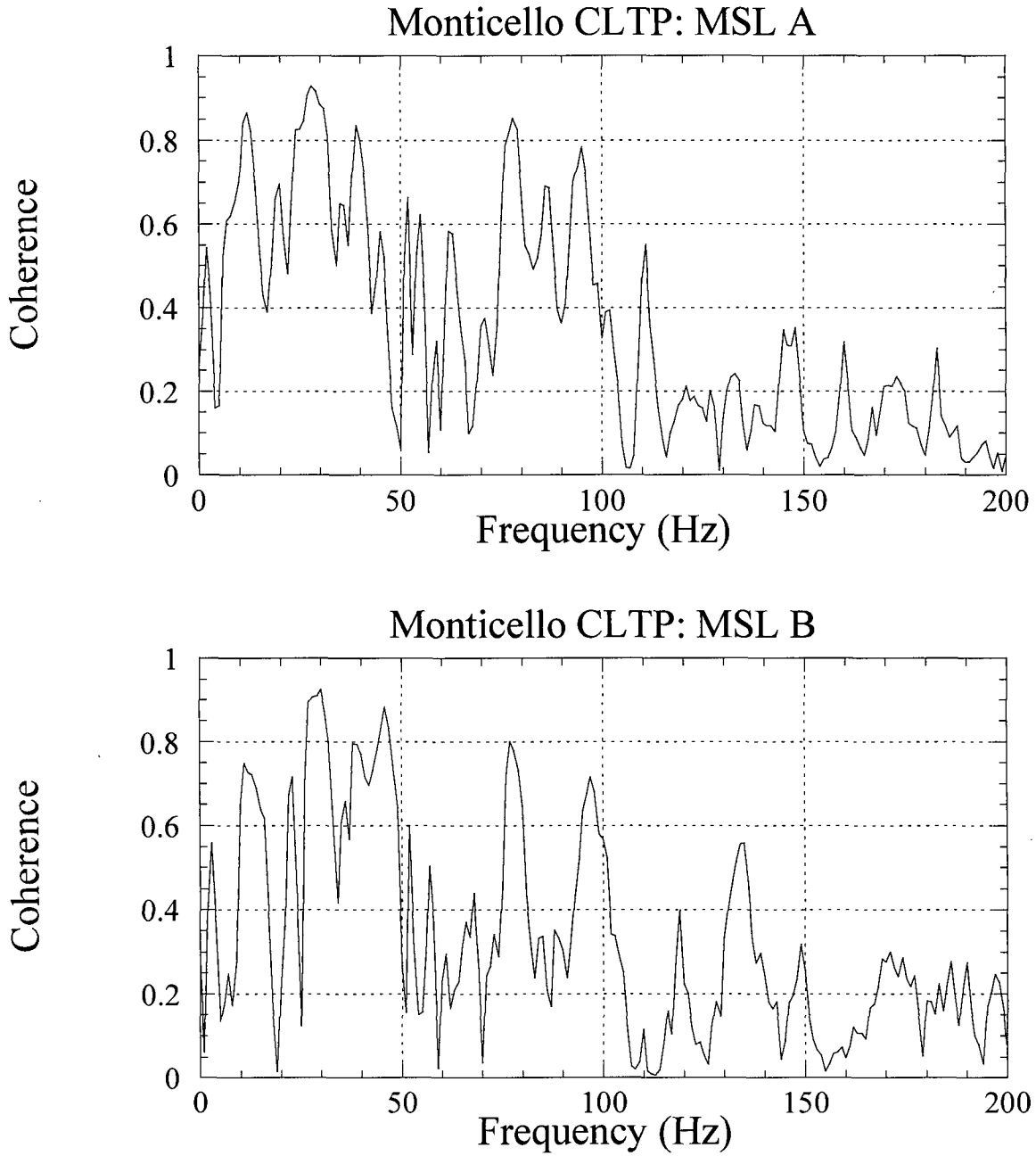


Figure 3.1a. Coherence between the upper and lower strain gage readings at Monticello: main steam line A (top); main steam line B (bottom).

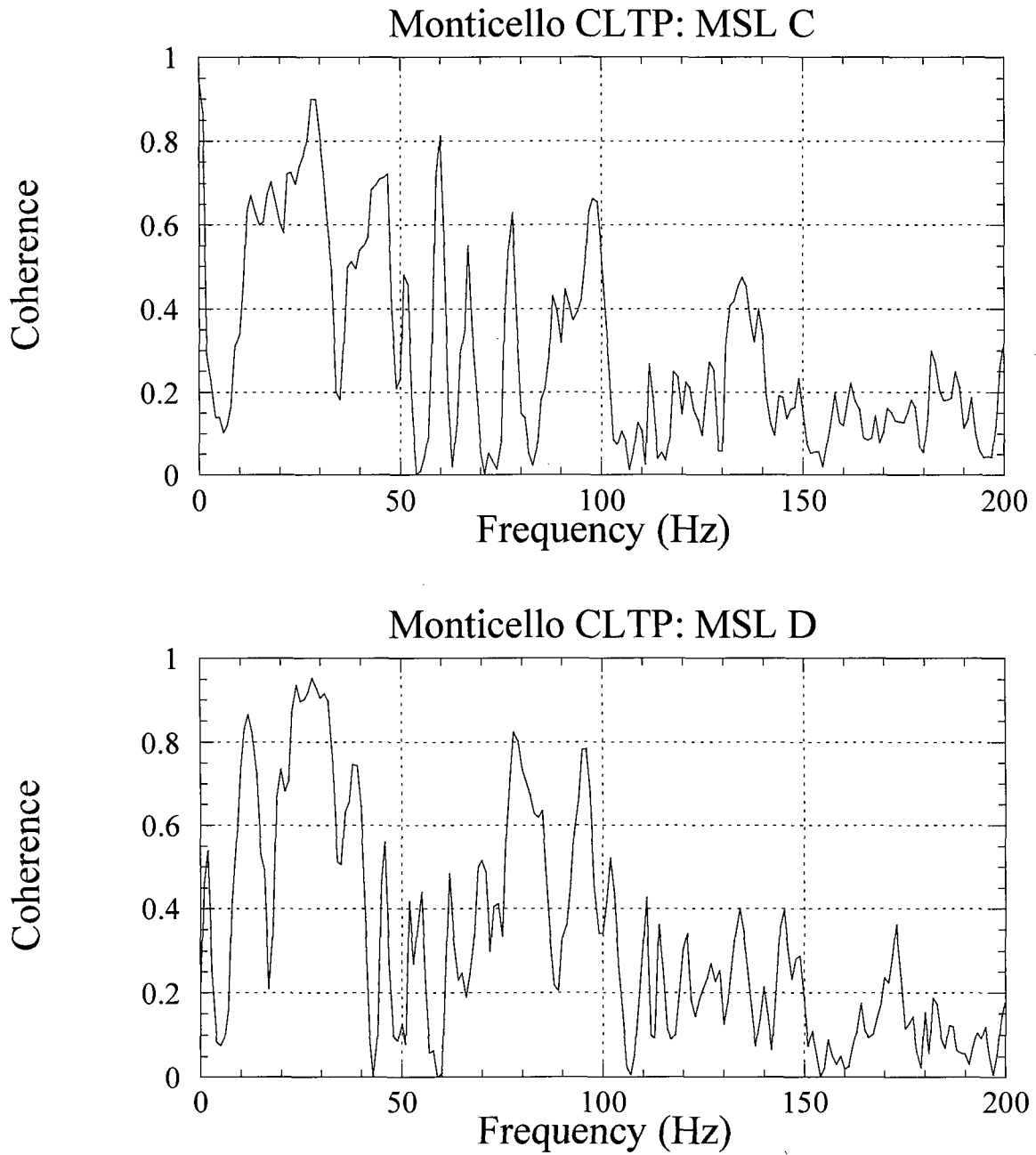


Figure 3.1b. Coherence between the upper and lower strain gage readings at Monticello: main steam line C (top); main steam line D (bottom).

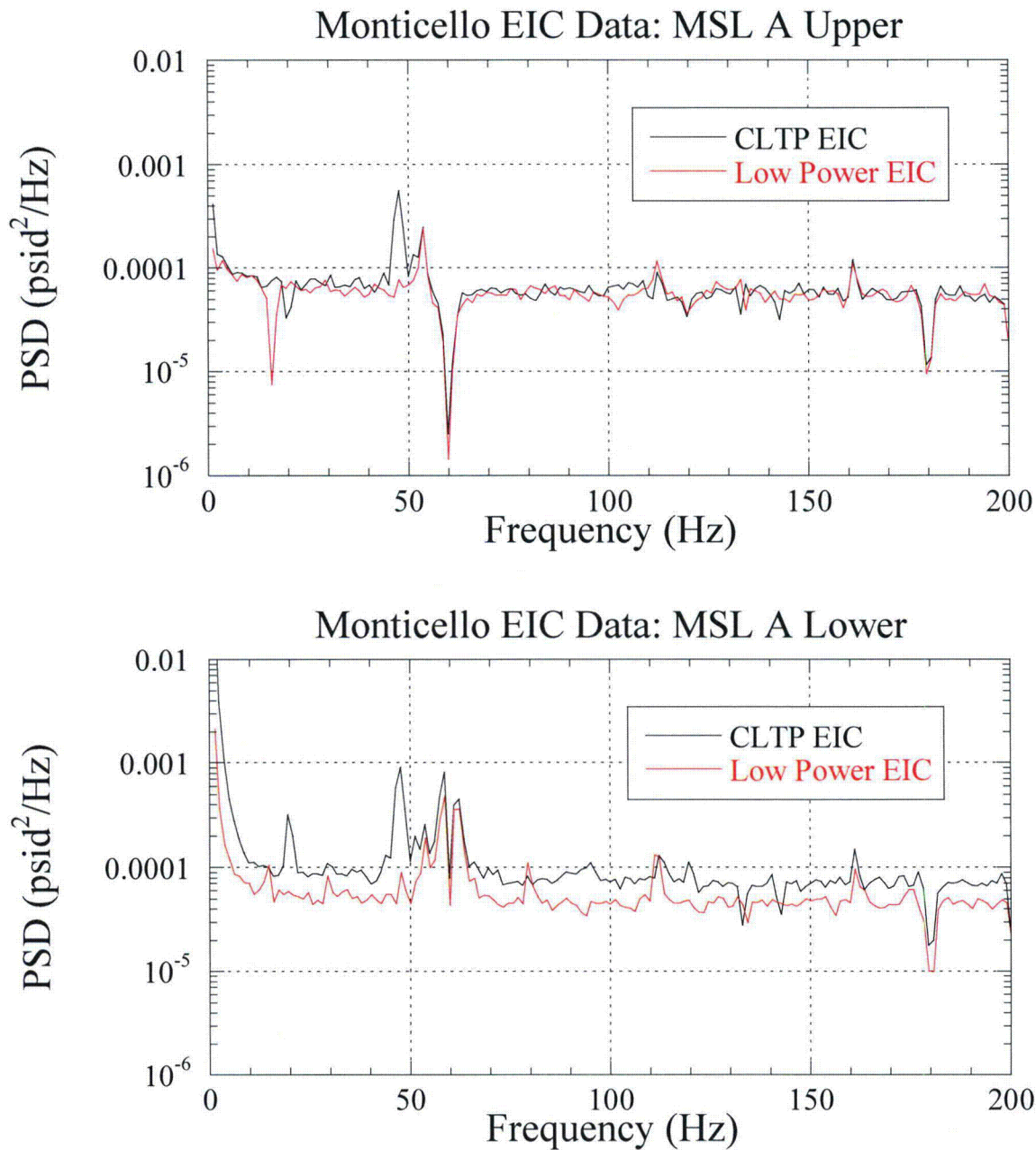


Figure 3.2a. PSD comparison of EIC pressure measurements at strain gage locations on main steam line A Upper (top) and A Lower (bottom).

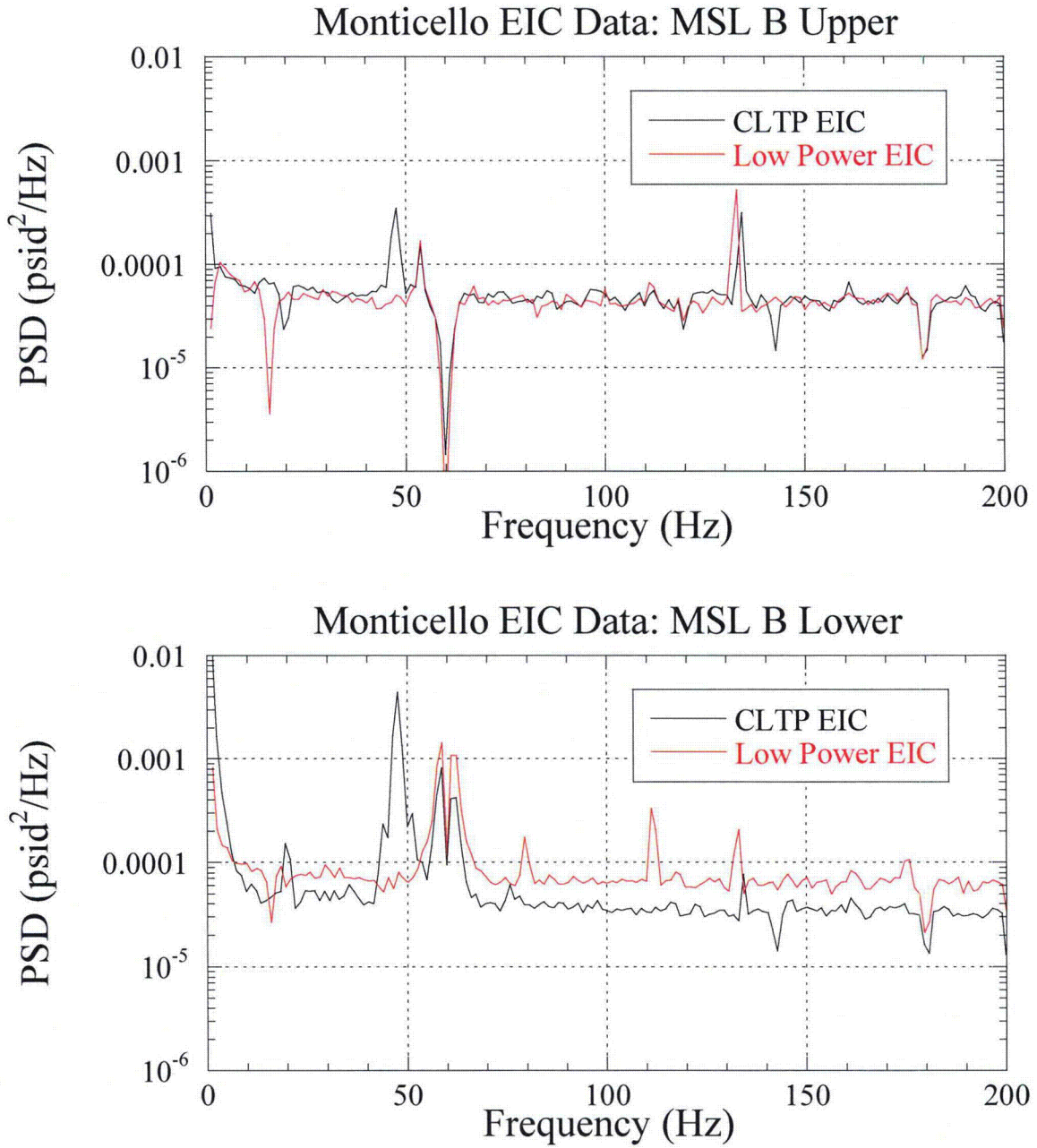


Figure 3.2b. PSD comparison of EIC pressure measurements at strain gage locations on main steam line B Upper (top) and B Lower (bottom).

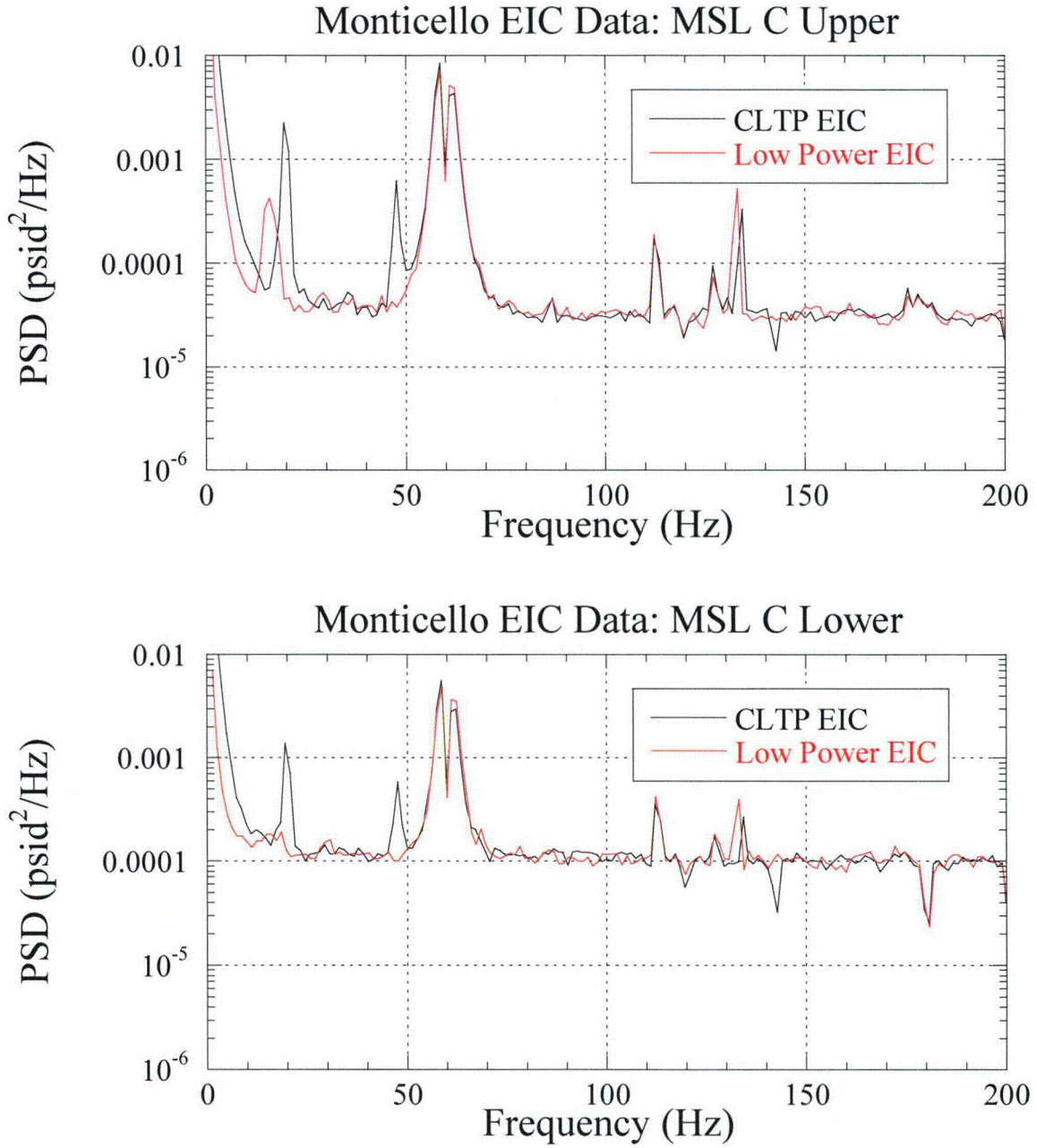


Figure 3.2c. PSD comparison of EIC pressure measurements at strain gage locations on main steam line C Upper (top) and C Lower (bottom).

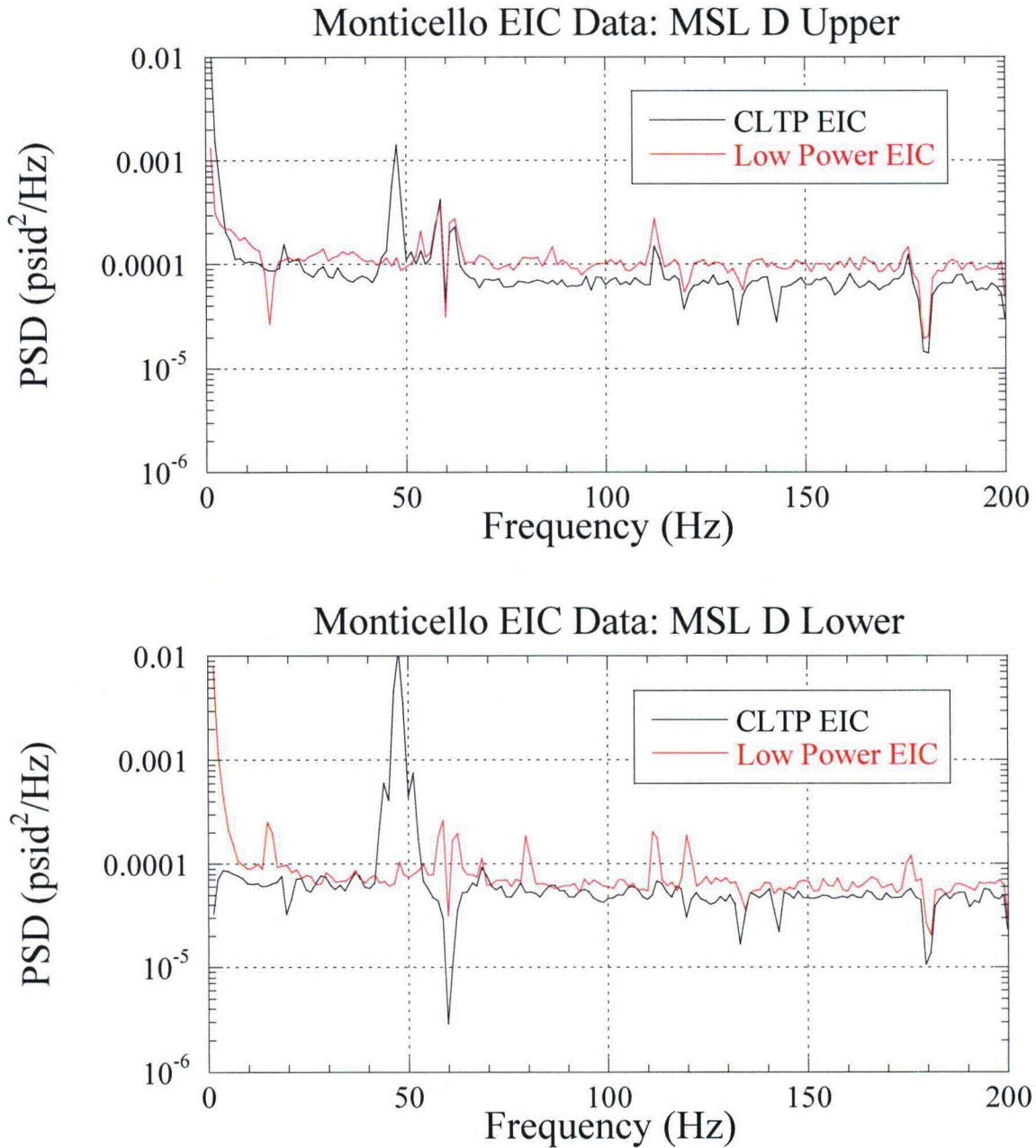


Figure 3.2d. PSD comparison of EIC pressure measurements at strain gage locations on main steam line D Upper (top) and D Lower (bottom).

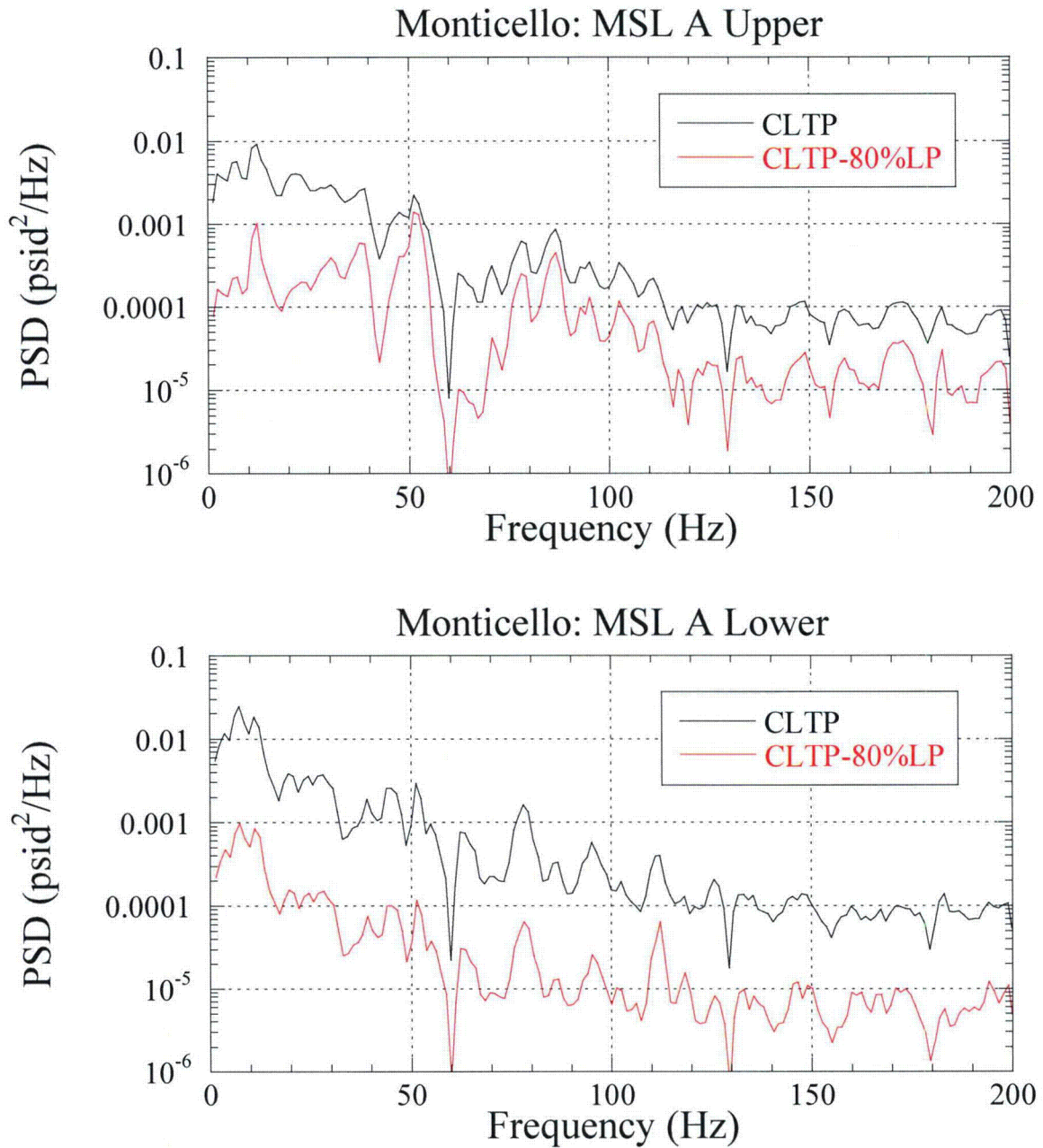


Figure 3.3a. PSD comparison of CLTP and CLTP minus 80% Low Power pressure measurements at strain gage locations on main steam line A Upper (top) and A Lower (bottom).

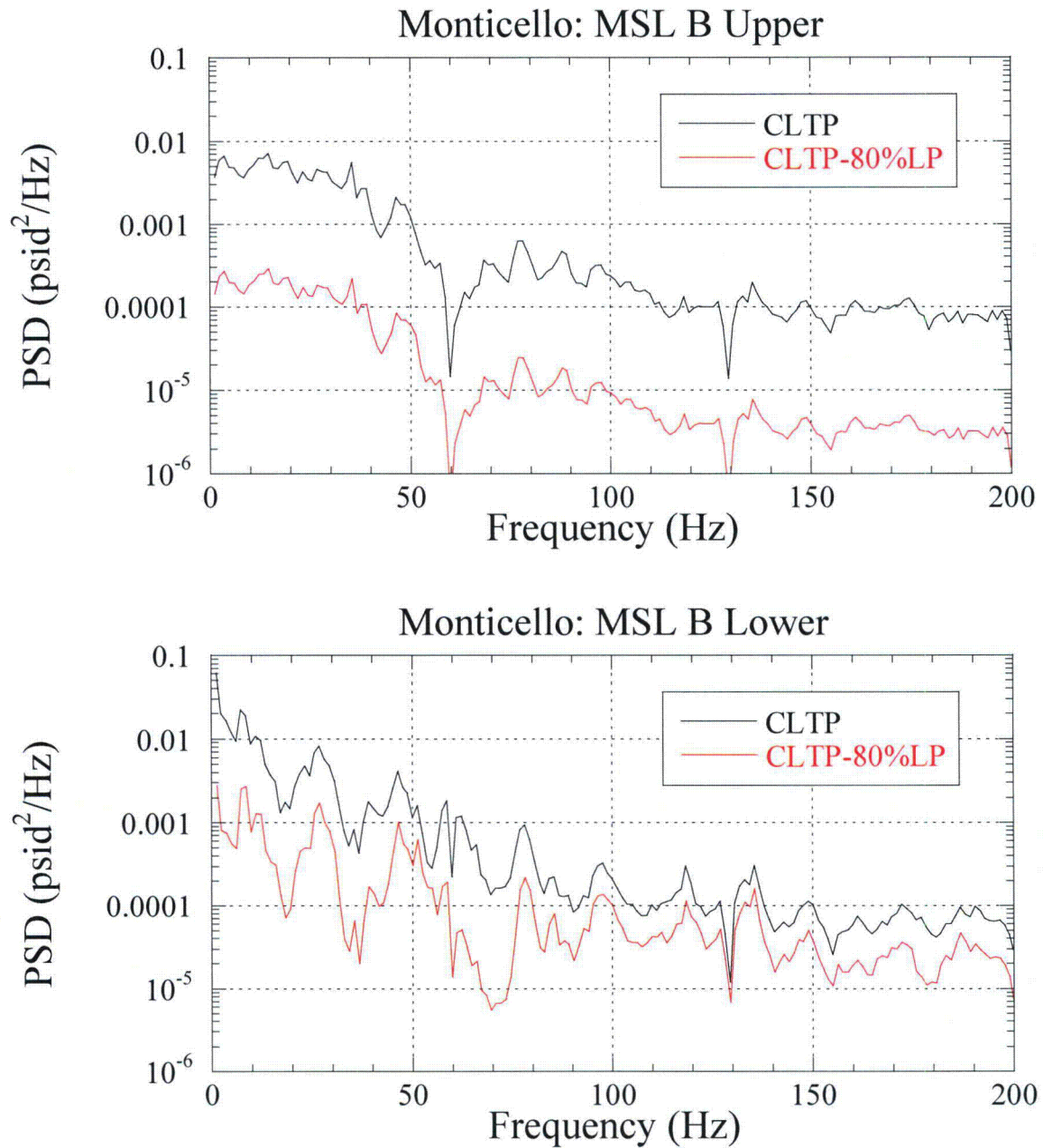


Figure 3.3b. PSD comparison of CLTP and CLTP minus 80% Low Power pressure measurements at strain gage locations on main steam line B Upper (top) and B Lower (bottom).

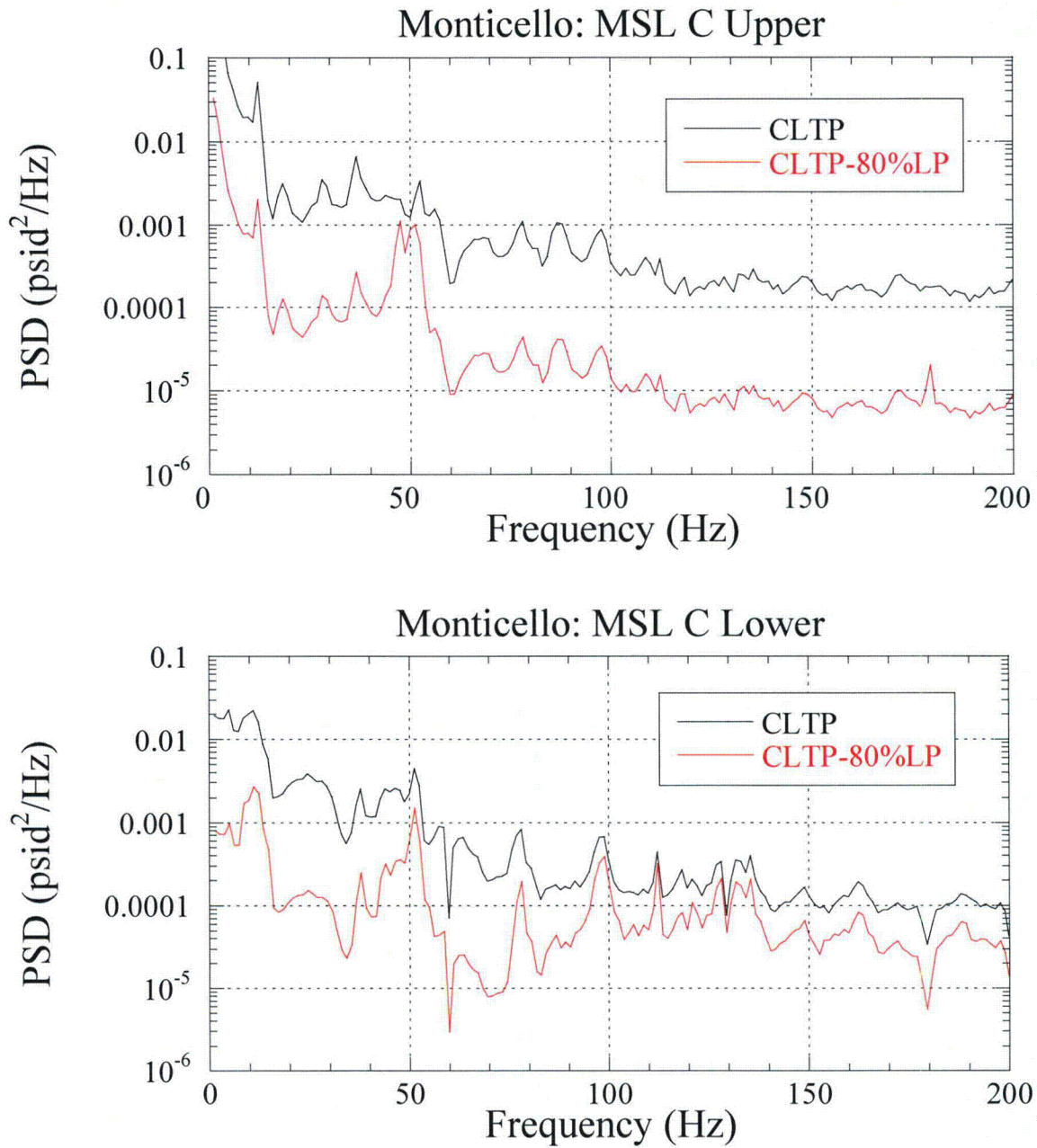


Figure 3.3c. PSD comparison of CLTP and CLTP minus 80% Low Power pressure measurements at strain gage locations on main steam line C Upper (top) and C Lower (bottom).

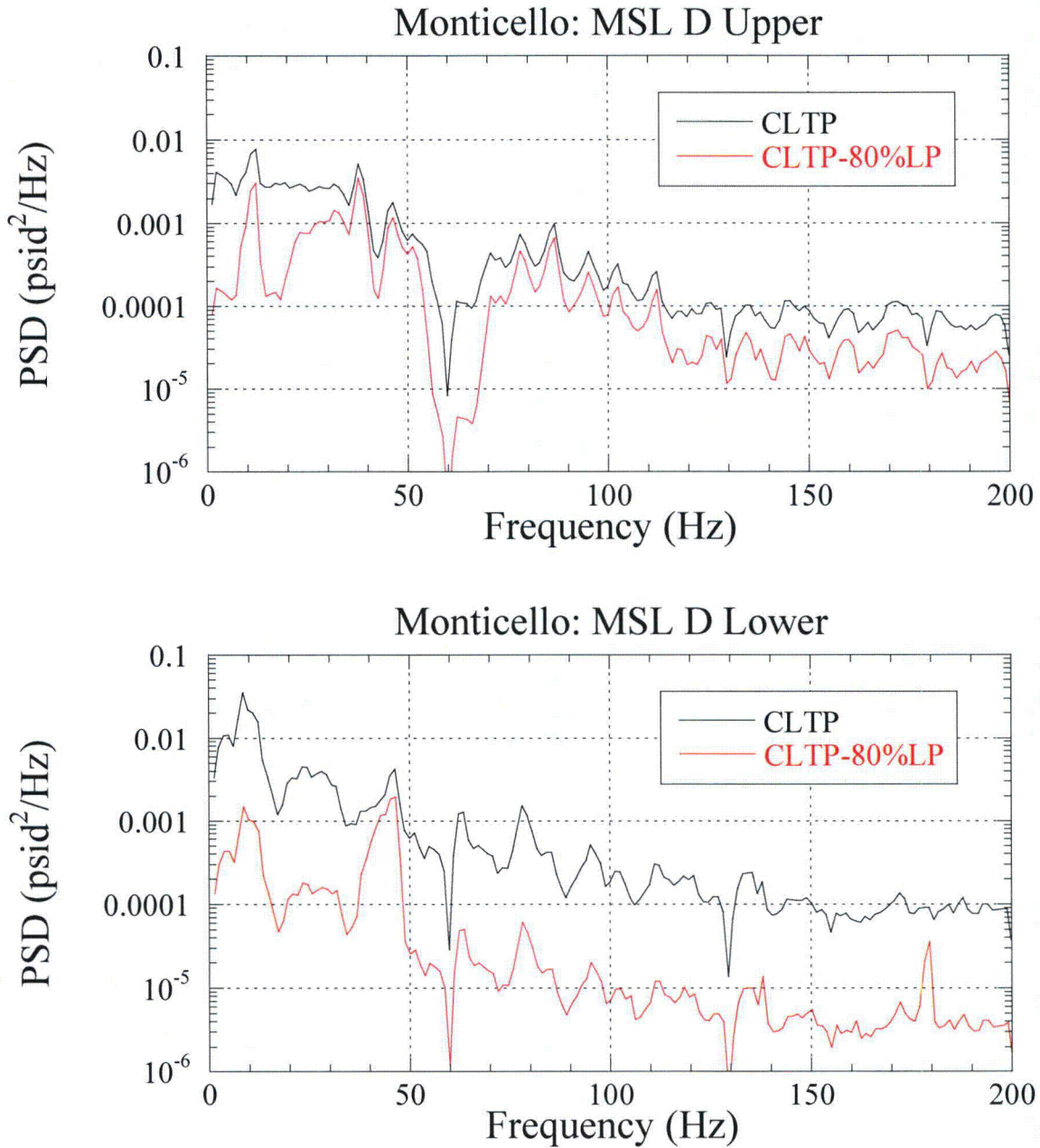


Figure 3.3d. PSD comparison of CLTP and CLTP minus 80% Low Power pressure measurements at strain gage locations on main steam line D Upper (top) and D Lower (bottom).

4. Results

The measured main steam line pressure data were used to drive the validated acoustic circuit methodology for the Monticello steam dome coupled to the main steam lines to make a pressure load prediction on the Monticello dryer. A low resolution CLTP load, developed at the nodal locations identified in Figures 4.1 to 4.4, produces the maximum differential and RMS pressure levels across the dryer as shown in Figure 4.5. PSDs of the peak loads on either side of the dryer are shown in Figure 4.6.

This load was obtained by applying the methodologies in BWRVIP-194 [1], with the exception that EIC data were not subtracted from the CLTP and low power data.

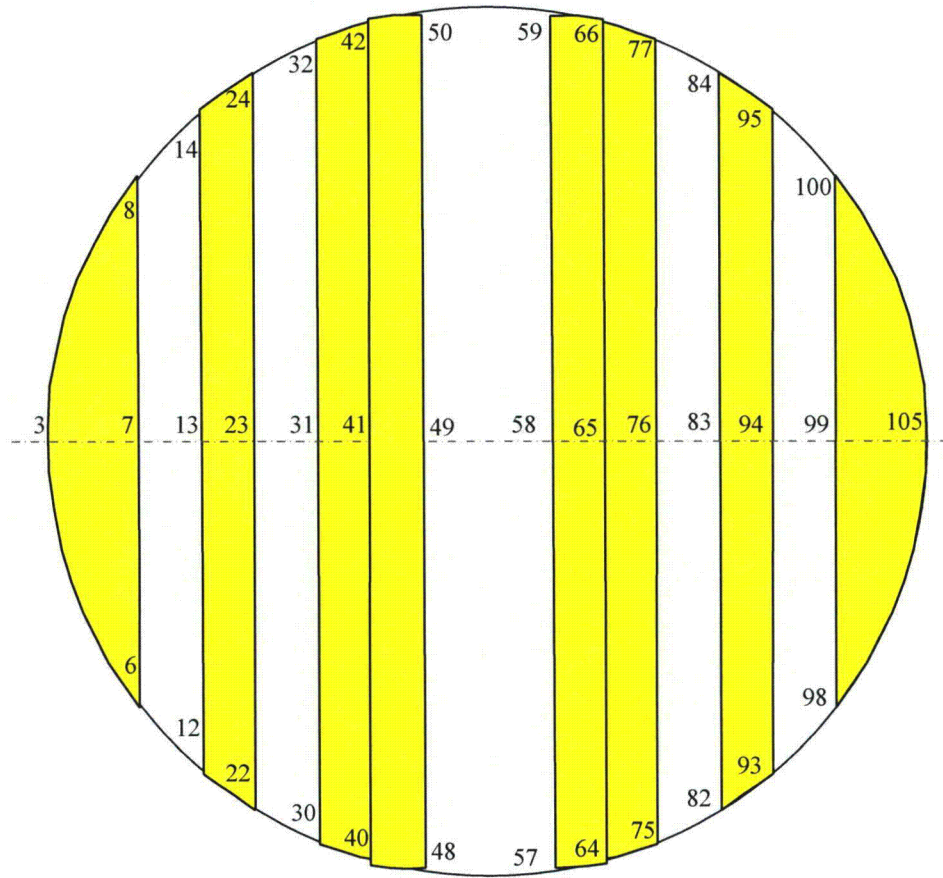


Figure 4.1. Bottom plates pressure node locations on the Monticello dryer, with pressures acting downward in the notation defined here. The high resolution grid mesh is spaced 3 inches on the cover plates, 6 inches on the first bottom plates, and 12 inches on the rest of the bottom plates.

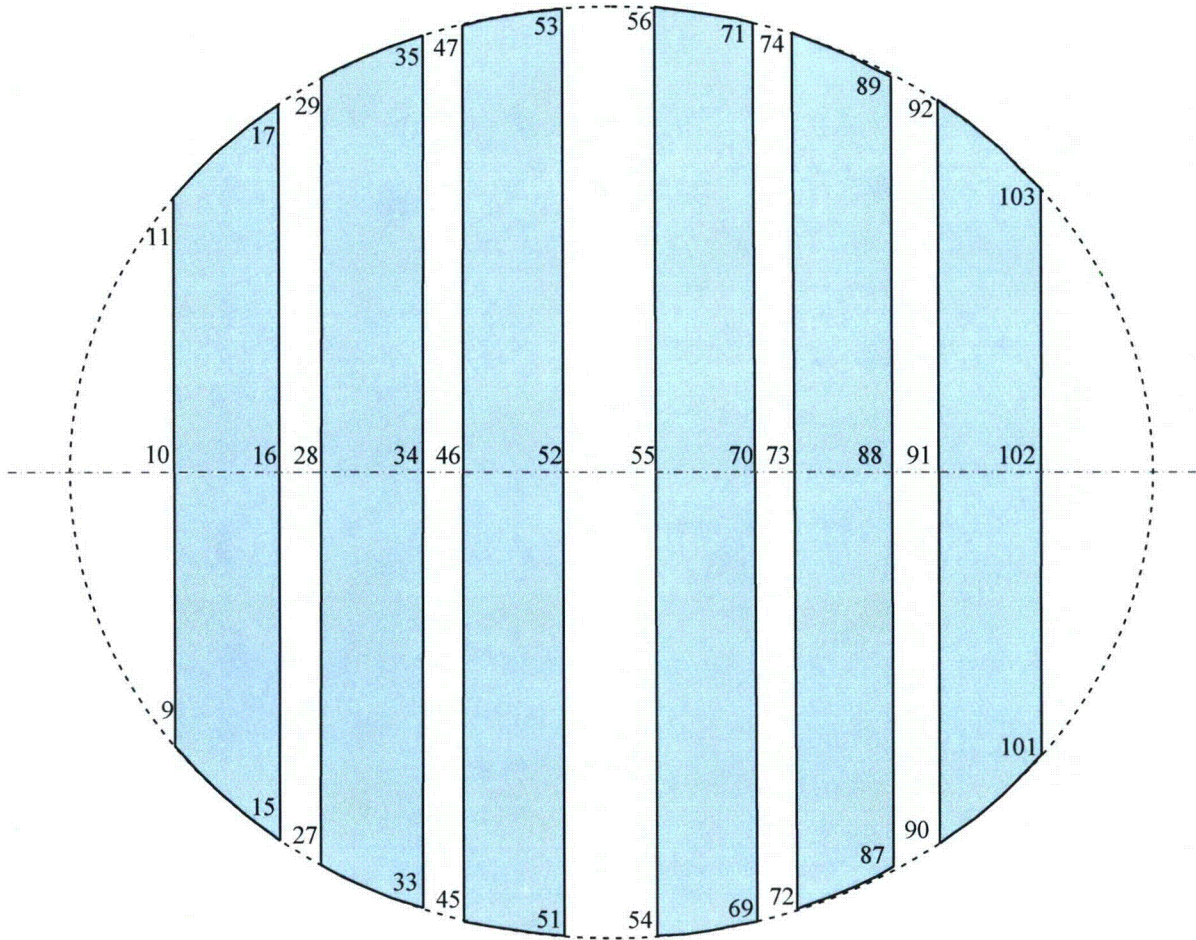


Figure 4.2. Upper plates pressure node locations on the Monticello dryer, with pressures acting downward in the notation defined here. The high resolution grid mesh is spaced 3 inches on the outer top plates, 6 inches on the first inner top plates, and 12 inches on the rest of the inner top plates.

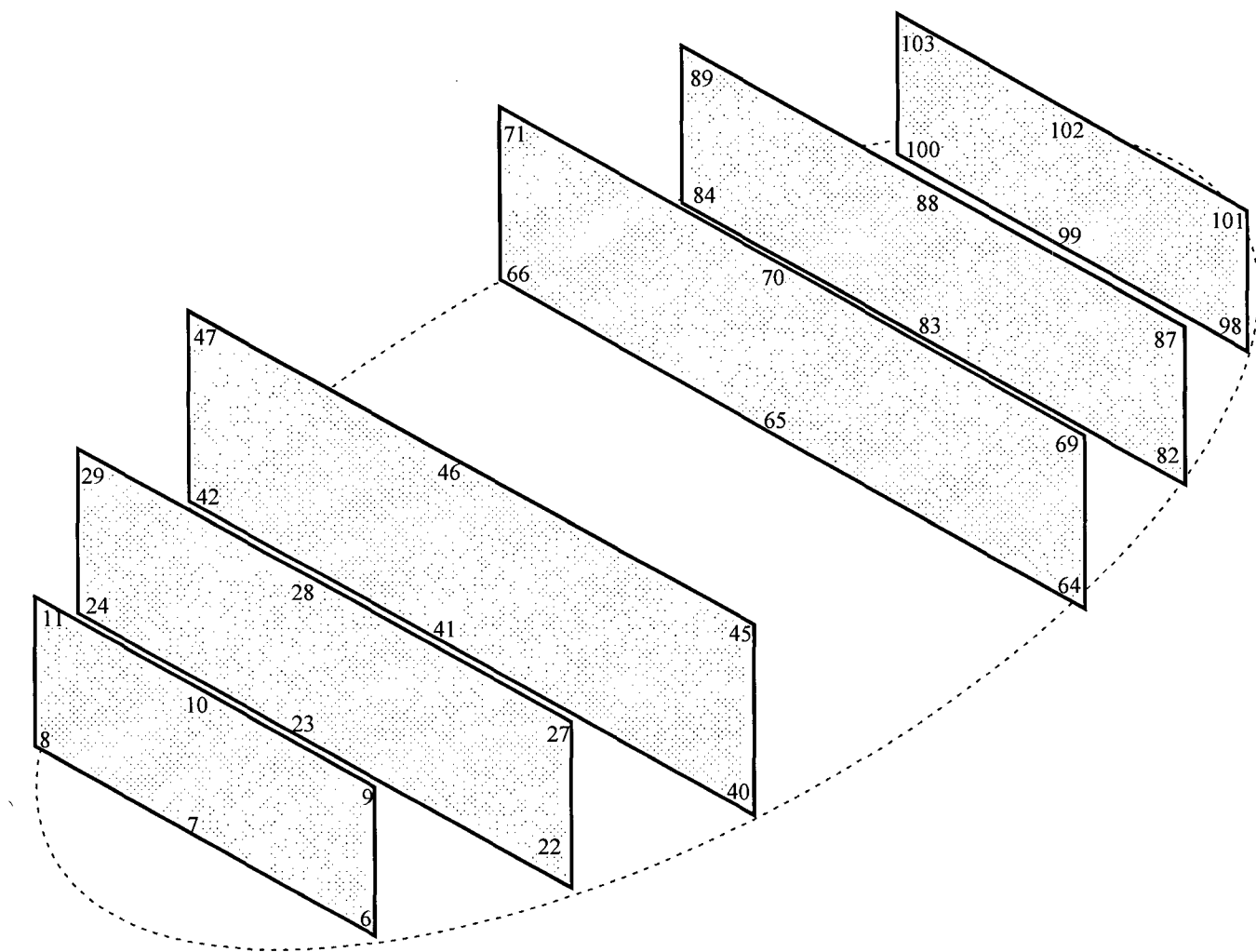


Figure 4.3. Vertical plates on the Monticello dryer: Pressures acting left to right on panels 6-11, 22-29, and 40-47, and acting right to left on panels 64-71, 82-89, and 98-103. The high resolution grid mesh is spaced 3 inches on the outer bank hoods, 6 inches on the first inside hoods, and 12 inches on the inside hoods.

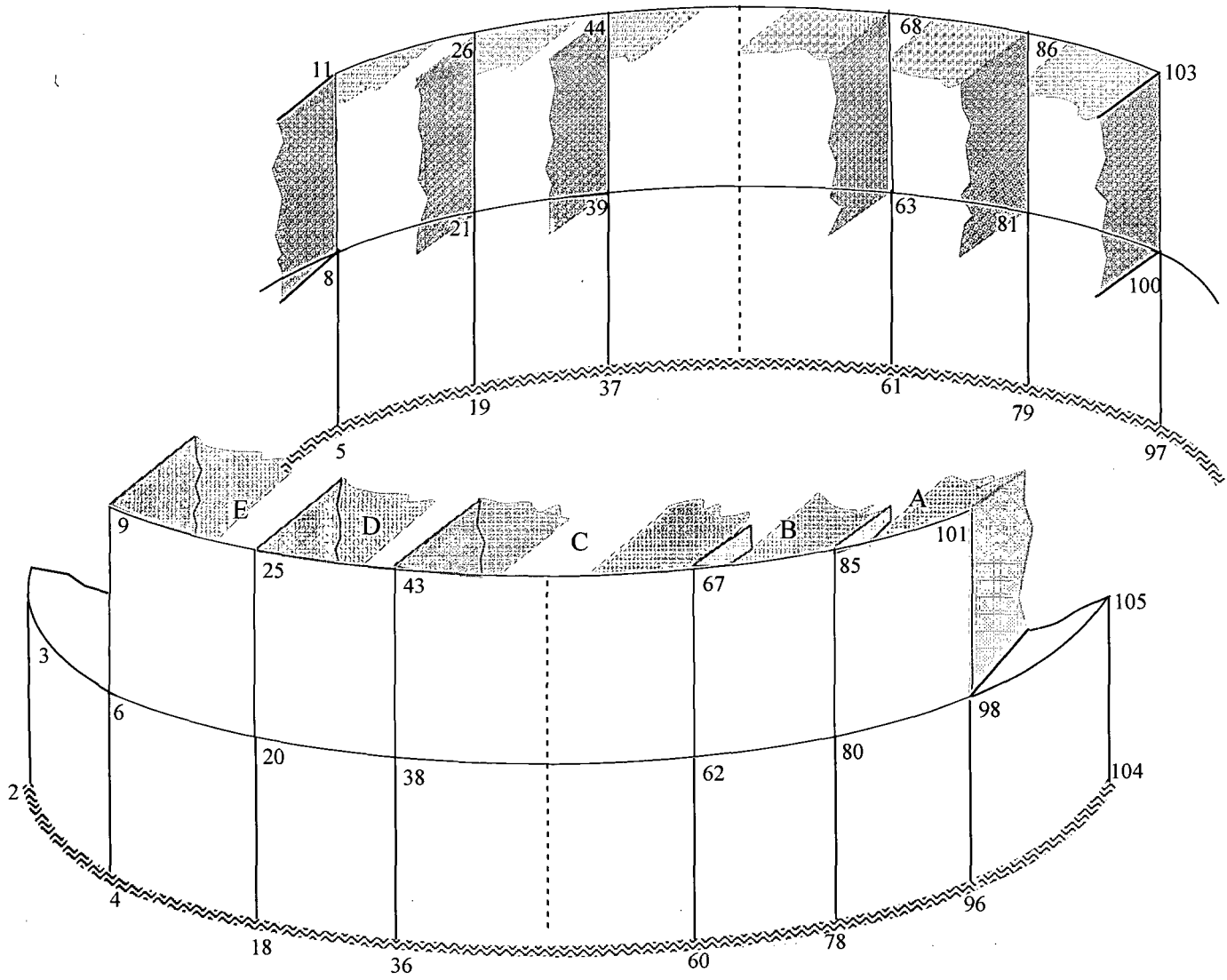


Figure 4.4. Skirt plates on the Monticello dryer: Pressure acting from the outside of the dryer to the inside. The high-resolution grid mesh is spaced 3 inches on the outer portion of the skirt closest to the main steam lines, 6 inches on the sections nearer the center of the dryer, and 12 inches on the center of the dryer.

[[

Figure 4.5. Predicted loads on the low resolution grid identified in Figures 4.1 to 4.4, as developed by the Modified Bounding Pressure model, to 200 Hz. Low-numbered nodes are on the C-D side of the dryer, while high-numbered nodes are on the A-B side of the dryer. ⁽³⁾]]

[[

Figure 4.6. PSD of the maximum pressure loads predicted on the C/D side of the Monticello dryer (top) and the A/B side (bottom).⁽³⁾]]

5. Uncertainty Analysis

The analysis of potential uncertainty occurring at Monticello consists of several contributions, including the uncertainty from collecting data on the main steam lines at locations other than the locations on Quad Cities Unit 2 (QC2) and the uncertainty in the Modified Bounding Pressure model. QC2 dryer data at Original Licensed Thermal Power (OLTP) conditions were used to generate an uncertainty analysis of the Acoustic Circuit Methodology (ACM) [3] for Monticello.

The approach taken for bias and uncertainty is similar to that used by Vermont Yankee for power uprate [7]. In this analysis, six “averaged pressures” are examined on the instrumented replacement dryer at QC2: averaging pressure sensors P1, P2, and P3; P4, P5, and P6; P7, P8, and P9; P10, P11, and P12; P18 and P20; and P19 and P21. These pressure sensors were all on the outer bank hoods of the dryer, and the groups are comprised of sensors located vertically above or below each other.

Bias is computed by taking the difference between the measured and predicted RMS pressure values for the six “averaged pressures”, and dividing the mean of this difference by the mean of the predicted RMS. RMS is computed by integrating the PSD across the frequency range of interest and taking the square root

$$\text{BIAS} = \frac{\frac{1}{N} \sum (\text{RMS}_{\text{measured}} - \text{RMS}_{\text{predicted}})}{\frac{1}{N} \sum \text{RMS}_{\text{predicted}}} \quad (5.1)$$

where $\text{RMS}_{\text{measured}}$ is the RMS of the measured data and $\text{RMS}_{\text{predicted}}$ is the RMS of the predicted data. Summations are over the number of “averaged pressures”, or $N = 6$.

Uncertainty is defined as the fraction computed by the standard deviation

$$\text{UNCERTAINTY} = \frac{\sqrt{\frac{1}{N} \sum (\text{RMS}_{\text{measured}} - \text{RMS}_{\text{predicted}})^2}}{\frac{1}{N} \sum \text{RMS}_{\text{predicted}}} \quad (5.2)$$

ACM bias and uncertainty results are compiled for specified frequency ranges of interest, as directed by [8] and summarized in Table 5.1. Other random uncertainties, specific to Monticello, are summarized in Table 5.2 and are typically combined with the ACM results by SRSS methods to determine an overall uncertainty for Monticello.

Table 5.1. Monticello bias and uncertainty for specified frequency intervals. A negative bias indicates that the ACM overpredicts the QC2 data in that interval.

[[

Table 5.2. Bias and uncertainty contributions to total uncertainty for Monticello plant data. ⁽³⁾]]

[[

|

⁽³⁾]]

6. Conclusions

The C.D.I. acoustic circuit analysis, using full-scale measured data for Monticello:

- a) [[(3)]]
- b) Predicts that the loads on dryer components are largest for components nearest the main steam line inlets and decrease inward into the reactor vessel.

7. References

1. BWRVIP-194: BWR Vessel and Internals Project, Methodologies for Demonstrating Steam Dryer Integrity for Power Uprate. EPRI, Palo Alto, CA, and Continuum Dynamics, Inc., Ewing, NJ: 2008. 1016578.
2. Continuum Dynamics, Inc. 2005. Methodology to Determine Unsteady Pressure Loading on Components in Reactor Steam Domes (Rev. 6). C.D.I. Report No. 04-09 (C.D.I. Proprietary).
3. Continuum Dynamics, Inc. 2007. Bounding Methodology to Predict Full Scale Steam Dryer Loads from In-Plant Measurements, with the Inclusion of a Low Frequency Hydrodynamic Contribution (Rev. 0). C.D.I. Report No. 07-09 (C.D.I. Proprietary).
4. Monticello Drawings. 2007. Information provided in files M00100V2.pdf, NX-7831-359.4.pdf, and an enhanced file detail.pdf from D. Dahlheimer dated 03/23/07.
5. Structural Integrity Associates, Inc. 2007. Monticello Main Steam Line 100% CLTP Strain Data Transmission. SIA Letter Report No. KKF-07-013 with inclusion of Channel 29.
6. J. Ferrante Email Correspondence: "Logic for Declaring Piping Vibrations." 02 February 2008.
7. Communication from Enrico Betti. 2006. Excerpts from Entergy Calculation VYC-3001 (Rev. 3), EPU Steam Dryer Acceptance Criteria, Attachment I: VYNPS Steam Dryer Load Uncertainty (Proprietary).
8. NRC Request for Additional Information on the Hope Creek Generating Station, Extended Power Uprate. 2007. TAC No. MD3002. RAI No. 14.67.
9. Continuum Dynamics, Inc. 2007. Letter Report Documenting Onset Speeds and Frequencies Anticipated for Flow Induced Vibration in Monticello Safety Valve Standpipes. Our Ref. F488/0018 dated 03/28/07.
10. Structural Integrity Associates, Inc. 2007. Evaluation of Monticello Strain Gage Uncertainty and Pressure Conversion (Rev. 0). SIA Calculation Package No. MONT-11Q-302.
11. Continuum Dynamics, Inc. 2005. Vermont Yankee Instrument Position Uncertainty. Letter Report Dated 01 August 2005.
12. Exelon Nuclear Generating LLC. 2005. An Assessment of the Effects of Uncertainty in the Application of Acoustic Circuit Model Predictions to the Calculation of Stresses in the Replacement Quad Cities Units 1 and 2 Steam Dryers (Revision 0). Document No. AM-21005-008.

This Document Does Not Contain Continuum Dynamics, Inc. Proprietary Information

13. Continuum Dynamics, Inc. 2007. Finite Element Modeling Bias and Uncertainty Estimates Derived from the Hope Creek Unit 2 Dryer Shaker Test (Rev. 0). C.D.I. Report No. 07-27 (Proprietary).
14. NRC Request for Additional Information on the Hope Creek Generating Station, Extended Power Uprate. 2007. RAI No. 14.79.
15. NRC Request for Additional Information on the Hope Creek Generating Station, Extended Power Uprate. 2007. RAI No. 14.110.

**Attachment III of
Enclosure 13 to L-MT-08-052**

CDI Report No. 07-26NP:
Stress Assessment of Monticello Steam Dryer,
Revision 2, November 2008

(Non-Proprietary)

Stress Assessment of Monticello Steam Dryer

Revision 2

Prepared by

Continuum Dynamics, Inc.
34 Lexington Avenue
Ewing, NJ 08618

Prepared under Purchase Order No. 13758 for

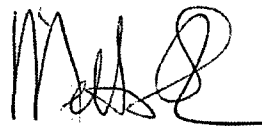
Northern States Power Company, a Minnesota Corporation (NSPM)
Monticello Nuclear Generating plant
2807 W. County Road 75
Monticello, MN 55362-9637

Approved by



Alan J. Bilanin

Reviewed by



Milton E. Teske

November 2008

This report complies with Continuum Dynamics, Inc. Nuclear Quality Assurance Program currently in effect.

Executive Summary

A harmonic finite element stress analysis method is used to assess stresses on the Monticello steam dryer resulting from acoustic and hydrodynamic loads. The harmonic stress analysis confers a number of useful computational advantages over a time-domain method including the ability to assess the effects of frequency scalings in the loads without the need for additional finite element calculations. [[

³⁾]]

The analysis first develops a series of unit stress solutions corresponding to the application of a unit pressure at a MSL at specified frequency, f . Each unit solution is obtained by calculating the associated acoustic pressure field using a separate analysis that solves the damped Helmholtz equation within the steam dryer [1]. This pressure field is then applied to a finite element structural model of the steam dryer and the stress response at frequency, f , calculated using the commercial ANSYS 10.0 finite element analysis software. This stress response constitutes the unit solution stress and is stored as a file for subsequent processing. Once all unit solutions have been computed, the stress response for any combination of MSL pressure spectrums (obtained by Fast Fourier Transform of the pressure histories in the MSLs) is determined by a simple matrix multiplication of these spectrums with the unit solutions.

This report provides details of the ANSYS 10.0 finite element structural model of the Monticello steam dryer and reviews pertinent modeling considerations. It also summarizes the framework underlying the development and application of unit solutions in the frequency domain and shows how these solutions are used to develop stress histories for general load conditions. Next, it reviews the assessment of these stresses for compliance with the ASME B&PV Code, Section III, subsection NG [2], for the load combination corresponding to normal operation (the Level A Service Condition).

Results obtained from application of the methodology to the Monticello steam dryer using the Rev. 4 acoustic/hydrodynamic loads [3] show that at nominal (no frequency shift) CLTP operation the smallest alternating stress ratio (SR-a) anywhere on the steam dryer is $SR-a=3.74$ and occurs on the outer hood/cover plate junction. These results account for all the end-to-end biases and uncertainties in the loads model [3,4] and finite element analysis. To account for uncertainties in the modal frequency predictions of the finite element model, the stresses are also computed for loads that are shifted in the frequency domain by $\pm 2.5\%$, $\pm 5\%$, $\pm 7.5\%$ and $\pm 10\%$. The minimum alternating stress ratio encountered at any frequency shift is found to be $SR-a=3.02$ occurring at the $+10\%$ shift. The stress ratio due to maximum stresses (SR-P) is $SR-P=2.89$ without frequency shifts and $SR-P=2.50$ when frequency shifts are considered.

The alternating stress ratios at EPU operation are obtained in two ways. The first scales the CLTP values by the steam flow velocity squared, $(U_{EPU}/U_{CLTP})^2=1.32$. Under this approach, the limiting alternating stress ratio becomes $SR-a=3.02/1.32=2.29$. The second approach [[

³⁾]]

resonance may occur. Outside this frequency range the CLTP signals are increased by the steam [[³⁾]] The limiting alternating stress ratios obtained using this second approach are SR-a=2.81 at zero frequency shift and 2.28 when all frequency shifts are considered. The limiting maximum stress intensity at any frequency shift for EPU is SR-P=2.03.

This Document Does Not Contain Continuum Dynamics, Inc. Proprietary Information

Summary of Changes from Revision 1 to Revision 2

Revision 2 of C.D.I. Report 07-26P differs from the previous Revision 1 in that minor editing changes and corrections of typos have been made. These are indicated in the text.

Table of Contents

Section	Page
Executive Summary	ii
Summary of Changes from Revision 1 to Revision 2.....	iv
Table of Contents	v
1. Introduction and Purpose	1
2. Methodology	3
2.1 Overview.....	3
[[⁽³⁾]]	5
2.3 Computational Considerations.....	6
3. Finite Element Model Description.....	9
3.1 Steam Dryer Geometry	9
3.2 Material Properties.....	10
3.3 Model Simplifications.....	10
3.4 Vane Bank Model	11
3.5 Water Inertia Effect on Submerged Panels.....	13
3.6 Structural Damping.....	13
3.7 Mesh Details and Element Types	14
3.8 Connections Between Structural Components.....	14
3.9 Pressure Loading.....	22
4. Structural Analysis.....	24
4.1 Static Analysis	24
4.2 Harmonic Analysis.....	24
4.3 Post-Processing	28
4.4 Computation of Stress Ratios for Structural Assessment	28
4.5 Submodeling	31
5. Results.....	32
5.1 General Stress Distribution and High Stress Locations.....	33
5.2 Load Combinations and Allowable Stress Intensities	45
5.3 Frequency Content and Sensitivity to Frequency Shift of the Stress Signals.....	58
[[⁽³⁾]]	66
6. Conclusions.....	76
7. References.....	78

1. Introduction and Purpose

Plans to qualify the Monticello nuclear plant for operation at Extended Power Uprate (EPU) operating condition require an assessment of the steam dryer stresses experienced under the increased loads. The steam dryer loads due to pressure fluctuations in the main steam lines (MSLs) are potentially damaging and the cyclic stresses from these loads can produce fatigue cracking if loads are sufficiently high. The industry has addressed this problem with physical modifications to the dryers, as well as a program to define steam dryer loads and their resulting stresses.

The purpose of the stress analysis discussed here is to calculate the maximum and alternating stresses generated during Current Licensed Thermal Power (CLTP) and EPU and determine the margins that exist when compared to stresses that comply with subsection NG of the ASME Code [2]. This step establishes whether the current dryer is adequately designed for sustaining structural integrity and preventing future weld cracking under planned EPU operating conditions. The load combination considered here corresponds to normal operation (the Level A Service Condition) and includes fluctuating pressure loads developed from Monticello main steam line data, and steam dryer weight. The fluctuating pressure loads, induced by the flowing steam, are predicted using a separate acoustic circuit analysis of the steam dome and main steam lines [6]. Level B service conditions, which include seismic loads, are not included in this evaluation since no physical modifications were made to the Monticello steam dryer for EPU operation.

[[

(3)]]

This report describes the overall methodology used to obtain the unit solutions in the frequency domain and how to assemble them into a stress response for a given combination of pressure signals in the MSLs. This is followed by details of the Monticello steam dryer finite element model including the elements used and overall resolution, treatment of connections between elements, the hydrodynamic model, the implementation of structural damping and key idealizations/assumptions inherent to the model. Post-processing procedures are also reviewed including the computation of maximum and alternating stress intensities, identification of high stress locations, adjustments to stress intensities at welds, and evaluation of stress ratios used to establish compliance with the ASME Code [2].

The results for Rev.4 acoustic/hydrodynamic loads [3] in terms of stress intensity distributions and stress ratios are presented next, together with accumulative PSDs of the dominant stress components. The latter show that the structural response is dominated by components in the 24-26 Hz and 149-151 Hz frequency ranges.

2. Methodology

2.1 Overview

Based on previous analysis undertaken at Quad Cities Units 1 and 2, the steam dryer can experience strong acoustic loads due to the fluctuating pressures in the MSLs connected to the steam dome containing the dryer. C.D.I. has developed an acoustic circuit model (ACM) that, given a collection of strain gauge measurements [7] of the fluctuating pressures in the MSLs, predicts the acoustic pressure field anywhere inside the steam dome and on the steam dryer [1,3,6]. The ACM is formulated in frequency space and contains two major components that are directly relevant to the ensuing stress analysis of concern here. [[

(1)

(2)

(3)]]

[[

(3)

(4)

(5)

⁽³⁾]]

[[

(6)

⁽³⁾]]

[[
[[

⁽³⁾]]

⁽³⁾]]

2.3 Computational Considerations

Focusing on the structural computational aspects of the overall approach, there are a number of numerical and computational considerations requiring attention. The first concerns the transfer of the acoustic forces onto the structure, particularly the spatial and frequency resolutions. The ANSYS finite element program inputs general distributed pressure differences using a table format. This consists of regular 3D rectangular (i.e., block) $n_x \times n_y \times n_z$ mesh where n_α is the number of mesh points in the α -th Cartesian direction and the pressure difference is provided at each mesh point (see Section 3.9). These tables are generated separately using a program that reads the loads provided from the ACM software, distributes these loads onto the finite element mesh using a combination of interpolation procedures on the surface and simple diffusion schemes off the surface (off-surface loads are required by ANSYS to ensure proper interpolation of forces), and written to ASCII files for input to ANSYS. A separate load file is written at each frequency for the real and imaginary component of the complex force.

The acoustic field is stored at 5 Hz intervals from 0 to 200 Hz. While a 5 Hz resolution is sufficient to capture frequency dependence of the acoustic field (i.e., the pressure at a point varies gradually with frequency), it is too coarse for representing the structural response especially at low frequencies. For 1% critical structural damping, one can show (as indicated in the design record file, DRF-CDI-174) that the frequency spacing needed to resolve a damped resonant peak at natural frequency, f_n , to within 5% accuracy is $\Delta f = 0.0064 \times f_n$. Thus for $f_n = 10$ Hz where the lowest structural response modes occur, a frequency interval of 0.064 Hz or less is required. In the calculations it is required that 5% maximum error be maintained over the range from $f_n = 5$ Hz to 200 Hz resulting in a finest frequency interval of 0.0321 Hz at the low frequency end (this adequately resolves all structural modes up to 200 Hz). Since there are no structural modes between 0 to 5 Hz, a 0.5 Hz spacing is used over this range with minimal (less than 5%) error. The unit load, $\hat{f}_n(\omega, \mathbf{R})$, at any frequency, ω_k , is obtained by linear interpolation of the acoustic solutions at the two nearest frequencies, ω_i and ω_{i+1} , spaced 5 Hz apart. Linear interpolation is sufficient since the pressure load varies slowly over each 5 Hz interval (linear interpolation of the structural response over these 5 Hz intervals would not be acceptable since it varies much more rapidly over these intervals).

[[

(3)]]

[[

(3)]]

Structural Damping

In harmonic analysis one has a broader selection of damping models than in transient simulations. A damping factor, z , of 1% critical damping is used in the structural analysis. In transient simulations, this damping can only be enforced exactly at two frequencies (where the damping model is "pinned"). Between these two frequencies the damping factor can be considerably smaller, for example 0.5% or less depending on the pinning frequencies. Outside the pinning frequencies, damping is higher. With harmonic analysis it is straightforward to enforce very close to 1% damping over the entire frequency range. In this damping model, the damping matrix, \mathbf{D} , is set to

$$\mathbf{D} = \frac{2z}{\omega} \mathbf{K} \quad (7)$$

where \mathbf{K} is the stiffness matrix and ω the forcing frequency. One can show that with this model the damping factor varies between 0.995% and 1.005% which is a much smaller variation than using the pinned model required in transient simulation.

Load Frequency Rescaling

As indicated above, one way to evaluate the sensitivity of the stress results to approximations in the structural modeling and applied loads is to rescale the frequency content of the applied loads. In this procedure the nominal frequencies, ω_k , are shifted to $(1+\lambda)\omega_k$, where the frequency shift, λ , ranges between $\pm 10\%$, and the response recomputed for the shifted loads. The objective of the frequency shifting can be explained by way of example. Suppose that in the actual dryer a strong structural-acoustic coupling exists at a particular frequency, ω^* . This means that the following conditions hold simultaneously: (i) the acoustic signal contains a significant signal at ω^* ; (ii) the structural model contains a resonant mode of natural frequency, ω_n , that is near ω^* ; and (iii) the associated structural mode shape is strongly coupled to the acoustic load (i.e., integrating the product of the mode shape and the surface pressure over the steam dryer surface produces a significant modal force). Suppose now that because of discretization errors and modeling idealizations that the predicted resonance frequency differs from ω^* by a small amount (e.g., 1.5%). Then condition (ii) will be violated and the response amplitude therefore significantly diminished. By shifting the load frequencies one re-establishes condition (ii) when $(1+\lambda)\omega^*$ is near ω_n . The other two requirements also hold and a strong structural acoustic interaction is restored.

[[

(3)]]

Evaluation of Maximum and Alternating Stress Intensities

Once the unit solutions have been obtained, the most intensive computational steps in the generation of stress intensities are: (i) the FFTs to evaluate stress time histories from (5); and (ii) the calculation of alternating stress intensities. [[

(3)]]

The high computational penalty incurred in calculating the alternating stress intensities is due to the fact that this calculation involves comparing the stress tensors at every pair of points in the stress history. This comparison is necessary since in general the principal stress directions can vary during the response, thus for N samples in the stress history, there will be $(N-1)N/2$ such pairs or, for $N=64K$ (the number required to accurately resolve the spectrum up to 200 Hz in 0.01 Hz intervals), 2.1×10^9 calculations per node each requiring the determination of the roots to a cubic polynomial. [[

(3)]]

3. Finite Element Model Description

A description of the ANSYS model of the Monticello steam dryer follows.

3.1 Steam Dryer Geometry

A geometric representation of the Monticello steam dryer was developed from available drawings (provided by the Nuclear Xcel Energy and included in the design record file DRF-MONT-244B) within the Workbench module of ANSYS. The completed model is shown in Figure 1.

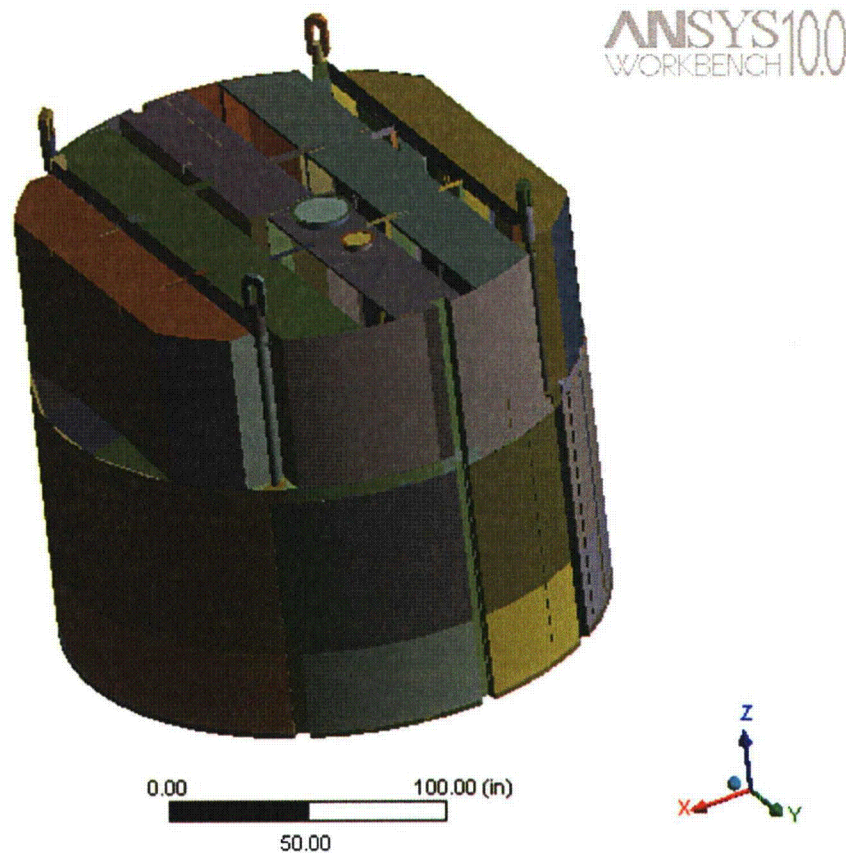


Figure 1. Overall geometry of the Monticello steam dryer model.

3.2 Material Properties

The steam dryer is constructed from Type 304 stainless steel and has an operating temperature of 550°F. Properties used in the analysis are summarized below in Table 1.

Table 1. Material properties.

	Young's Modulus (10 ⁶ psi)	Density (lbm/in ³)	Poisson's Ratio
stainless steel	25.55	0.284	0.3
structural steel with added water inertia	25.55	2.722	0.3

The structural steel modulus for Type 304 Stainless Steel at an operating temperature of 550°F is taken from Table I-6.0 in Appendix I of the ASME Code [12]. The density of steel is taken from pg. 6-44 of [13]. The effective properties of submerged parts are discussed in Section 3.5. Note that the increased effective density for submerged components is only used in the harmonic analysis. When calculating the stress distribution due to the static dead weight load, the unmodified density of steel (0.284 lbm/in³) is used throughout.

3.3 Model Simplifications

The following simplifications were made to achieve reasonable model size while maintaining good modeling fidelity for key structural properties:

- The drying vanes were replaced by point masses attached to the corresponding bottom and top supports. The vane bank end plates and vane bank top covers were explicitly modeled (see Section 3.4).
- The added mass properties of the lower part of the skirt below the reactor water level were obtained using a separate hydrodynamic analysis (see Section 3.5).
- Fixed constraints were imposed at the underside of the steam dryer upper support ring where it makes contact with the four steam dryer support brackets that are located on the reactor vessel (Figure 2). No constraints were applied to the tops of the reactor vessel lift lugs.
- Most welds were replaced by node-to-node connections; interconnected parts share common nodes along the welds. In other locations the constraint equations between nodal degrees of freedom were introduced as described in Section 3.8.

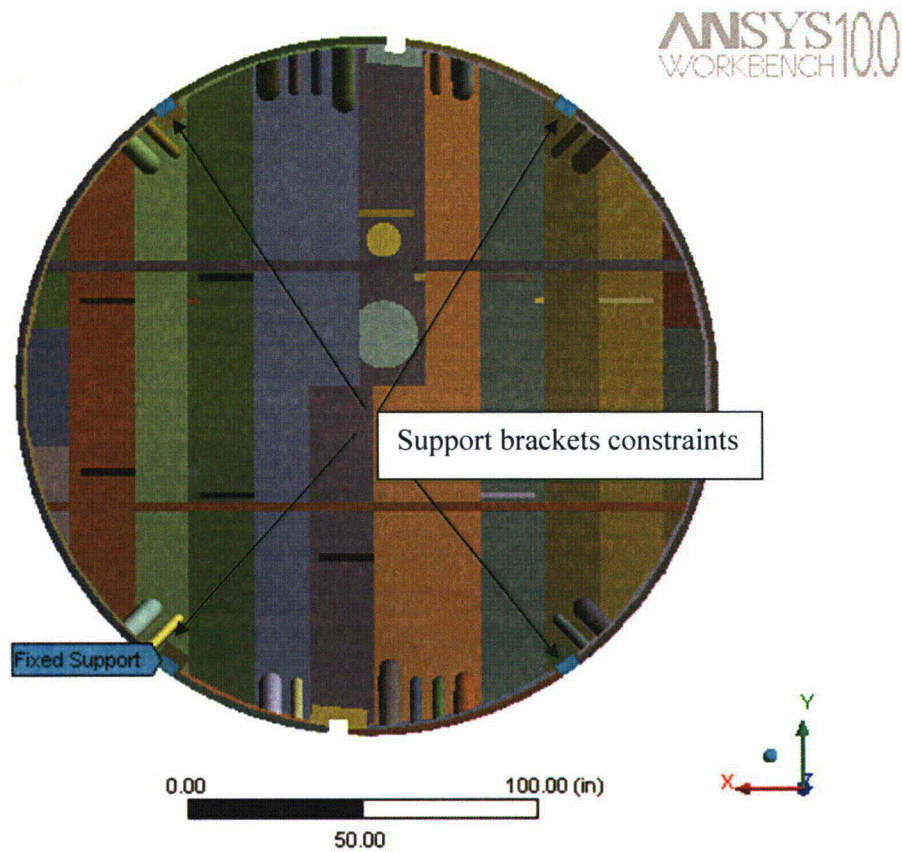


Figure 2. Fixed support constraints. View from under the dryer.

3.4 Vane Bank Model

The vane bank assemblies consist of many vertical angled plates that are computationally expensive to model explicitly, since a prohibitive number of elements would be required. These parts have significant weight which is transmitted through the surrounding structure, so it is important to capture their gross inertial properties. Here the vane banks are modeled as a collection of point masses located at the center of mass for each vane bank section (see Figure 3 and Figure 4). The following masses were used for the vane bank sections, based on data found on provided drawings:

inner banks:	2 sections, each 850 lbm
middle banks:	3 sections, each 1087 lbm; and
outer banks:	3 sections, each 850 lbm.

These masses were applied to the top and bottom vane bank supports using the standard ANSYS point mass modeling option, element MASS21. Note that in static analysis all weight was applied to the bottom supports only. ANSYS automatically distributes the point mass inertial loads to the nodes of the selected structure. The distribution algorithm minimizes the sum of the squares of the nodal inertial forces, while ensuring that the net forces and moments are

conserved. Vane banks are not exposed to main steam lines directly, but rather shielded by the hoods.

The collective stiffness of the vane banks is expected to be small compared to the surrounding support structure and is neglected in the model. In the static case it is reasonable to expect that this constitutes a conservative approach, since neglecting the stiffness of the vane banks implies that the entire weight is transmitted through the adjacent vane bank walls and supports. In the dynamic case the vane banks exhibit only a weak response since (i) they have large inertia so that the characteristic acoustically-induced forces divided by the vane masses and inertias yield small amplitude motions, velocities and accelerations; and (ii) they are shielded from acoustic loads by the hoods, which transfer dynamic loads to the rest of the structure. Thus, compared to the hoods, less motion is anticipated on the vane banks so that approximating their inertial properties with equivalent point masses is justified. Nevertheless, the bounding parts, such as side panels, and top covers, are retained in the model since they can individually exhibit a strong modal response. Errors associated with the point mass representation of the vane banks are compensated for by frequency shifting of the applied loads.

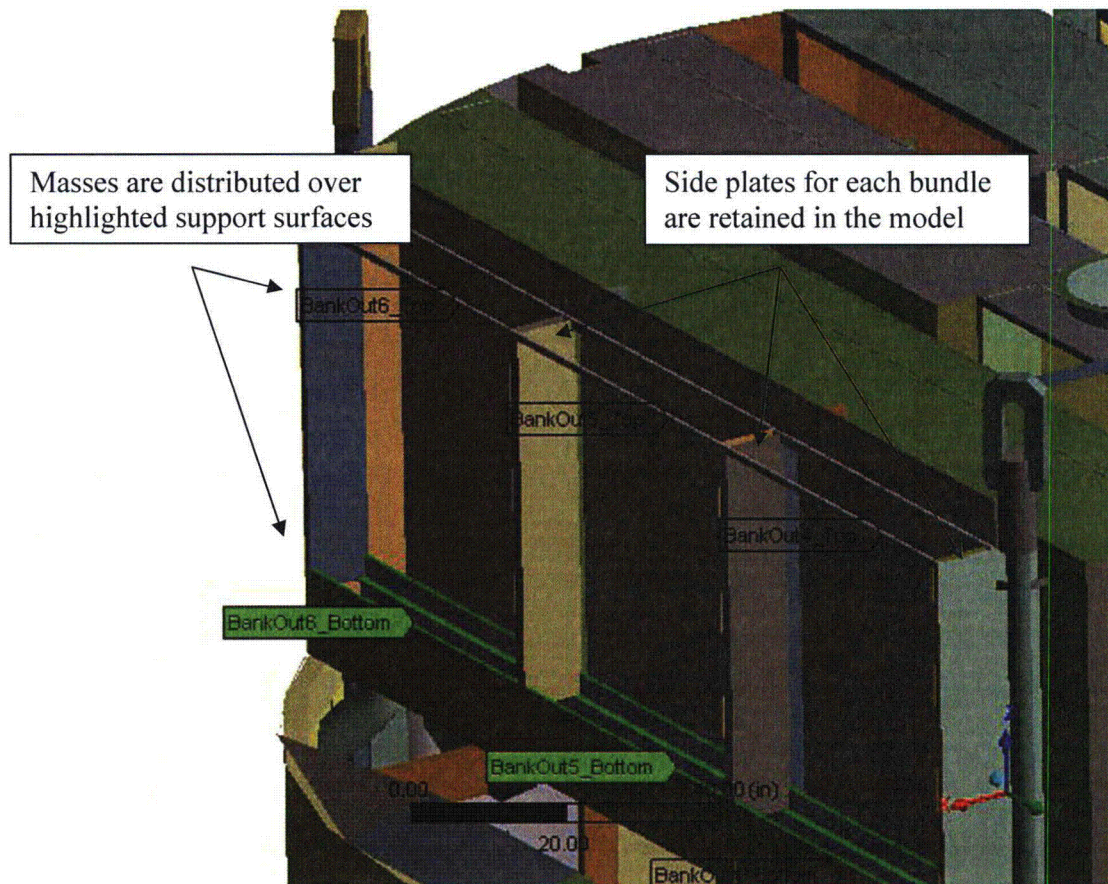


Figure 3. Structural model of vane banks. Outer hood assembly is removed for clarity.

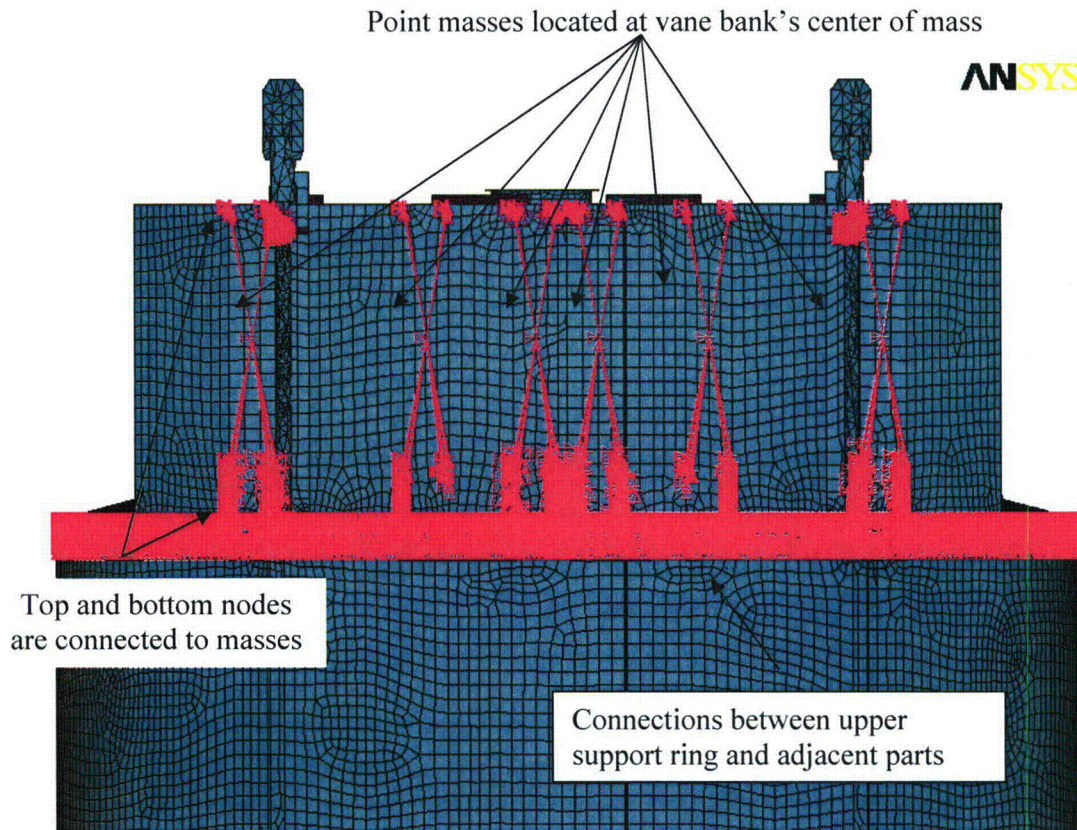


Figure 4. Point masses representing the vanes. The pink shading represents where constraint equations between nodes are applied.

3.5 Water Inertia Effect on Submerged Panels

Water inertia was modeled by an increase in density of the submerged structure to account for the added hydrodynamic mass. This added mass was found by a separate hydrodynamic analysis (included in DRF-MONT-244B supporting this report) to be 0.6095 lbm/in^2 on the submerged skirt area. This is modeled by effectively increasing the material density for the submerged portions of the skirt. Since the skirt is 0.25 inches thick, the added mass is equivalent to a density increase to 2.722 lbm/in^3 . This added water mass was included in the ANSYS model by appropriately modifying the density of the submerged structural elements when computing harmonic response. For the static stresses, the unmodified density of steel is used throughout.

3.6 Structural Damping

Structural damping was defined as 1% of critical damping for all frequencies. This damping is consistent with guidance given on pg. 10 of NRC RG-1.20 [14], which permits 1% damping to be used in this structural analysis (for higher than 1% damping, justification must be provided).

3.7 Mesh Details and Element Types

ANSYS shell elements (SHELL 63) were employed to model the skirt, hoods, side and end plates, trough bottom plates, reinforcements, base plates and cover plates. The SHELL 63 element models bending and membrane stresses, but omits transverse shear. The use of shell elements is appropriate for most of the structure where the characteristic thickness is small compared to the other plate dimensions. For thicker structures, such as the upper and lower support rings, vane bank top and bottom supports, solid brick elements were used to provide the full 3D stress. The elements SURF154 are used to assure proper application of pressure loading to the structure. Mesh details and element types are shown in Table 2 and Table 3.

Table 2. FE Model Summary.

Description	Quantity
No. of Nodes	173,327
No. of Elements	145,663
No. of Element Types	5

Table 3. Listing of Element Types.

Generic Element Type Name	Element Name	ANSYS Name
20-Node Quadratic Hexahedron	SOLID186	20-Node Hexahedral Structural Solid
10-Node Quadratic Solid Element	SOLID187	10-Node Tetrahedral Structural Solid
4-Node Elastic Shell	SHELL63	4-Node Elastic Shell
Mass Element	MASS21	Structural Mass
Pressure Surface Definition	SURF154	3D Structural Surface Effect

The mesh is generated automatically by ANSYS with refinement near edges. The maximum allowable mesh spacing is specified by the user. Here a 3.5 inch maximum allowable spacing is specified everywhere with local refinement in the areas including drain pipes (0.75 inch maximum spacing); cover plates (1.75 inches); tie bars (0.5 inches); and the curved portions of the risers (1.25 inches). Details of the finite element mesh are shown in Figure 5. Numerical experiments carried out using the ANSYS code applied to simple analytically tractable plate structures with dimensions and mesh spacing similar to the ones used for the steam dryer, confirm that the natural frequencies are accurately recovered (less than 1% errors for the first modes). These errors are compensated for by the use of frequency shifting.

3.8 Connections Between Structural Components

Most connections between parts are modeled as node-to-node connections. This is the correct manner (i.e., within the finite element framework) of joining elements away from discontinuities. At joints between shells, this approach omits the additional stiffness provided by the extra weld material. Also, locally 3D effects are more pronounced. The latter effect is accounted for using weld factors. The deviation in stiffness due to weld material is negligible, since weld dimensions are on the order of the shell thickness. The consequences upon modal frequencies and amplitude are, to first order, proportional to t/L where t is the thickness and L a

characteristic shell length. The errors committed by ignoring additional weld stiffness are thus small and readily compensated for by performing frequency shifts.

When joining shell and solid elements, however, the problem arises of properly constraining the rotations, since shell element nodes contain both displacement and rotational degrees of freedom at every node whereas solid elements model only the translations. A node-to-node connection would effectively appear to the shell element as a simply supported, rather than (the correct) cantilevered restraint and significantly alter the dynamic response of the shell structure.

To address this problem, constraint equations are used to properly connect adjacent shell- and solid-element modeled structures. Basically, all such constraints express the deflection (and rotation for shell elements) of a node, R_1 , on one structural component in terms of the deflections/rotations of the corresponding point, P_2 , on the other connected component. Specifically, the element containing P_2 is identified and the deformations at P_2 determined by interpolation between the element nodes. The following types of shell-solid element connections are used in the steam dryer model including the following:

1. Connections of shell faces to solid faces (Figure 6a). While only displacement degrees of freedom are explicitly constrained, this approach also implicitly constrains the rotational degrees of freedom when multiple shell nodes on a sufficiently dense grid are connected to the same solid face.
2. Connections of shell edges to solids (e.g., connection of the bottom of end plates with the upper ring). Since solid elements do not have rotational degrees of freedom, the coupling approach consists of having the shell penetrate into the solid by one shell thickness and then constraining both the embedded shell element nodes (inside the solid) and the ones located on the surface of the solid structure (see Figure 6b). Numerical tests involving simple structures show that this approach and penetration depth reproduce both the deflections and stresses of the same structure modeled using only solid elements or ANSYS' bonded contact technology. Continuity of rotations and displacements is achieved.

The use of constraint conditions rather than the bonded contacts advocated by ANSYS for connecting independently meshed structural components confers better accuracy and useful numerical advantages to the structural analysis of the steam dryer including better conditioned and smaller matrices. The smaller size results from the fact that equations and degrees of freedom are eliminated rather than augmented (in Lagrange multiplier-based methods) by additional degrees of freedom. Also, the implementation of contact elements relies on the use of very high stiffness elements (in penalty function-based implementations) or results in indefinite matrices (Lagrange multiplier implementations) with poorer convergence behavior compared to positive definite matrices.



Figure 5a. Mesh overview. The colors emphasize element type.

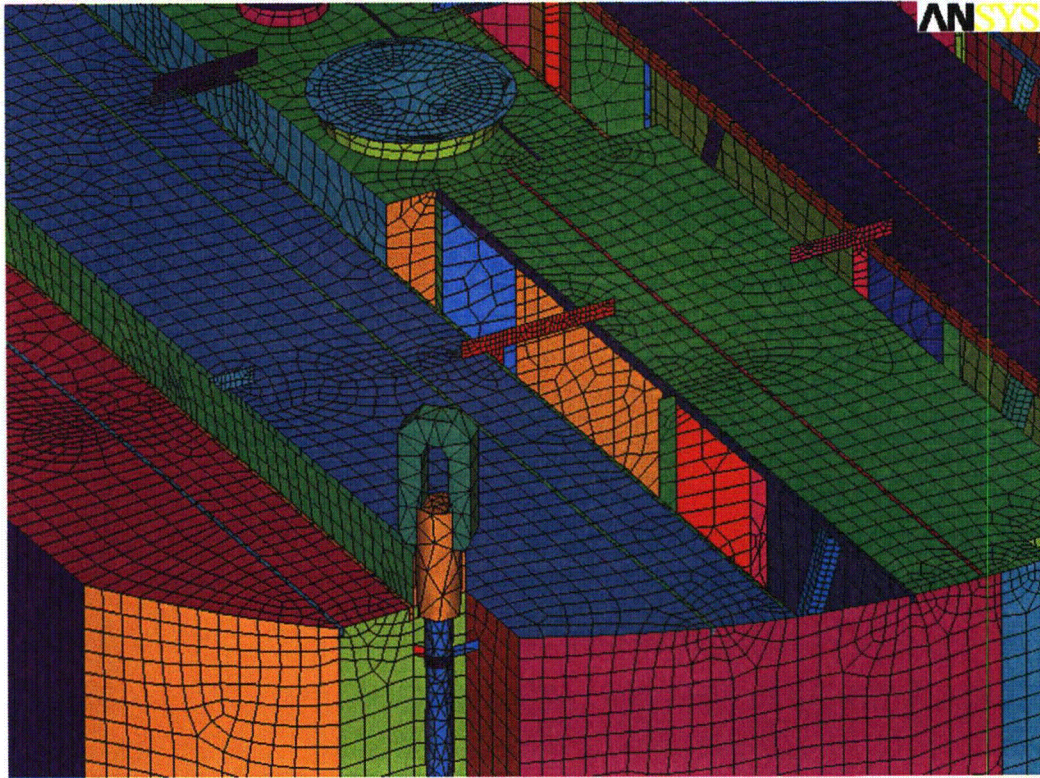


Figure 5b. Close up of mesh showing hoods and tie bars. The colors emphasize element type.

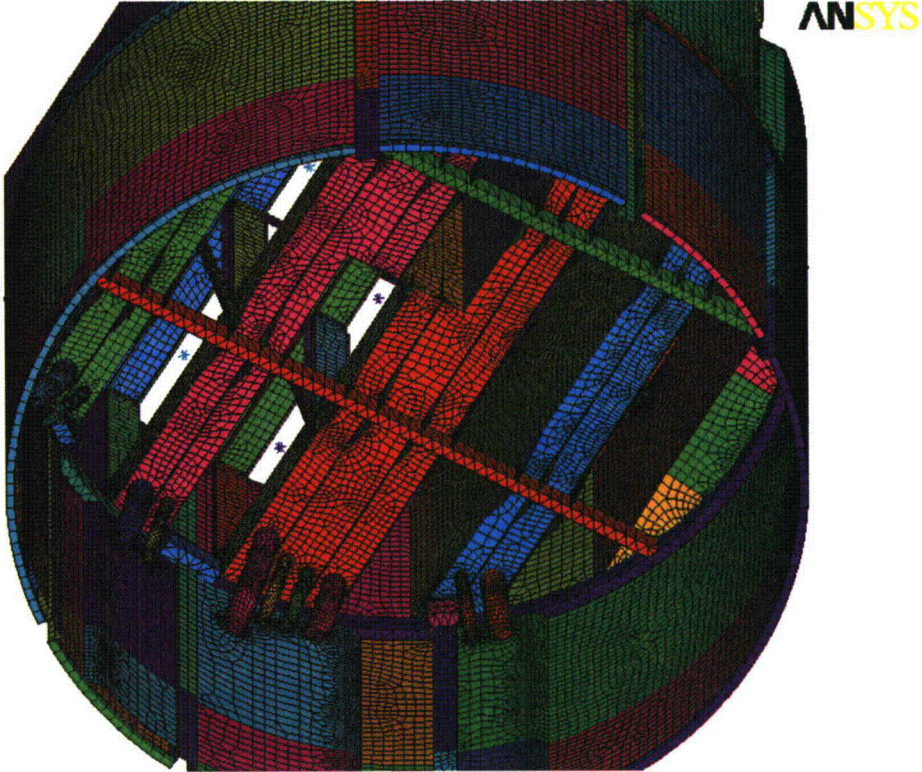


Figure 5c. Close up of mesh showing drain pipes, risers and cover plate supports. The colors emphasize element type.



Figure 5d. Close up of mesh showing node-to-node connections between end panels, top plates, and hoods. The colors emphasize element types. View from the top of the dryer.



Figure 5e. Close up of mesh showing node-to-node connections between the skirt and risers, drain pipes and cover plates. The colors emphasize element type. View from underneath the dryer.

Shell nodes DOF are related to solid element shape functions

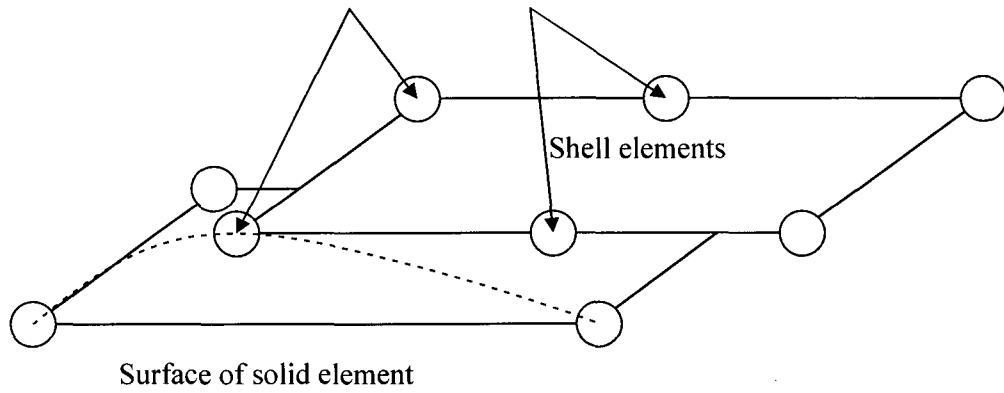


Figure 6a. Face-to-face shell to solid connection.

Shell node displacements are related to solid element shape functions

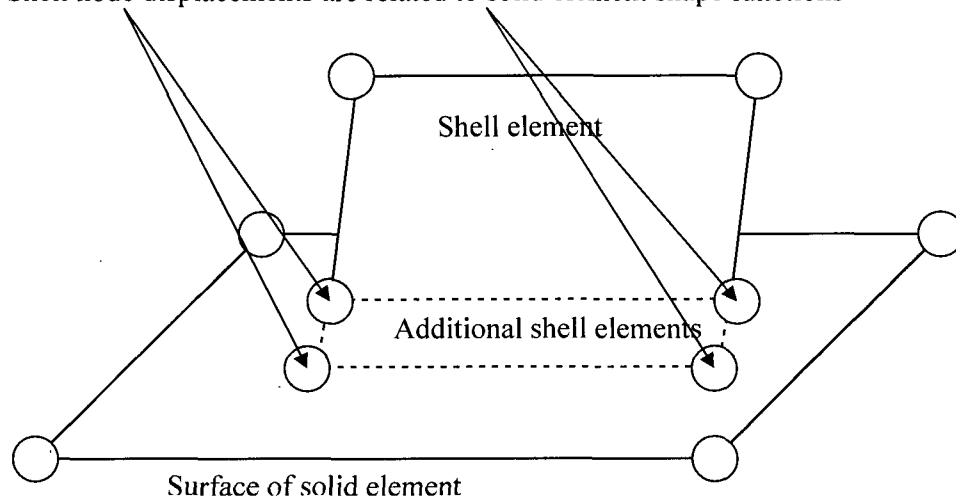


Figure 6b. Shell edge-to-solid face connection.

3.9 Pressure Loading

The harmonic loads are produced by the pressures acting on the exposed surfaces of the steam dryer. At every frequency and for each MSL, the pressure distribution corresponding to a unit pressure at the MSL inlet is represented on a three-inch grid lattice grid (i.e., a mesh whose lines are aligned with the x-, y- and z-directions) that is superimposed over the steam dryer surface. This grid is compatible with the "Table" format used by ANSYS to "paint" general pressure distributions upon structural surfaces. The pressures are obtained from the Helmholtz solver routine in the acoustic analysis [1].

In general, the lattice nodes do not lie on the surface, so that to obtain the pressure differences at the surface, it is necessary to interpolate the pressure differences stored at the lattice nodes. This is done using simple linear interpolation between the eight forming nodes of the lattice cell containing the surface point of interest. Inspection of the resulting pressures at selected nodes shows that these pressures vary in a well-behaved manner between the nodes with prescribed pressures. Graphical depictions of the resulting pressures and comparisons between the peak pressures in the original nodal histories and those in the final surface load distributions produced in ANSYS, all confirm that the load data are interpolated accurately and transferred correctly to ANSYS.

The harmonic pressure loads are only applied to surfaces above the water level, as indicated in Figure 7. In addition to the pressure load, the static loading induced by the weight of the steam dryer is analyzed separately. The resulting static and harmonic stresses are linearly combined to obtain total values which are then processed to calculate maximum and alternating stress intensities for assessment in Section 5.

[[

^{(3)]]} This is useful since revisions in the loads model do not necessitate recalculation of the unit stresses.

The results produced here utilize the Rev. 4 acoustic/hydrodynamic loads model described in [3] to calculate the MSL pressure signals $P_n(\omega)$ and associated biases and uncertainties.

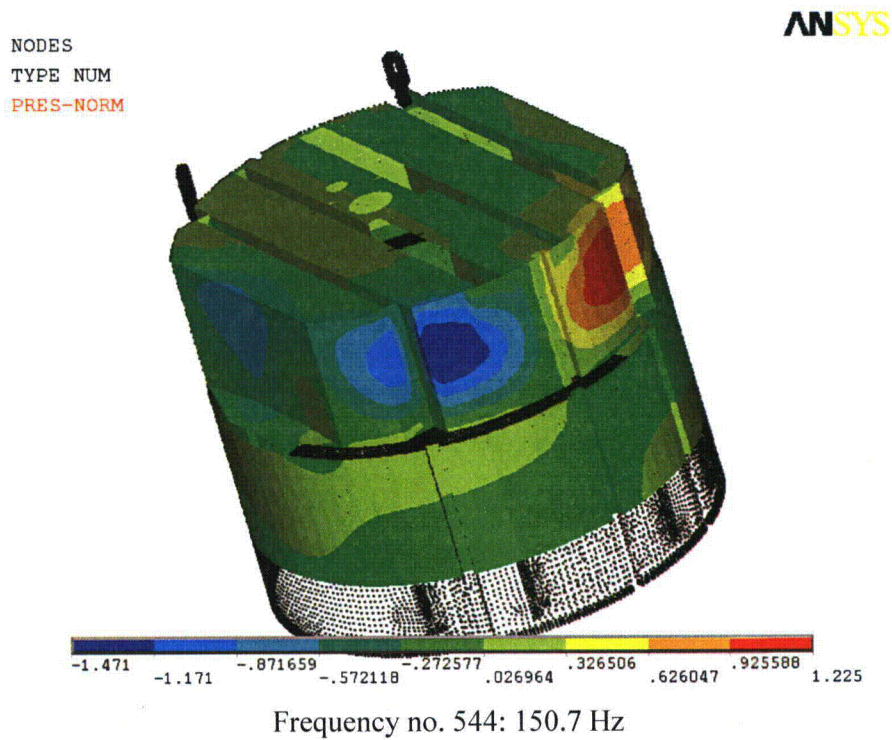
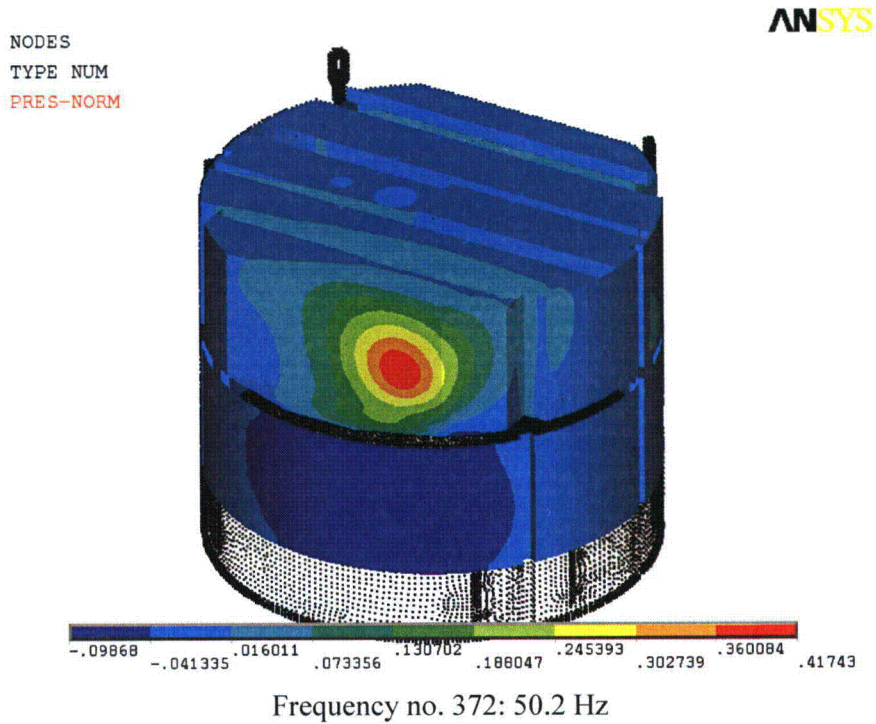


Figure 7. Real part of unit pressure loading MSL C (in psid) on the steam dryer at different frequencies. No loading is applied to submerged parts (nodes at the bottom).

4. Structural Analysis

The solution is decomposed into static and harmonic parts, where the static solution produces the stress field induced by the supported structure subjected to its own weight and the harmonic solution accounts for the harmonic stress field due to the unit pressure of given frequency in one of the main steam lines. All solutions are linearly combined, with amplitudes provided by signal measurements in each steam line, to obtain the final displacement and stress time histories. This decomposition facilitates the prescription of the added mass model accounting for hydrodynamic interaction and allows one to compare the stress contributions arising from static and harmonic loads separately. Proper evaluation of the maximum membrane and membrane+bending stresses requires that the static loads due to weight be accounted for. Hence both static and harmonic analyses are carried out.

4.1 Static Analysis

The results of the static analysis are shown in Figure 8. Only a few locations exhibited high stress intensity levels. These locations include the top cover plate/end plate connection with stress intensity 3,510 psi. High stress locations are also near the steam dryer support brackets and on tie bars. Close up views of these locations are shown in Figure 9. Note that these locations have high stress intensity also when static and transient runs are combined, primarily due to static loading.

4.2 Harmonic Analysis

The harmonic pressure loads were applied to the structural model at all surface nodes described in Section 3.9. Typical stress intensity distributions over the structure are shown in Figure 10. Stresses were calculated for each frequency, and results from static and harmonic calculations were combined.

To evaluate maximum stresses, the stress harmonics including the static component are transformed into a time history using FFT, and the maximum and alternating stress intensities for the response, evaluated. According to subsection NG-3216.2 of the ASME B&PV Code [2] the following procedure was established to calculate alternating stresses. For every node, the stress difference tensors, $\sigma'_{nm} = \sigma_n - \sigma_m$, are considered for all possible pairs of the stresses σ_n and σ_m at different time levels, t_n and t_m . Note that all possible pairs require consideration, since there are no "obvious" extrema in the stress responses. However, in order to contain computational cost, extensive screening of the pairs takes place (see Section 2.3), so that pairs known to produce alternating stress intensities less than 250 psi are rejected. For each remaining stress difference tensor, the principal stresses S_1, S_2, S_3 are computed and the maximum absolute value among principal stress differences, $S_{nm} = \max\{|S_1 - S_2|, |S_1 - S_3|, |S_2 - S_3|\}$, obtained. The alternating stress at the node is then one-half the maximum value of S_{nm} taken over all combinations (n,m), i.e., $S_{alt} = \frac{1}{2} \max_{n,m} \{S_{nm}\}$. This alternating stress is compared against allowable values, depending on the node location with respect to welds.

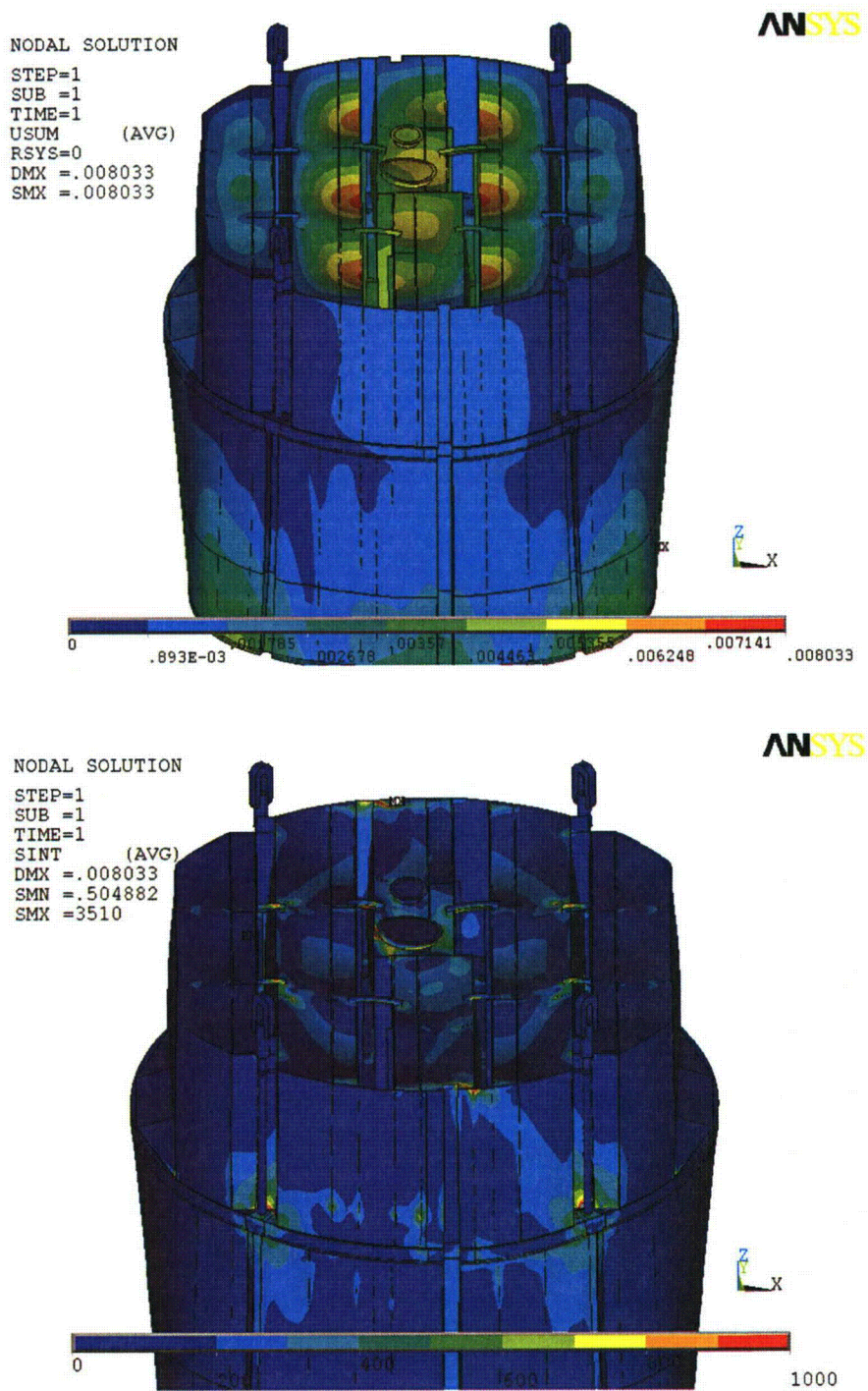


Figure 8. Overview of static calculations showing displacements (top, in inches) and stress intensities (bottom, in psi). The maximum displacement (DMX) is 0.008"; the maximum stress intensity (SMX) is 3,510 psi. Note that displacements are amplified for visualization.

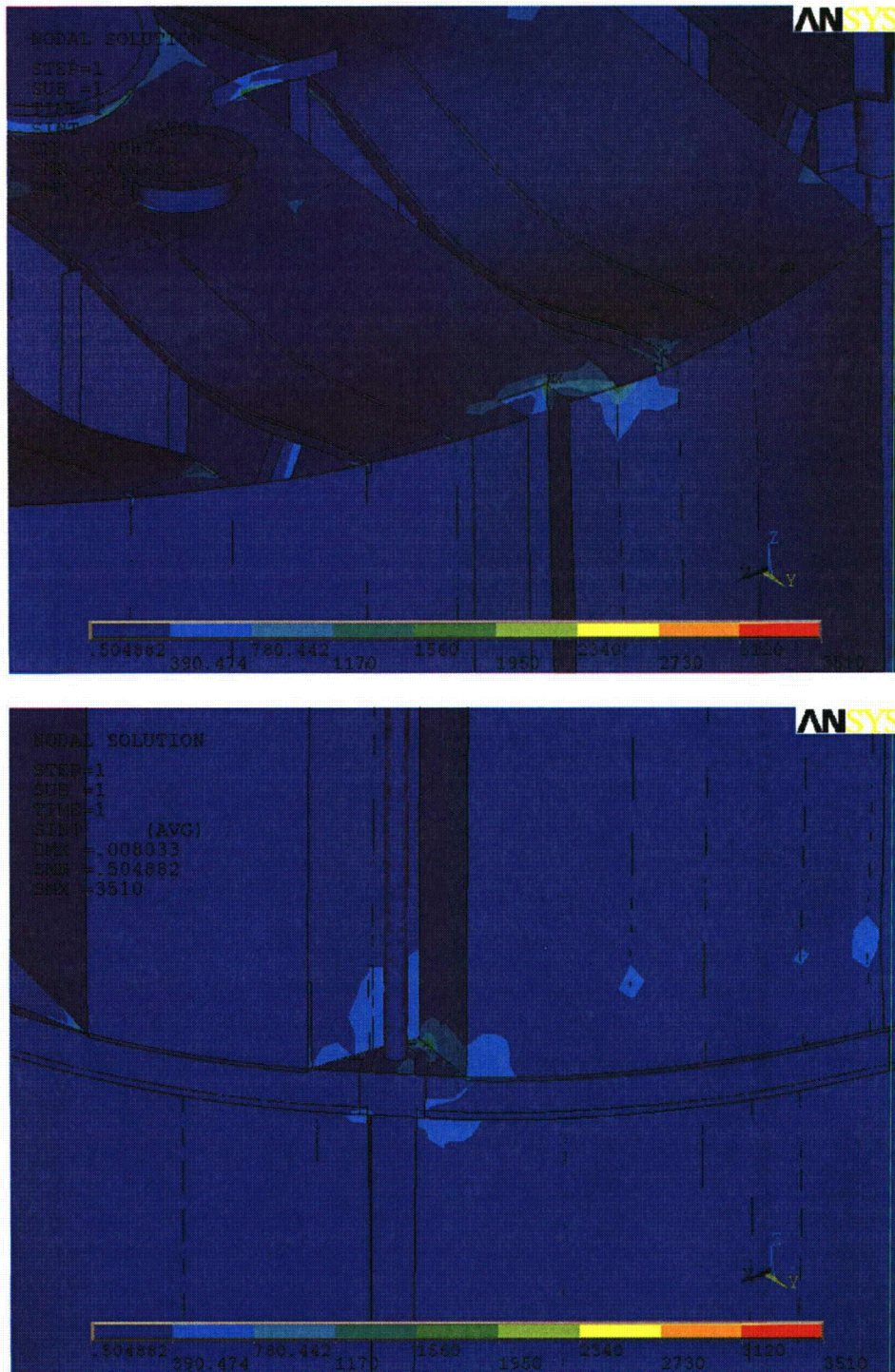
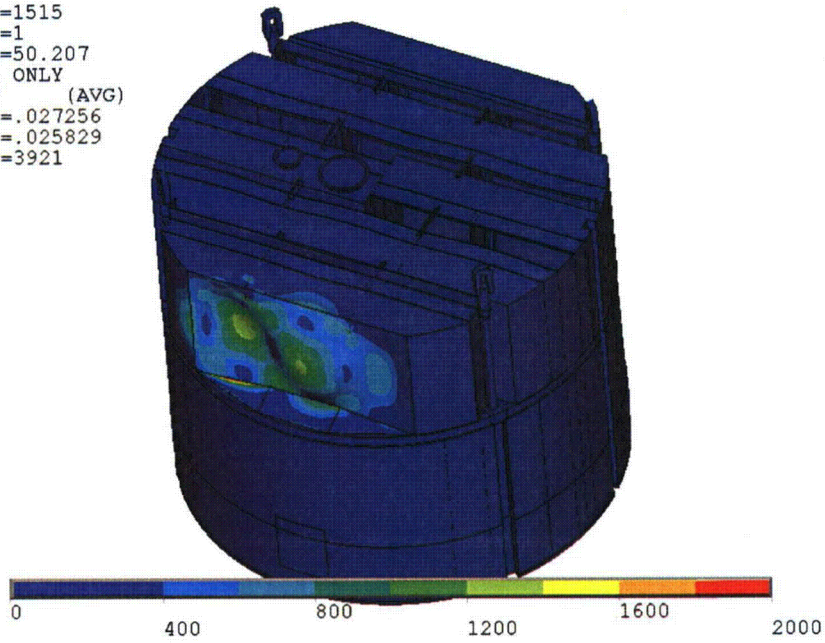


Figure 9. Close up of high static stress intensity (in psi) locations at top cover plates, top, and near support brackets, bottom.

ANSYS

```
NODAL SOLUTION
STEP=1515
SUB =1
FREQ=50.207
REAL ONLY
SINT      (AVG)
DMX =.027256
SMN =.025829
SMX =3921
```



ANSYS

```
NODAL SOLUTION
STEP=579
SUB =1
FREQ=150.685
REAL ONLY
SINT      (AVG)
DMX =.05261
SMN =1.563
SMX =32285
```

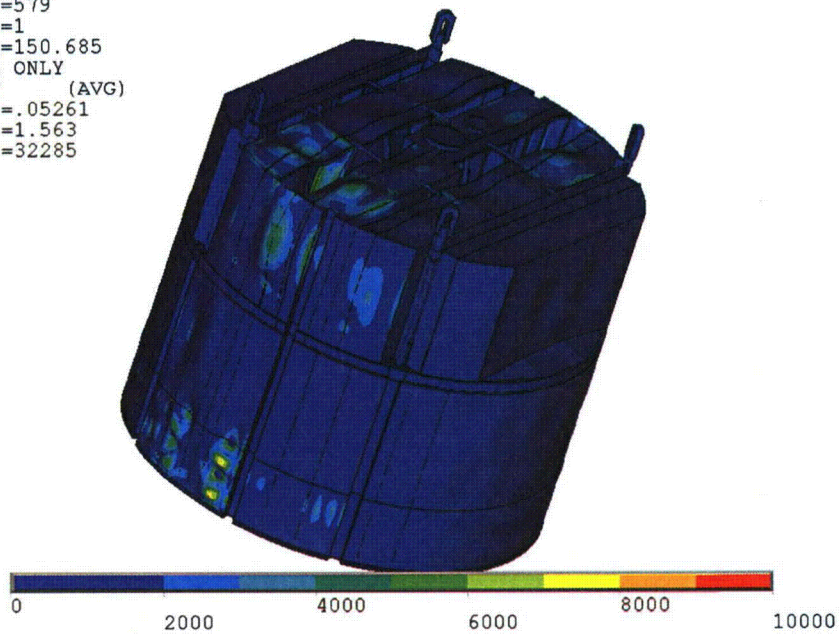


Figure 10. Overview of harmonic calculations showing real part of stress intensities (in psi) along with displacements. Unit loading MSL C for frequencies 50.2 Hz (top) and 150.7 Hz (bottom).

4.3 Post-Processing

The static and unsteady stresses computed at every node with ANSYS were exported into files for subsequent post-processing. These files were then read into separate customized software to compute the maximum and alternating stresses at every node. The maximum stress was defined for each node as the largest stress intensity occurring during the time history. Alternating stresses were calculated according to the ASME procedure [2] described above. For shell elements the maximum stresses were calculated separately at the mid-plane, where only membrane stress is present, and at top/bottom of the shell, where bending stresses are also present.

For nodes that are shared between several structural components or lie on junctions, the maximum and alternating stress intensities are calculated as follows. First, the nodal stress tensor is computed separately for each individual component by averaging over all finite elements meeting at the node and belonging to the same structural component. The time histories of these stress tensors are then processed to deduce the maximum and alternating stress intensities for each structural component. Finally, for nodes shared across multiple components, the highest of the component-wise maximum and alternating stresses is recorded as the "nodal" stress. This approach prevents averaging of stresses across components and thus yields conservative estimates for nodal stresses at the weld locations where several components are joined together.

The maximum stresses are compared against allowable values which depend upon the stress type (membrane, membrane+bending, alternating – P_m , P_m+P_b , S_{alt}) and location (at a weld or away from welds). These allowables are specified in the following section. For solid elements the most conservative allowable for membrane stress, P_m , is used, although bending stresses are nearly always present also. The structure is then assessed in terms of stress ratios formed by dividing allowables by the computed stresses at every node. Stress ratios less than unity imply that the associated maximum and/or alternating stress intensities exceed the allowable levels. Post-processing tools calculate the stress ratios, identifying the nodes with low stress ratios and generating files formatted for input to the 3D graphics program, TecPlot [15], which provides more general and sophisticated plotting options than currently available in ANSYS.

4.4 Computation of Stress Ratios for Structural Assessment

The ASME B&PV Code [2] provides different allowable stresses for different load combinations and plant conditions. The stress levels of interest in this analysis are for the normal operating condition, which is the Level A service condition. The load combination for this condition is:

$$\text{Normal Operating Load Combination} = \text{Weight} + \text{Pressure} + \text{Thermal}$$

The weight and fluctuating pressure contributions have been calculated in this analysis and are included in the stress results. The static pressure differences and thermal expansion stresses are small, since the entire steam dryer is suspended inside the reactor vessel and all surfaces are exposed to the same conditions. Seismic loads only occur in Level B and C cases, and are not considered in this analysis.

Allowable Stress Intensities

Section NG-3222 of the ASME B&PV Code [2] shows the following (Table 4) for the maximum allowable stress intensity (S_m) and alternating stress intensity (S_a) for the Level A service condition. The allowable stress intensity values for type 304 stainless steel at operating temperature 550°F are taken from Table I-1.2 and Fig. I-9.2.2 of Appendix I of Section III, in the ASME B&PV Code. The calculation for different stress categories is performed in accordance with Fig. NG-3221-1 in [2].

Table 4. Maximum allowable stress intensity and alternating stress intensity for all areas other than welds. The notation P_m represents membrane stress; P_b represents stress due to bending; Q represents secondary stresses (from thermal effects and gross structural discontinuities, for example); and F represents additional stress increments (due to local structural discontinuities, for example).

Type	Notation	Service Limit	Allowable Value (psi)
<i>Maximum Stress Allowables:</i>			
General Membrane	P_m	S_m	16,900
Membrane + Bending	$P_m + P_b$	1.5 S_m	25,350
Primary + Secondary	$P_m + P_b + Q$	3.0 S_m	50,700
<i>Alternating Stress Allowable:</i>			
Peak = Primary + Secondary + F	S_{alt}	S_a	13,600

When evaluating welds, either the calculated or allowable stress was adjusted, to account for stress concentration factor and weld quality. Specifically:

- For maximum allowable stress intensity, the allowable value is decreased by multiplying its value in Table 4 by 0.55.
- For alternating stress intensity, the calculated weld stress intensity is multiplied by a weld stress intensity (fatigue) factor of 1.8, before comparison to the S_a value given above.

The factors (0.55 and 1.8) conservatively presume that the structure is joined using fillet welds unless specified otherwise. Since fillet welds correspond to larger stress concentration factors than other types of welds, this assumption is a conservative one. Moreover, it is understood that the factors must be used in conjunction with stress *intensities* prior to comparison against allowables. The resulting allowable values at welds are summarized in Table 5.

Table 5. Weld Stress Intensities.

Type	Notation	Service Limit	Allowable Value (psi)
<i>Maximum Stress Allowables:</i>			
General Membrane	Pm	0.55 Sm	9,295
Membrane + Bending	Pm + Pb	0.825 Sm	13,943
Primary + Secondary	Pm + Pb + Q	1.65 Sm	27,885
<i>Alternating Stress Allowables:</i>			
Peak = Primary + Secondary + F	S _{alt}	Sa	13,600

Comparison of Calculated and Allowable Stress Intensities

The classification of stresses into general membrane or membrane + bending types was made according to the exact location, where the stress intensity was calculated; namely, general membrane, Pm, for middle surface of shell element, and membrane + bending, Pm + Pb, for other locations. For solid elements the most conservative, general membrane, Pm, allowable is used.

The structural assessment is carried out by computing stress ratios between the computed maximum and alternating stress intensities, and the allowable levels. Locations where any of the stresses exceed allowable levels will have stress ratios less than unity. Since computation of stress ratios and related quantities within ANSYS is time-consuming and awkward, a separate FORTRAN code was developed to compute the necessary maximum and alternating stress intensities, Pm, Pm+Pb, and S_{alt}, and then compare it to allowables. Specifically, the following quantities were computed at every node:

1. The maximum membrane stress intensity, Pm (evaluated at the mid-thickness location for shells),
2. The maximum membrane+bending stress intensity, Pm+Pb, (taken as the largest of the maximum stress intensity values at the bottom, top, and mid thickness locations, for shells),
3. The alternating stress, S_{alt}, (the maximum value over the three thickness locations is taken).
4. The stress ratio due to a maximum stress intensity assuming the node lies at a non-weld location (note that this is the minimum ratio obtained considering both membrane stresses and membrane+bending stresses):

$$SR-P(nw) = \min \{ Sm/Pm, 1.5 * Sm/(Pm+Pb) \}.$$
5. The alternating stress ratio assuming the node lies at a non-weld location,

$$SR-a(nw) = Sa / (1.1 * S_{alt}),$$
6. The same as 4, but assuming the node lies on a weld,

$$SR-P(w) = SR-P(nw) * 0.55$$
7. The same as 5, but assuming the node lies on a weld,

$$SR-a(w) = SR-a(nw) / 1.8.$$

Note that in steps 4 and 6, the minimum of the stress ratios based on P_m and P_m+P_b , is taken. The allowables listed in Table 4, $S_m=16,900$ psi and $S_a=13,600$ psi. The factors, 0.55 and 1.8, are the weld factors discussed above. The factor of 1.1 accounts for the differences in Young's moduli for the steel used in the steam dryer and the values assumed in alternating stress allowable. According to NG-3222.4 in [2], the effect of elastic modulus upon alternating stresses is taken into account by multiplying alternating stress S_{alt} at all locations by the ratio, $E/E_{model}=1.1$, where:

$$E = 28.3 \cdot 10^6 \text{ psi, as shown on Fig. I-9.2.2. ASME BP\&V Code [2]}$$
$$E_{model} = 25.55 \cdot 10^6 \text{ psi (Table 1)}$$

The appropriate maximum and alternating stress ratios, SR-P and SR-a, are thus determined and a final listing of nodes having the smallest stress ratios is generated. The nodes with stress ratios lower than 4 are plotted in TecPlot (a 3D graphics plotting program widely used in engineering communities [15]). These nodes are tabulated and depicted in the following Results Section.

4.5 Submodeling

In order to maintain computational costs at a feasible level, the steam dryer model is predominantly comprised of shell elements. These elements are well suited for structures such as the steam dryer consisting of shell-like components and tend to produce conservative estimates of the stresses. In some cases however, such as welded junctions involving multiple components, shell element models can overestimate the nominal stress intensities in the vicinity of the junctions. In such cases a more refined analysis using solid elements to capture the complete 3D stress distribution, is warranted. Therefore, to efficiently analyze complex structures such as steam dryers, a standard engineering practice is to first analyze the structure using a shell-based model. If any locations with high stresses are identified these regions are examined in greater detail using 3D solid elements to obtain a more definitive stress prediction.

In the Monticello steam dryer, one location was identified as requiring a more refined stress analysis. This is the weld joining a vertical plate to the outer hood. This vertical plate also connects to a diagonal brace that acts to reinforce the outer hood. The vertical plate also connects to the top cover plate, but submodeling was not used for this weld connection. This location was examined using a detailed 3D solid element submodel analysis as reported in [16]. Based on this model, the nominal stress intensities computed by the 3D solid element model is lower than that obtained with the shell-based FEA used to analyze the complete steam dryer by a factor of 0.39. The stress intensities predicted by the shell element-based analysis at this location is therefore first multiplied by these factors to obtain more accurate estimates of the nominal stresses. These are then multiplied by the 1.8 weld factor before comparing against allowables to obtain the alternating stress ratios.

5. Results

The stress intensities and associated stress ratios resulting from the Rev.4 acoustic/hydrodynamic loads [3] with associated biases and uncertainties factored in, are presented below. The bias due to finite frequency discretization and uncertainty associated with the finite element model itself, are also factored in. In the following sections the highest maximum and alternating stress intensities are presented to indicate which points on the dryer experience significant stress concentration and/or modal response (Section 5.1). The lowest stress ratios obtained by comparing the stresses against allowable values, accounting for stress type (maximum and alternating) and location (on or away from a weld), are also reported (Section 5.2). The frequency dependence of the stresses at nodes experiencing the lowest stress ratios is depicted in the form of accumulative PSDs (Section 5.3). Finally section 5.4 reports the predicted stress ratios at EPU conditions. This section also reflects the most recent revisions of biases and uncertainties in the finite element model as well the low flow noise removal procedure.

In each section results are presented both at nominal conditions (no frequency shift) and with frequency shift included. Unless specified otherwise, frequency shifts are generally performed at 2.5% increments. The tabulated stresses and stress ratios are obtained using a 'blanking' procedure that is designed to prevent reporting a large number of high stress nodes from essentially the same location on the structure. In the case of stress intensities this procedure is as follows. The relevant stress intensities are first computed at every node and then nodes sorted according to stress level. The highest stress node is noted and all neighboring nodes within 10 inches of the highest stress node and its symmetric images (i.e., reflections across the $x=0$ and $y=0$ planes) are "blanked" (i.e., excluded from the search for subsequent high stress locations). Of the remaining nodes, the next highest stress node is identified and its neighbors (closer than 10 inches) blanked. The third highest stress node is similarly located and the search continued in this fashion until all nodes are either blanked or have stresses less than half the highest value on the structure. For stress ratios, an analogous blanking procedure is applied. Thus the lowest stress ratio of a particular type in a 10" neighborhood and its symmetric images is identified and all other nodes in these regions excluded from listing in the table. Of the remaining nodes, the one with the lowest stress ratio is reported and its neighboring points similarly excluded, and so on until all nodes are either blanked or have a stress ratio higher than 4.

The measured CLTP strain gage signals contain significant contributions from non-acoustic sources such as sensor noise, MSL turbulence and pipe bending vibration that contribute to the hoop strain measurements. The ACM analysis does not distinguish between the acoustic and non-acoustic fluctuations in the MSL signals that could lead to sizeable, but fictitious acoustic loads and resulting stresses on the dryer. One way to remove these fictitious loads is to collect data with the system maintained at operating pressure (1000 psi) and temperature, but low (less than 30% of CLTP) flow. By operating the recirculation pumps at this condition, the background plant noise and vibrations remain present. At these conditions the acoustic loads are known to be negligible so that collected data, referred to as the low flow data, originate entirely from non-acoustic sources such as sensor noise and mechanical vibrations. This information is valuable since it allows one to now distinguish between the acoustic and non-acoustic content in the CLTP signal and therefore modify the CLTP loads so that only the acoustic component is

retained. For consistency, the low flow strain gage signals are filtered in the same manner as the CLTP data and are fed into the ACM model to obtain the monopole and dipole signals at the MSL inlets. Since there is negligible flow, these signals are fictitious, i.e., the hoop strains measured by the strain gages are not due to pressure fluctuations, but rather due to noise. However, under the supposition that these signals are acoustic in origin the hypothetical stresses due to these signals can nevertheless be computed.

The contribution of background noise in the Monticello steam dryer was quantified by taking strain gage measurements at 28% power. At this level there are no significant acoustic sources. To compensate for the non-acoustic noise source represented in the low flow data, the CLTP MSL inlet pressure signals are modified according to:

$$P(f) = P_0(f) * \max \left[0.2, 1 - \frac{\bar{N}(f)}{\bar{P}_0(f)} \right] \quad (8)$$

where f is the frequency (in Hz), $P_0(f)$ is the MSL inlet pressure (monopole or dipole) at CLTP conditions before correction, $P(f)$ is the corresponding post-correction pressure and $\bar{N}(f)$ and $\bar{P}_0(f)$ are averaged pressure amplitudes associated with the low flow data and CLTP data respectively. Specifically,

$$\bar{P}_0(f) = \frac{1}{2} \int_{f-1}^{f+1} |P_0(f)| df \quad (9)$$

where $|P_0(f)|$ denotes the absolute value of the complex quantity. Hence $\bar{P}_0(f)$ is the average amplitude of the CLTP pressure in the ± 1 Hz interval about frequency, f . The same definition, but using the low flow pressure signal, is used for $\bar{N}(f)$. Note that this modification leaves the phase information in the original CLTP signal unchanged.

The applied load includes all biases and uncertainties for both the ACM (summarized in [3]) and the FEM. For the latter there are three main contributors to the finite element bias and uncertainty. The first is an uncertainty (21.5%) that accounts for modeling idealizations (e.g., vane bank mass model), geometrical approximations and other discrepancies between the modeled and actual dryer such as neglecting of weld mass and stiffness in the FEA. The second contributor accounts for discretization errors associated with using a finite size mesh, upon computed stresses. This error is subsumed in the modeling idealizations error above since the associated FE analysis was performed using a similar finite mesh spacing. The third contributor is also a bias and compensates for the use of a finite discretization schedule in the construction of the unit solutions. The frequencies are spaced such that at 1% damping the maximum (worst case) error in a resonance peak is 5%. The average error for this frequency schedule is 1.72%.

5.1 General Stress Distribution and High Stress Locations

The largest stress intensities obtained by post-processing the ANSYS stress histories for CLTP at nominal frequency and with frequency shift operating conditions are listed in Table 6. Contour plots of the stress intensities over the steam dryer structure are shown on Figure 11

(nominal frequency) and Figure 12 (maximum stress over all nine frequency shifts including nominal). The figures are oriented to emphasize the high stress regions. Note that these stress intensities *do not* account for weld factors but do include end-to-end bias and uncertainty. Further, it should be noted that since the allowable stresses vary with location, stress intensities do not necessarily correspond to regions of primary structural concern. Instead, structural evaluation is more accurately made in terms of the stress ratios which compare the computed stresses to allowable levels with due account made for stress type and weld factors. Comparisons on the basis of stress ratios are made in Section 5.2.

The maximum stress intensities in most areas are low (less than 250 psi, or 5% of the most conservative critical stress). For the membrane stresses (P_m) the high stress regions tend to be very localized and occur on: (i) the base of the lifting lug (note that the membrane and membrane+bending stress intensities – P_m and P_m+P_b - are identical because they occur in solid elements for which no distinction is made between the membrane and bending stresses); (ii) the top edges of the inner and middle vane bank support plates and (iii) the tie bars. In most cases the stress is dominated by the static deadweight component as evidenced by the low alternating stress values in the rightmost columns in the table.

The membrane + bending stress (P_m+P_b) distributions evidence a more pronounced modal response in all cases. Modal excitations are most pronounced on the hoods. The skirt also evidences a modal response, but the associated stresses there and on the drain channels are low. Other than the outer hood high stresses tend to be localized near junctions and weld lines. The most pronounced such line is where the base of the outer hood connects to the outer cover plate.

The highest reported value of the alternating stresses at nominal operation is 1837 psi and occurs on the weld joining the base of the outer hood to the outer cover plate. The cover plate consists of three parts that are welded together and the high stress point lies at the junction of two welds – the weld joining adjacent cover plates and the weld joining cover plates to the outer hood. Given the arrangement of plates and hoods at this intersection, it is reasonable to expect higher stresses at this point. The second highest stress also occurs on the outer hood where it joins to the small vertical plate underneath the hood that in turn is connected to the diagonal support brace. As frequencies are shifted the spatial distributions of stress do not change significantly. The highest alternating stress amplitudes increases by 24% at the +10% frequency shift.

Finally, for reference the stresses obtained without filtering of the background noise using the low flow data are listed in Table 7.

Table 6a. Locations with highest predicted stress intensities at CLTP conditions at zero frequency shift. Signal noise has been removed using low flow data. Stress plots are shown in Figure 11.

Stress Category	Location	Weld	Location (in) ^(a)			node ^(b)	Stress Intensities (psi)		
			x	y	z		P _m	P _m +P _b	S _{alt}
P _m	Lifting Rod Support	Yes	-50.6	77.8	0	152128	3217	3217	<250
"	Inner Vane Bank CD	Yes	-10.8	-99.7	12	21519	2620	2620	761
"	Tie Bar	No	-22.8	30.4	61.5	96902	2511	2606	274
"	Middle Vane Bank AB	Yes	23.2	94.9	12	11016	2277	2277	507
"	Side Plate	No	31.8	32.4	9	100433	2269	2271	323
P _m +P _b	Inner Top Cover/Rail	Yes	-11.1	95.4	61.5	141731	1336	3795	289
"	Mid Plate/Inner Cover Plate AB	Yes	1.8	0	0	143461	1234	3408	<250
"	Lifting Rod Support	Yes	-50.6	77.8	0	152128	3217	3217	<250
"	Diagonal Brace/Inner Cover Plate B/Gusset	Yes	32.2	32.4	0	142843	1036	3004	310
"	Inner Cover Plate C D	Yes	-32.2	91.7	0	112814	610	2997	253
S _{alt}	Outer Hood/Outer Cover Plate (AB)	Yes	84.8	-17	3.6	140583	307	1845	1837
"	Outer Top Cover AB/Vertical Plate Inside Hood	Yes	79.8	-25.6	61.5	140248	857	1657	1282
"	Outer Hood A B/Outer Cover Plate A B	Yes	84.8	-6.5	3.6	140578	117	1142	1081
"	Outer Cover Plate Ext/Outer Cover Plate C D	Yes	-98.2	2.9	0	141480	59	1086	941
"	Middle Vane Bank A B	Yes	32.2	-94.9	12	13858	2143	2143	910

Notes for Table 6.

- (a) Spatial coordinates are in a reference frame whose origin is located at the intersection of the steam dryer centerline and the plane containing the base plates (this plane also contains the top of the upper support ring and the bottom edges of the hoods). The y-axis is parallel to the hoods, the x-axis is normal to the hoods pointing from MSL C/D to MSL A/B, and the z-axis is vertical, positive up.
- (b) Node numbers are retained for further reference.
- (c) In accordance with [16], the nominal stress intensities at the vertical plate/hood support junction are multiplied by 0.39.

Table 6b. Locations with highest predicted stress intensities taken over all frequency shifts at CLTP conditions. Signal noise has been removed using low flow data. Stress contour plots are shown in Figure 12.

Stress Category	Location	Weld	Location (in) ^(a)			node ^(b)	Stress Intensities (psi)			% Freq. Shift
			x	y	z		Pm	Pm+Pb	S _{alt}	
Pm	Inner Vane Bank CD	Yes	-10.8	-99.7	12	21519	3716	3716	1818	10
"	Lifting Rod Support	Yes	-50.6	77.8	0	152128	3317	3317	<250	10
"	Middle Vane Bank CD	Yes	-23.2	-94.9	12	12560	2739	2739	1023	10
"	Middle Vane Bank AB	Yes	32.2	-94.9	12	13858	2738	2738	1502	10
"	Side Plate	No	31.8	32.4	9	100433	2663	2669	758	10
Pm+Pb	Inner Top Cover/Rail	Yes	-11.1	95.4	61.5	141731	1349	3835	331	10
"	Inner Vane Bank CD	Yes	-10.8	-99.7	12	21519	3716	3716	1818	10
"	Mid Plate/Inner Cover Plate AB	Yes	1.8	0	0	143461	1287	3554	332	5
"	Diagonal Brace/Inner Cover Plate AB/Gusset	Yes	32.2	32.4	0	142843	1180	3509	786	10
"	Lifting Rod Support	Yes	-50.6	77.8	0	152128	3317	3317	<250	10
S _{alt}	Outer Hood/Outer Cover Plate (AB)	Yes	84.8	-17	3.6	140583	341	2374	2276	10
"	Outer Top Cover AB/Vertical Plate Inside Hood	Yes	79.8	25.6	61.5	143720	1047	2285	2023	10
"	Inner Vane Bank (CD)	Yes	-10.8	-99.7	12	21519	3716	3716	1818	10
"	Middle Vane Bank (AB)	Yes	32.2	-94.9	12	13858	2738	2738	1502	10
"	Outer Hood /Outer Cover Plate (AB)	Yes	84.8	-1.3	3.6	140581	128	1472	1355	10

See Table 6a for notes (a)-(c).

Table 7a. Stress intensities at zero frequency shift for the nodes listed in Table 6a computed using the unfiltered CLTP loads (i.e., signal noise has *not* been removed).

Stress Category	Location	Weld	Location (in) ^(a)			node ^(b)	Stress Intensities (psi)		
			x	y	z		Pm	Pm+Pb	S _{alt}
Pm	Lifting Rod Support	Yes	-50.6	77.8	0	152128	3481	3481	389
"	Inner Vane Bank CD	Yes	-10.8	-99.7	12	21519	4509	4509	2638
"	Tie Bar	No	-22.8	30.4	61.5	96902	2919	3007	627
"	Middle Vane Bank AB	Yes	23.2	94.9	12	11016	3148	3148	1413
"	Side Plate	No	31.8	32.4	9	100433	2865	2870	923
Pm+Pb	Inner Top Cover/Rail	Yes	-11.1	95.4	61.5	141731	1473	4179	659
"	Mid Plate/Inner Cover Plate AB	Yes	1.8	0	0	143461	1314	3630	435
"	Lifting Rod Support	Yes	-50.6	77.8	0	152128	3481	3481	389
"	Diagonal Brace/Inner Cover Plate A B/Gusset/Diagonal Brace Ext	Yes	32.2	32.4	0	142843	1190	3586	882
"	Inner Cover Plate C D	Yes	-32.2	91.7	0	112814	654	3231	496
S _{alt}	Outer Hood A B/Outer Cover Plate AB/Outer Cover Plate AB	Yes	84.8	-17	3.6	140583	370	2391	2293
"	Outer Top Cover AB/Vertical Plate Inside Hood	Yes	79.8	-25.6	61.5	140248	1021	1914	1557
"	Outer Hood A B/Outer Cover Plate A B	Yes	84.8	-6.5	3.6	140578	127	1231	1175
"	Outer Cover Plate C D Ext/Outer Cover Plate C D	Yes	-98.2	2.9	0	141480	74	1380	1307
"	Middle Vane Bank A B	Yes	32.2	-94.9	12	13858	3555	3555	2355

See Table 6a for notes (a)-(c).

Table 7b. Highest stress intensities at any frequency shift for the nodes listed in Table 6b computed using the unfiltered CLTP loads (i.e., signal noise has *not* been removed).

Stress Category	Location	Weld	Location (in) ^(a)			node ^(b)	Stress Intensities (psi)			% Freq. Shift
			x	y	z		Pm	Pm+Pb	S _{alt}	
Pm	Inner Vane Bank CD	Yes	-10.8	-99.7	12	21519	5670	5670	3881	10
"	Lifting Rod Support	Yes	-50.6	77.8	0	152128	3826	3826	756	10
"	Middle Vane Bank CD	Yes	-23.2	-94.9	12	12560	3915	3915	2267	10
"	Middle Vane Bank AB	Yes	32.2	-94.9	12	13858	4671	4671	3406	10
"	Side Plate	No	31.8	32.4	9	100433	3662	3668	1695	10
Pm+Pb	Inner Top Cover/Rail	Yes	-11.1	95.4	61.5	141731	1576	4477	1014	10
"	Inner Vane Bank CD	Yes	-10.8	-99.7	12	21519	5670	5670	3881	10
"	Mid Plate/Inner Cover Plate AB	Yes	1.8	0	0	143461	1465	4042	812	7.5
"	Diagonal Brace/Inner Cover Plate AB/Gusset/Diagonal Brace Ext	Yes	32.2	32.4	0	142843	1466	4492	1755	10
"	Lifting Rod Support	Yes	-50.6	77.8	0	152128	3826	3826	756	10
S _{alt}	Outer Hood/Outer Cover Plate (AB)	Yes	84.8	-17	3.6	140583	449	3016	2820	10
"	Outer Top Cover AB/Vertical Plate Inside Hood	Yes	79.8	25.6	61.5	143720	1287	3255	2836	10
"	Inner Vane Bank (CD)	Yes	-10.8	-99.7	12	21519	5670	5670	3881	10
"	Middle Vane Bank (AB)	Yes	32.2	-94.9	12	13858	4671	4671	3406	10
"	Outer Hood /Outer Cover Plate (AB)	Yes	84.8	-1.3	3.6	140581	153	1746	1639	10

See Table 6a for notes (a)-(c).

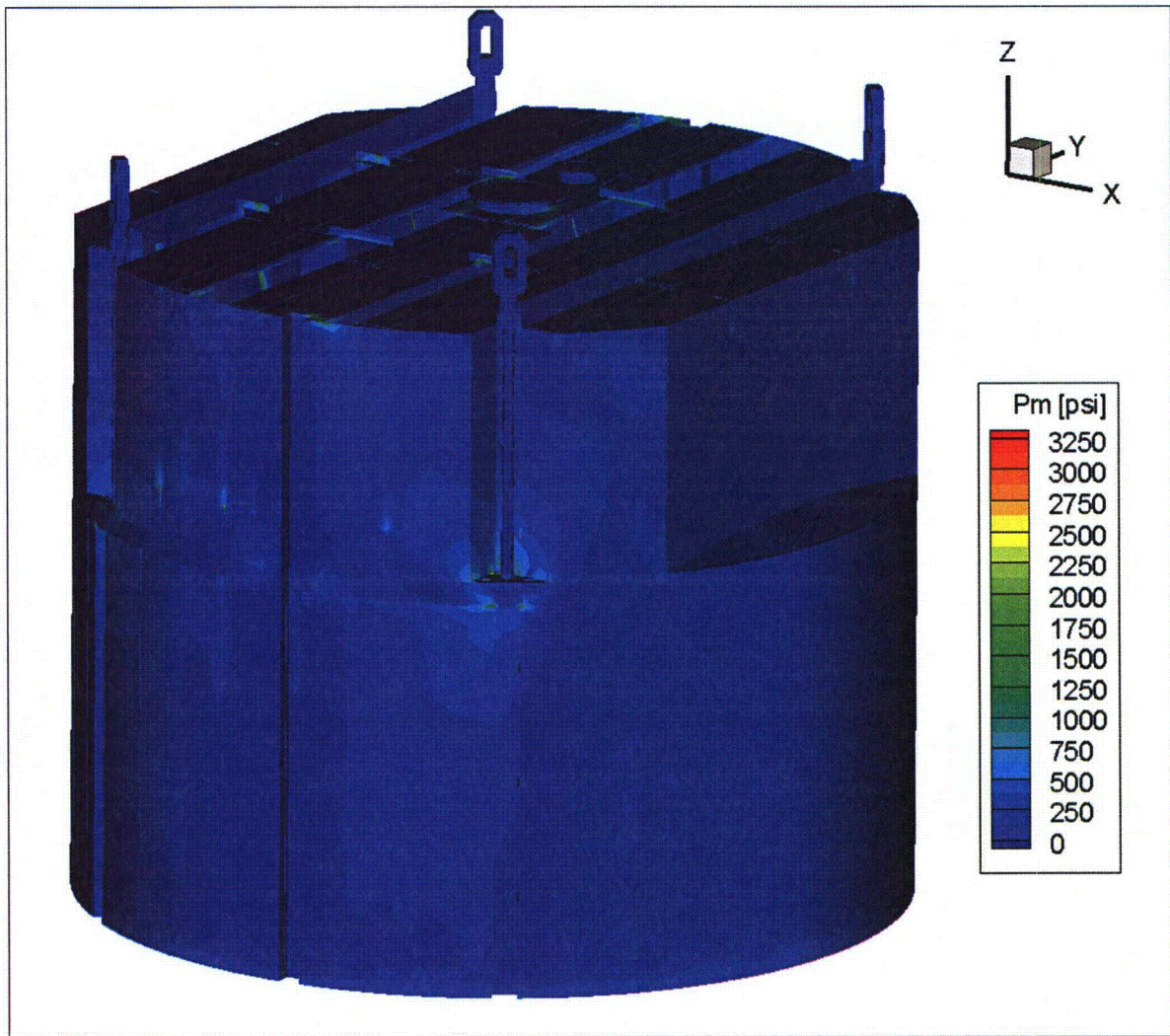


Figure 11a. Contour plot of maximum membrane stress intensity, P_m , for CLTP load. The maximum stress intensity is 3217 psi.

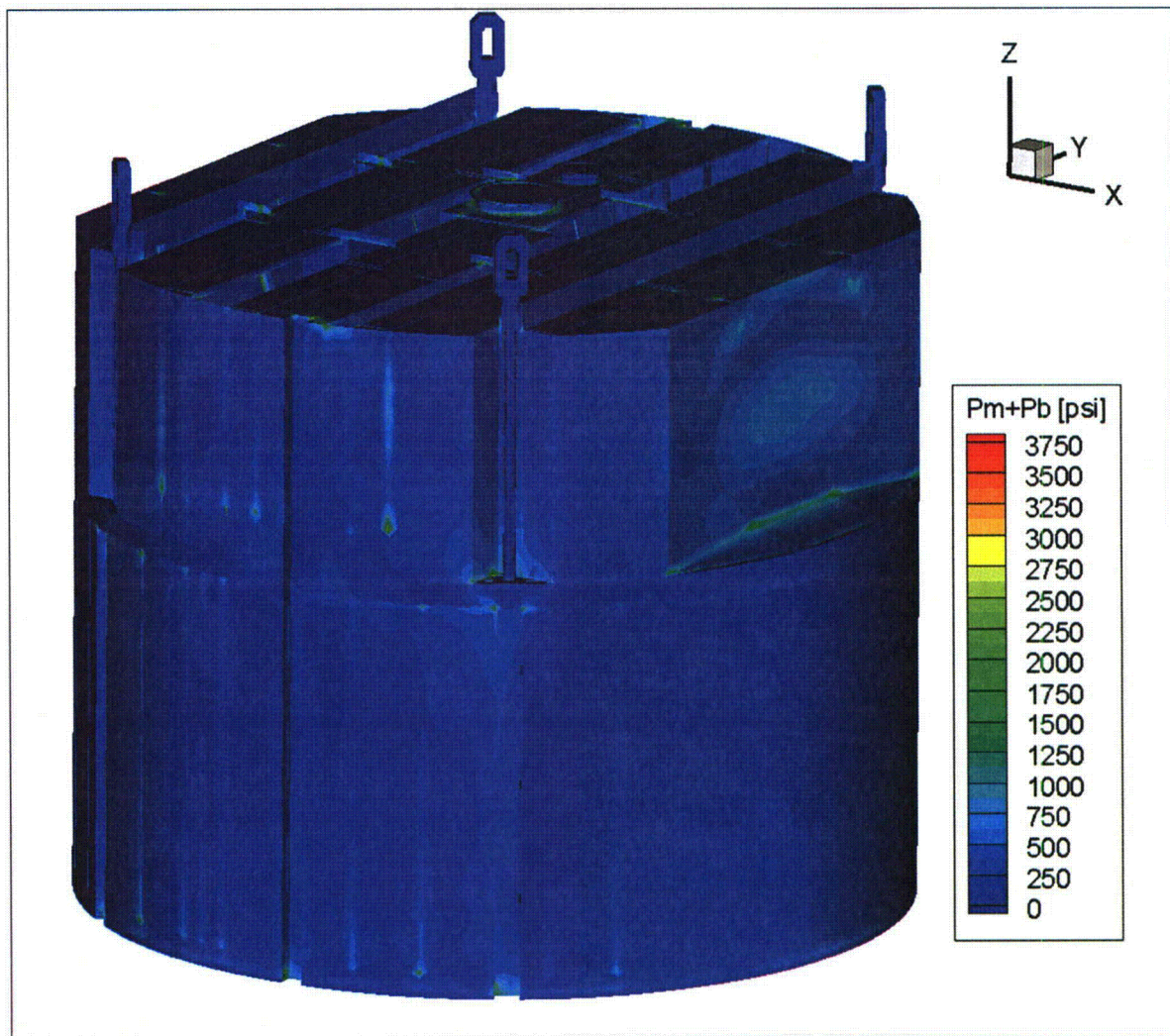


Figure 11b. Contour plot of maximum membrane+bending stress intensity, P_m+P_b , for CLTP load. The maximum stress intensity is 3795 psi.

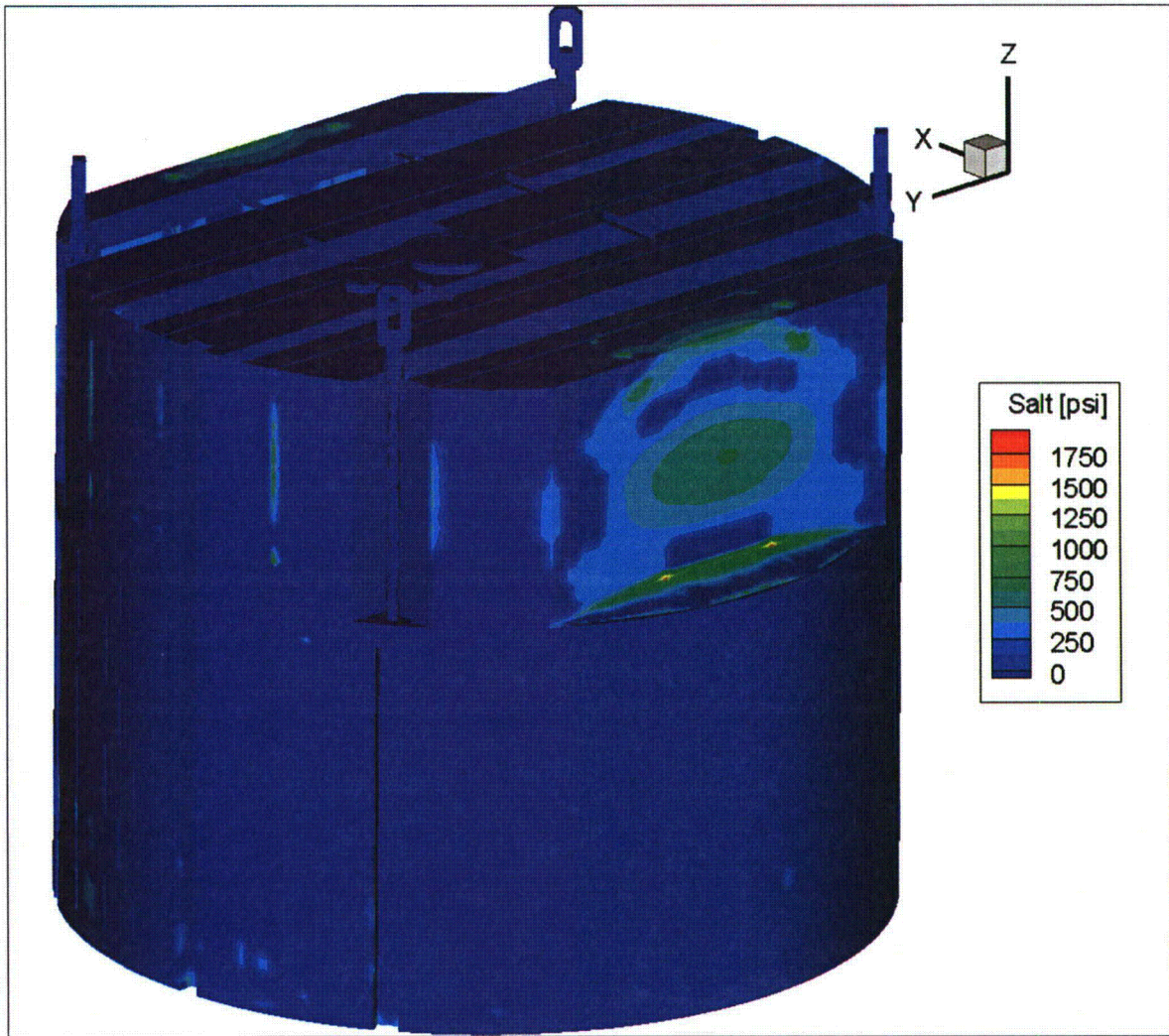


Figure 11c. Contour plot of alternating stress intensity, S_{alt} , for CLTP load. The highest alternating stress intensity is 1837 psi.

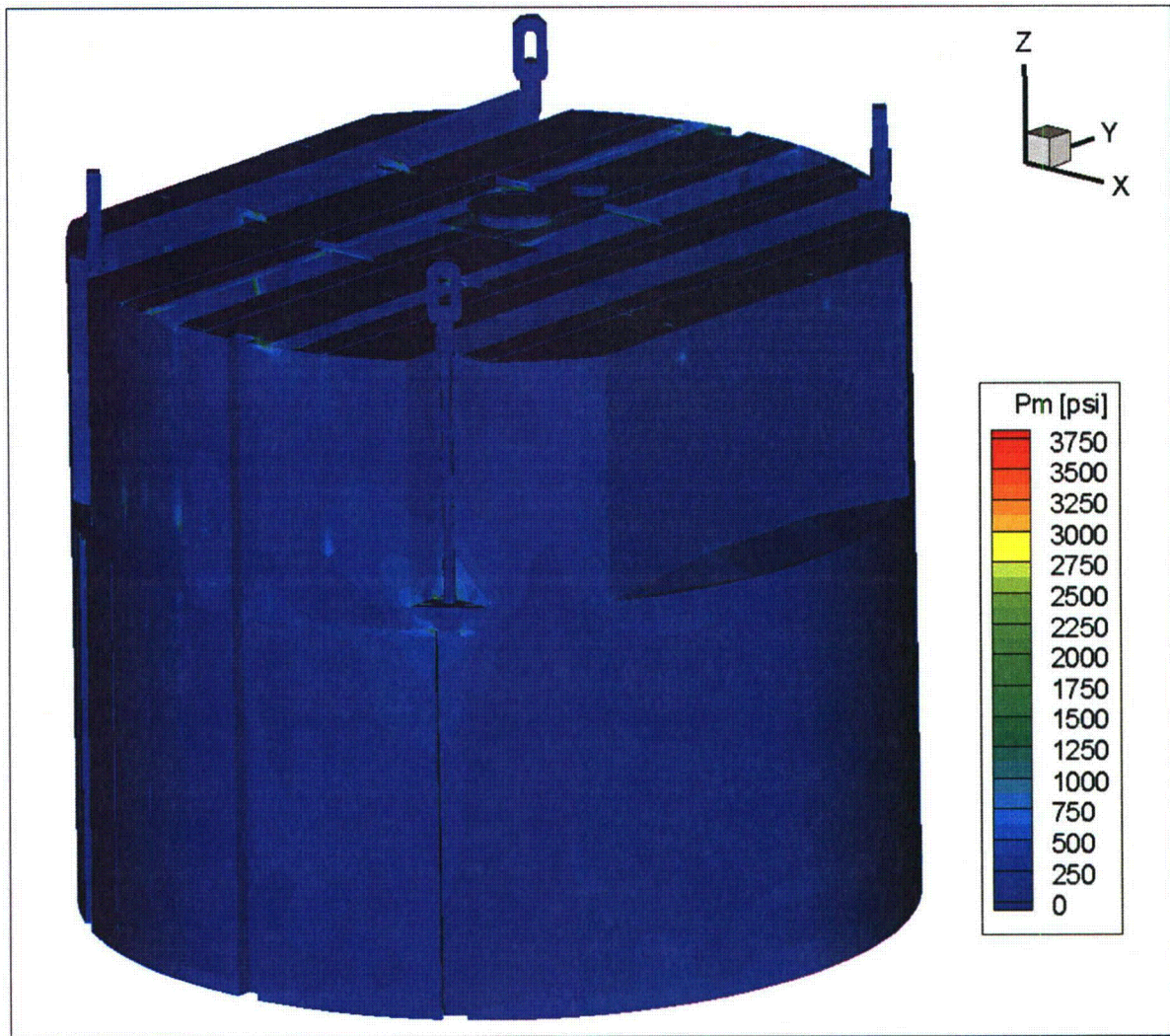


Figure 12a. Contour plot of maximum membrane stress intensity, P_m , for CLTP operation with frequency shifts. The recorded stress at a node is the maximum value taken over all frequency shifts. The maximum stress intensity is 3716 psi.

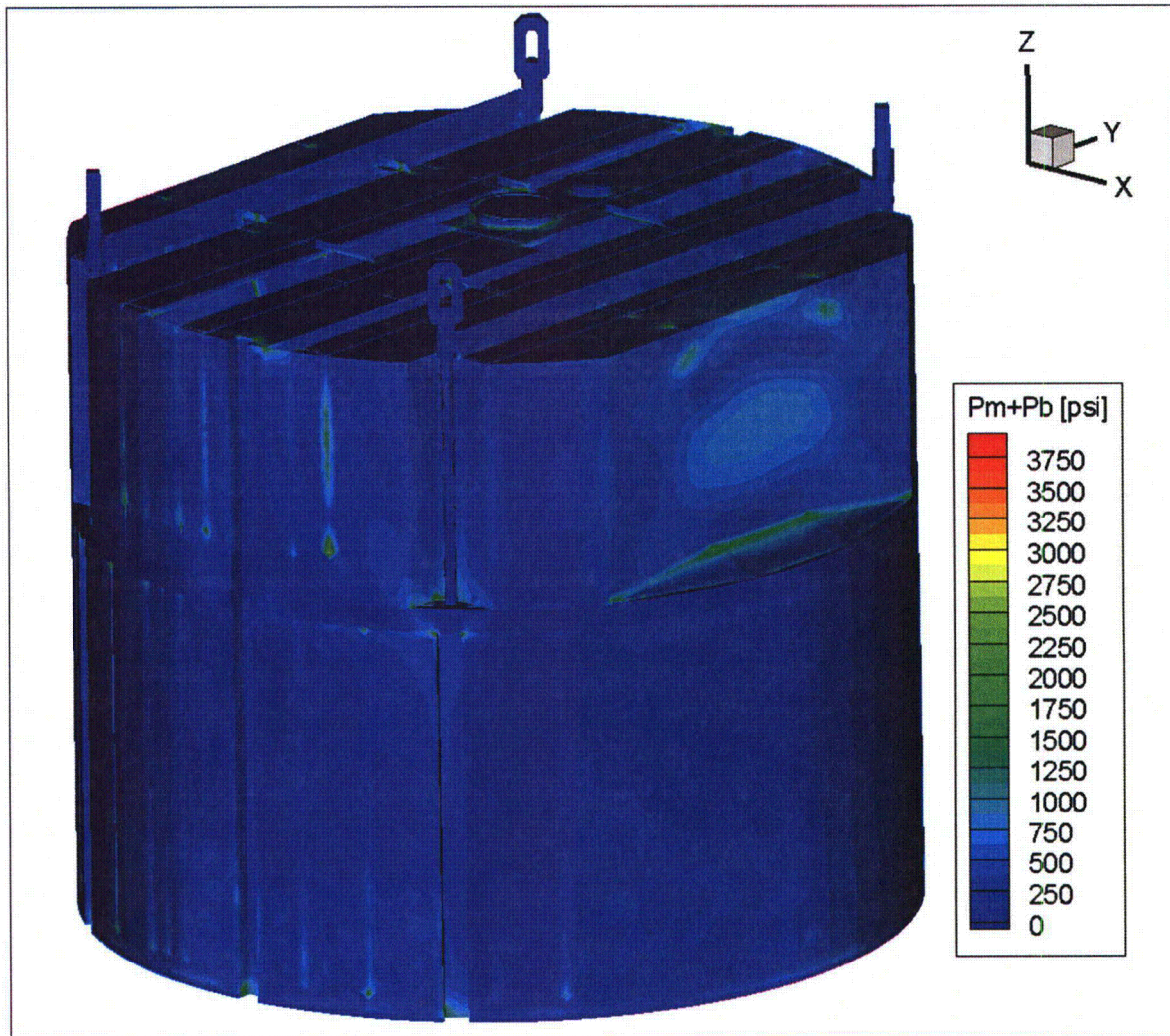


Figure 12b. Contour plot of maximum membrane+bending stress intensity, P_m+P_b , for CLTP operation with frequency shifts. The recorded stress at a node is the maximum value taken over all frequency shifts. The maximum stress intensity is 3835 psi.

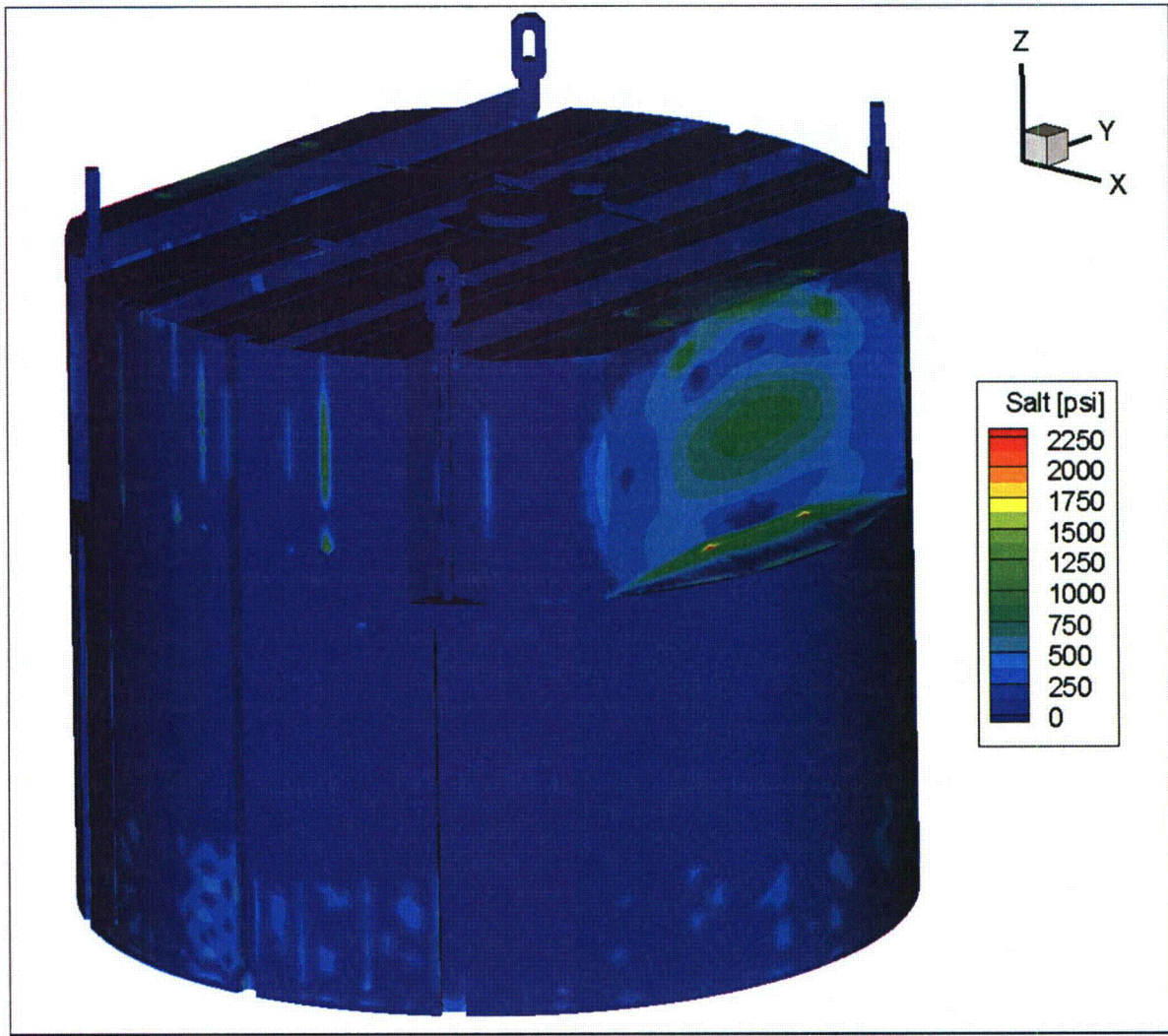


Figure 12c. Contour plot of alternating stress intensity, S_{alt} , for CLTP operation with frequency shifts. The recorded stress at a node is the maximum value taken over all frequency shifts. The maximum alternating stress intensity is 2276 psi.

5.2 Load Combinations and Allowable Stress Intensities

The stress ratios computed for CLTP at nominal frequency and with frequency shifting are listed in Table 8. The stress ratios are grouped according to type (SR-P for maximum membrane and membrane+bending stress, SR-a for alternating stress) and location (away from welds or on a weld). However, away from welds, stress ratios are everywhere above 4.0. The locations of the tabulated nodes are shown in Figure 13 (nominal frequencies) and Figure 14 (with frequency shifts included). These figures show all low stress ratio nodes (i.e., the upper bound is given by the figure legend) as well as the tabulated entries. Table 8 and the associated figures all correspond to the stresses obtained when the background noise is filtered out using the low flow data. The lowest stress ratio nodes obtained without this noise filtering are listed in Table 9.

For CLTP operation at nominal frequency the minimum stress ratio is identified as a maximum stress, SR-P=2.89, and occurs at the base of the lifting rod support as indicated in Figure 13a by label '1'. The next highest location occurs on the weld connecting the inner vane bank to the outer wall and has stress intensity, SR-P=3.55. The lowest alternating stress ratio is SR-a=3.74 and occurs at the junction between the outer hood and cover plate.

The effects of frequency shifts can be conservatively accounted for by identifying the minimum stress ratio at every node, where the minimum is taken over all the frequency shifts considered (including the nominal or 0% shift case). The resulting stress ratios are then processed as before to identify the smallest stress ratios anywhere on the structure, categorized by stress type (maximum or alternating) and location (on or away from a weld). The results are summarized in Table 8b and show that the minimum stress ratio, SR-P=2.50, is identified with a maximum stress and occurs on the inner vane bank. This is the smallest stress ratio encountered anywhere on the structure for any frequency shift at the CLTP condition. The lowest alternating stress ratio at any frequency shift lies at the same location as for the 0% shift and has the value SR-a=3.02.

Table 8a. Locations with minimum stress ratios for CLTP conditions with no frequency shift. Stress ratios are grouped according to stress type (maximum – SR-P; or alternating – SR-a) and location (away from a weld or at a weld). Bold text indicates minimum stress ratio of any type on the structure. Stress ratios away from welds are all greater than 4.0. Locations are depicted in Figure 13. Signal noise has been removed using low flow data.

Stress Ratio	Weld	Location	Location (in) ^(a)			node ^(b)	Stress Intensity (psi)			Stress Ratio	
			x	y	z		Pm	Pm+Pb	S _{alt}	SR-P	SR-a
SR-P	No	NONE (All SR-P > 4)									
SR-a	No	NONE (All SR-a > 4)									
SR-P	Yes	1. Lifting Rod Support	-50.6	77.8	0	152128	3217	3217	<250	2.89	>20
"	"	2. Inner Vane Bank (CD)	-10.8	-99.7	12	21519	2620	2620	761	3.55	9.03
"	"	3. Inner Top Cover/Rail	-11.1	95.4	61.5	141731	1336	3795	289	3.67	23.78
"	"	4. Middle Vane Bank (AB)	23.2	94.9	12	11016	2277	2277	507	4.08	13.55
"	"	5. Middle Plate/Inner Cover Plate (AB)	1.8	0	0	143461	1234	3408	<250	4.09	>20
SR-a	Yes	1. Outer Hood/Outer Cover Plate (AB)	84.8	-17	3.6	140583	307	1845	1837	7.56	3.74

See Table 6a for notes (a)-(c).

Table 8b. Locations with minimum stress ratios for CLTP conditions with frequency shifts. Stress ratios at every node are recorded as the lowest stress ratio identified during the frequency shifts. Stress ratios are grouped according to stress type (maximum – SR-P; or alternating – SR-a) and location (away from a weld or at a weld). Bold text indicates minimum stress ratio of any type on the structure. Stress ratios away from welds are all higher than 4.0. Locations are depicted in Figure 14. Signal noise has been removed using low flow data.

Stress Ratio	Weld	Location	Location (in.) ^(a)			node ^(b)	Stress Intensity (psi)			Stress Ratio		% Freq. Shift
			x	y	z		Pm	Pm+Pb	Salt	SR-P	SR-a	
SR-P	No	NONE (All SR-P > 4)										
SR-a	No	NONE (All SR-P > 4)										
SR-P	Yes	1. Inner Vane Bank (CD)	-10.8	-99.7	12	21519	3716	3716	1818	2.5	3.78	10
"	"	2. Lifting Rod Support	-50.6	77.8	0	152128	3317	3317	<250	2.8	>20	10
"	"	3. Middle Vane Bank (CD)	-23.2	-94.9	12	12560	2739	2739	1023	3.39	6.71	10
"	"	4. Middle Vane Bank (AB)	32.2	-94.9	12	13858	2738	2738	1502	3.39	4.57	10
"	"	5. Inner Top Cover/Rail	-11.1	95.4	61.5	141731	1349	3835	331	3.64	20.73	10
"	"	6. Mid Plate/Inner Cover Plate (AB)	1.8	0	0	143461	1287	3554	332	3.92	20.67	5
"	"	7. Diagonal Brace/Inner Cover Plate AB/Gusset	32.2	32.4	0	142843	1180	3509	786	3.97	8.74	10
SR-a	Yes	1. Outer Hood/Outer Cover Plate (AB)	84.8	-17	3.6	140583	341	2374	2276	5.87	3.02	10
"	"	2. Outer Top Cover (AB)/Vertical Plate Inside Hood	79.8	25.6	61.5	143720	1047	2285	2023	6.1	3.39	10
"	"	3. Inner Vane Bank (CD)	-10.8	-99.7	12	21519	3716	3716	1818	2.5	3.78	10
"	"	4. Middle Vane Bank (AB)	32.2	-94.9	12	13858	2738	2738	1502	3.39	4.57	10

See Table 6a for notes (a)-(c).

Table 9a. Minimum stress ratios at zero frequency shift for the nodes listed in Table 8a computed using the unfiltered CLTP loads (i.e., signal noise has *not* been removed). Locations are depicted in Figure 13.

Stress Ratio	Weld	Location	Location (in) ^(a)			node ^(b)	Stress Intensity (psi)			Stress Ratio	
			x	y	z		Pm	Pm+Pb	S _{alt}	SR-P	SR-a
SR-P	No	NONE (All SR-P > 4)									
SR-a	No	NONE (All SR-a > 4)									
SR-P	Yes	1. Lifting Rod Support	-50.6	77.8	0	152128	3481	3481	389	2.67	17.67
"	"	2. Inner Vane Bank (CD)	-10.8	-99.7	12	21519	4509	4509	2638	2.06	2.60
"	"	3. Inner Top Cover/Rail	-11.1	95.4	61.5	141731	1473	4179	659	3.34	10.43
"	"	4. Middle Vane Bank (AB)	23.2	94.9	12	11016	3148	3148	1413	2.95	4.86
"	"	5. Middle Plate/Inner Cover Plate (AB)	1.8	0	0	143461	1314	3630	435	3.84	15.79
SR-a	Yes	1. Outer Hood/Outer Cover Plate (AB)	84.8	-17	3.6	140583	370	2391	2293	5.83	3.00

See Table 6a for notes (a)-(c).

Table 9b. Minimum stress ratios at any frequency shift for the nodes listed in Table 8b computed using the unfiltered CLTP loads (i.e., signal noise has *not* been removed). Locations are depicted in Figure 14.

Stress Ratio	Weld	Location	Location (in.) ^(a)			node ^(b)	Stress Intensity (psi)			Stress Ratio		% Freq. Shift
			x	y	z		Pm	Pm+Pb	S _{alt}	SR-P	SR-a	
SR-P	No	NONE (All SR-P > 4)										
SR-a	No	NONE (All SR-P > 4)										
SR-P	Yes	1. Inner Vane Bank (CD)	-10.8	-99.7	12	21519	5670	5670	3881	1.64	1.77	10
"	"	2. Lifting Rod Support	-50.6	77.8	0	152128	3826	3826	756	2.43	9.09	10
"	"	3. Middle Vane Bank (CD)	-23.2	-94.9	12	12560	3915	3915	2267	2.37	3.03	10
"	"	3. Middle Vane Bank (AB)	32.2	-94.9	12	13858	4671	4671	3406	1.99	2.02	10
"	"	5. Inner Top Cover/Rail	-11.1	95.4	61.5	141731	1576	4477	1014	3.11	6.77	10
"	"	6. Mid Plate/Inner Cover Plate (AB)	1.8	0	0	143461	1465	4042	812	3.45	8.46	7.5
"	"	7. Diagonal Brace/Inner Cover Plate AB/Gusset/Diagonal Brace Ext	32.2	32.4	0	142843	1466	4492	1755	3.10	3.91	10
SR-a	Yes	1. Outer Hood/Outer Cover Plate (AB)	84.8	-17	3.6	140583	449	3016	2820	4.62	2.44	10
"	"	2. Outer Top Cover (AB)/Vertical Plate Inside Hood	79.8	25.6	61.5	143720	1287	3255	2836	4.28	2.42	10
"	"	3. Inner Vane Bank (CD)	-10.8	-99.7	12	21519	5670	5670	3881	1.64	1.77	10
"	"	4. Middle Vane Bank (AB)	32.2	-94.9	12	13858	4671	4671	3406	1.99	2.02	10

See Table 6a for notes (a)-(c).

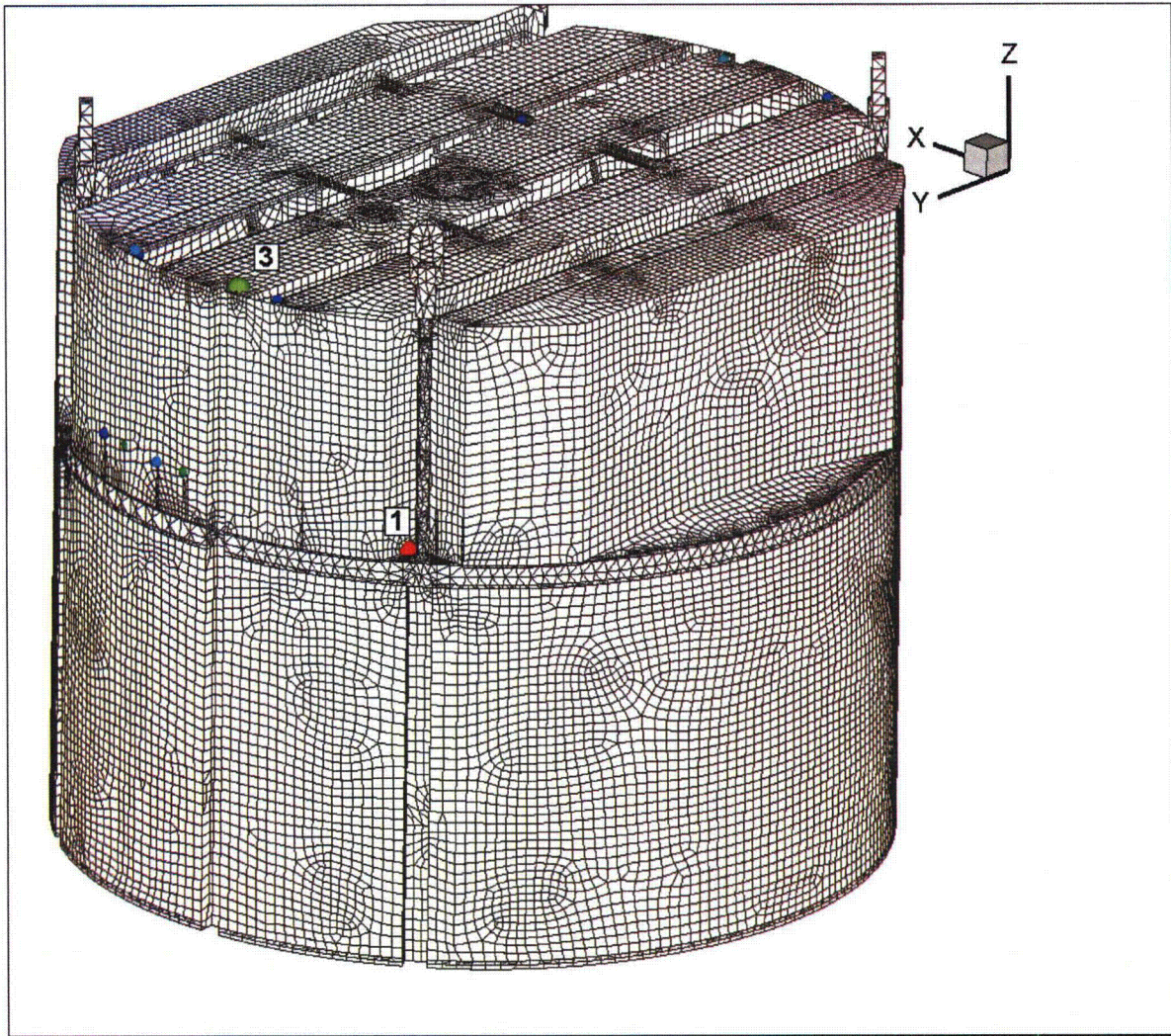


Figure 13a. Locations of smallest maximum stress ratios, $SR-P \leq 5$, at welds for nominal CLTP operation. Numbers refer to the enumerated locations for SR-P values at welds in Table 8a. First view showing locations 1 and 3.

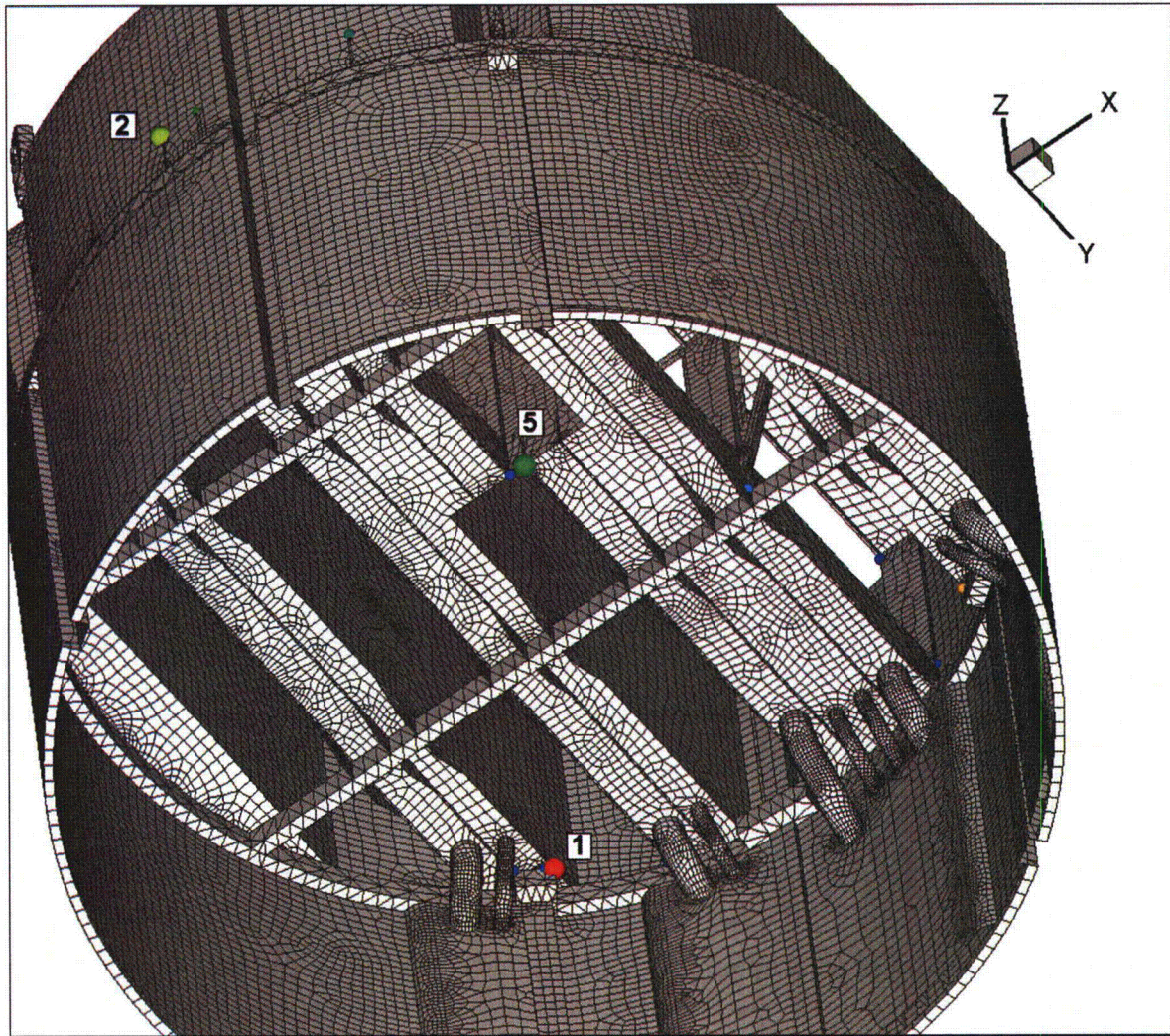


Figure 13b. Locations of smallest maximum stress ratios, $SR-P \leq 5$, at welds for nominal CLTP operation. Numbers refer to the enumerated locations for $SR-P$ values at welds in Table 8a. Second view showing locations 1-2 and 5.

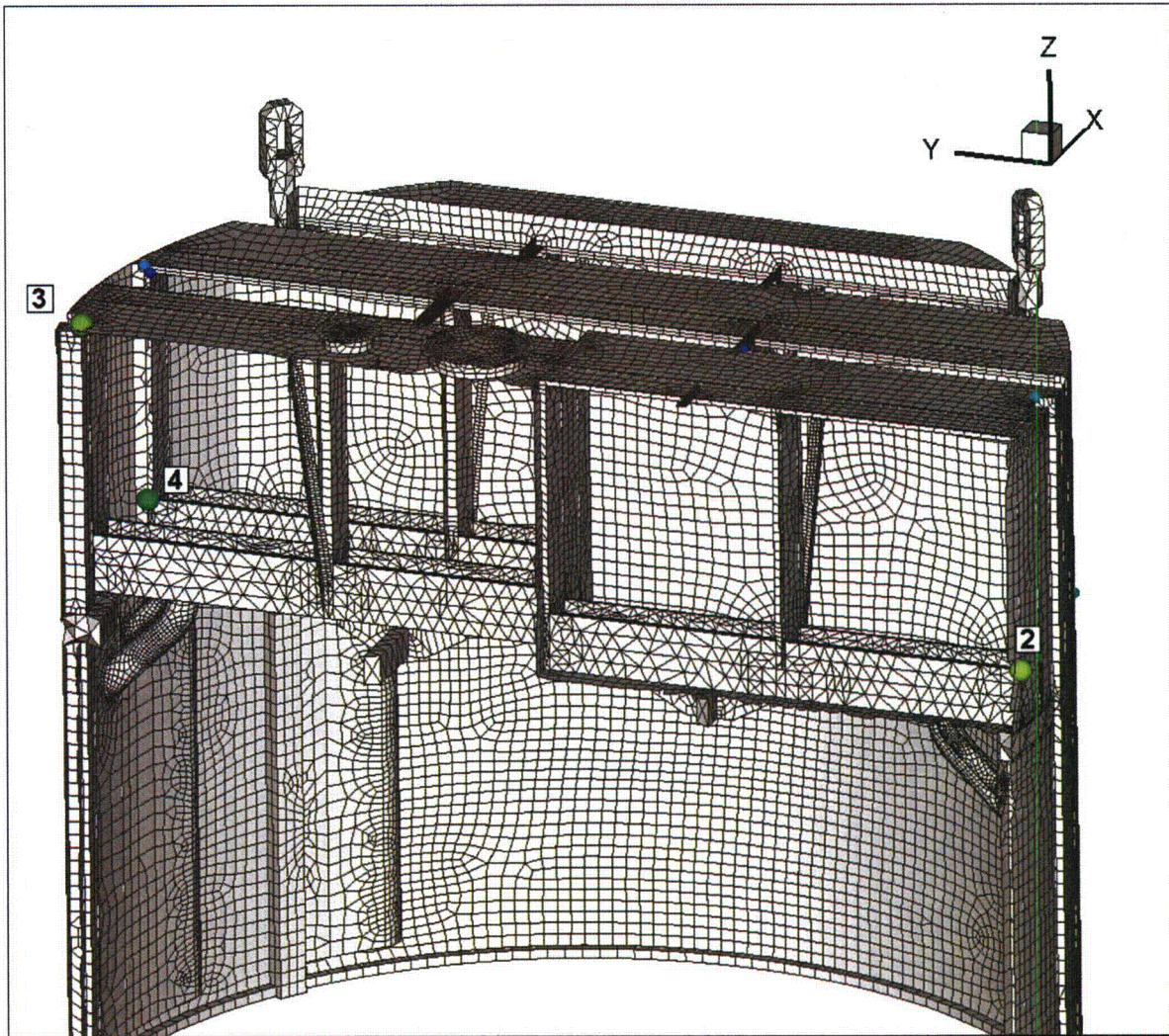


Figure 13c. Locations of smallest maximum stress ratios, $SR-P \leq 5$, at welds for nominal CLTP operation. Numbers refer to the enumerated locations for SR-P values at welds in Table 8a. Third cutaway view showing locations 2-4.

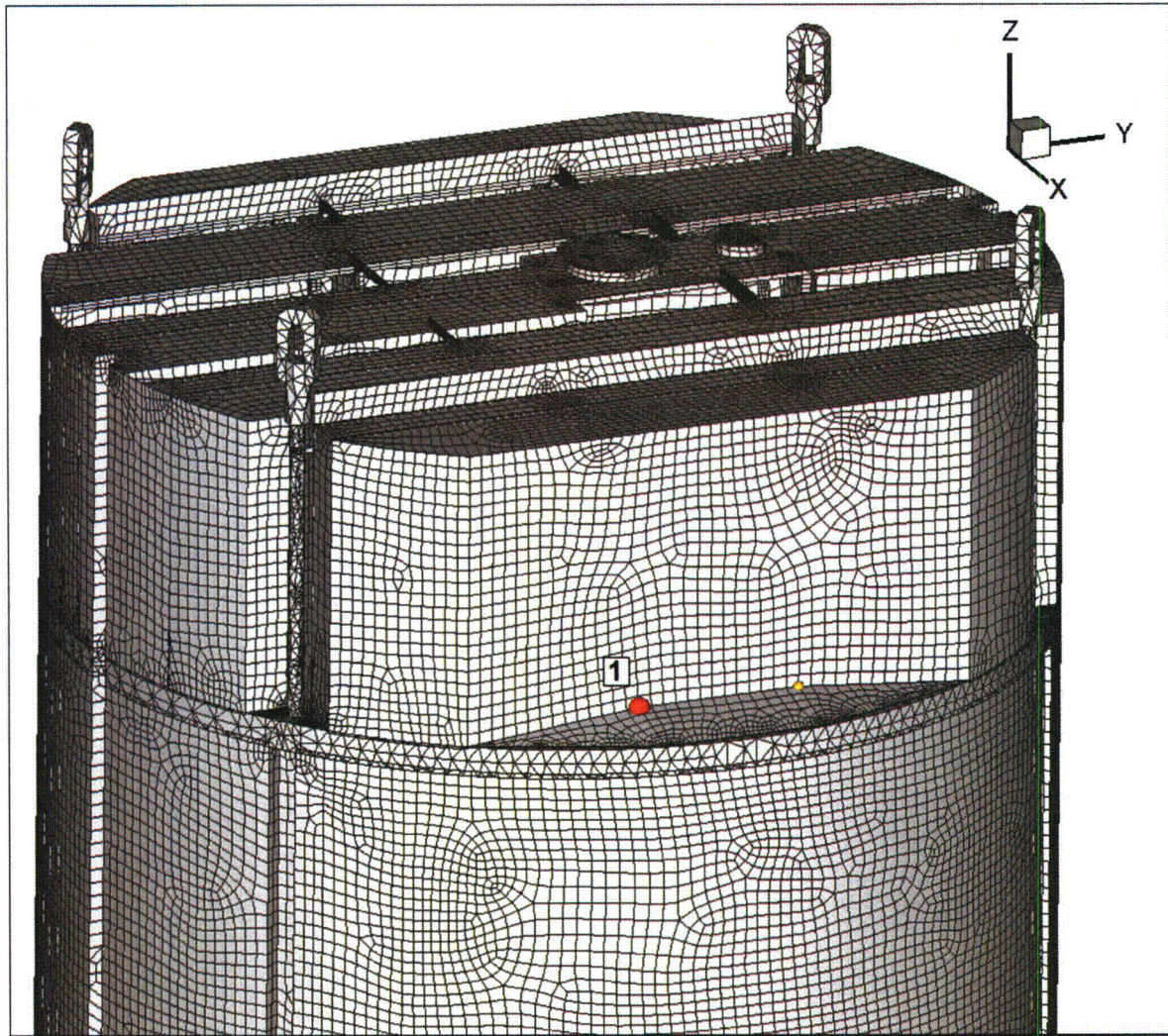


Figure 13d. Locations of smallest alternating stress ratios, $SR-a \leq 5$, at welds for nominal CLTP operation. Number refers to the enumerated location for $SR-a$ values at welds in Table 8a.

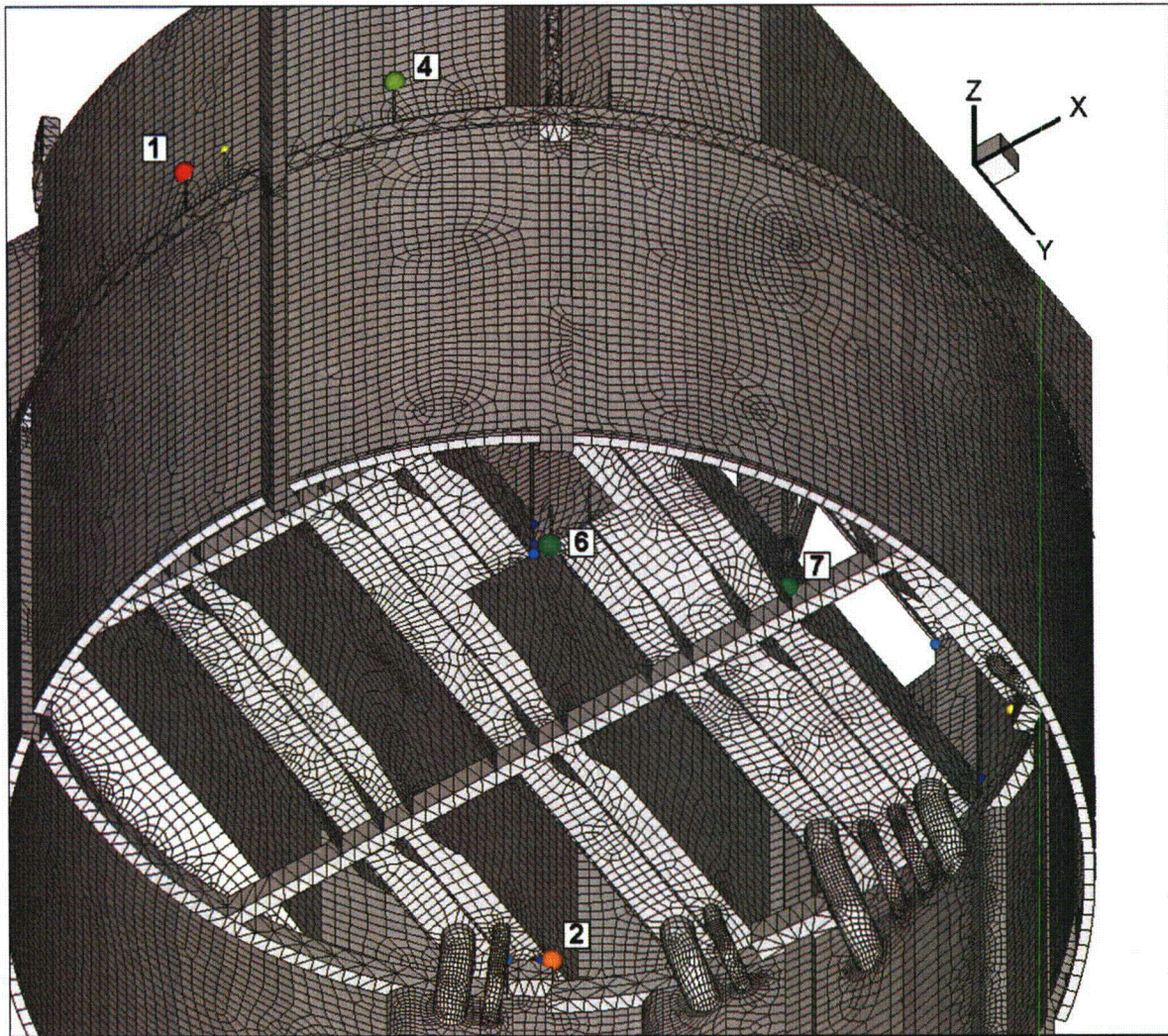


Figure 14a. Locations of minimum stress ratios, $SR-P \leq 5$, associated with maximum stress intensities at welds for CLTP operation with frequency shifts. The recorded stress ratio at a node is the minimum value taken over all frequency shifts. Numbers refer to the enumerated locations for SR-P values at welds in Table 8b. This view shows locations 1, 2, 4, 6 and 7.

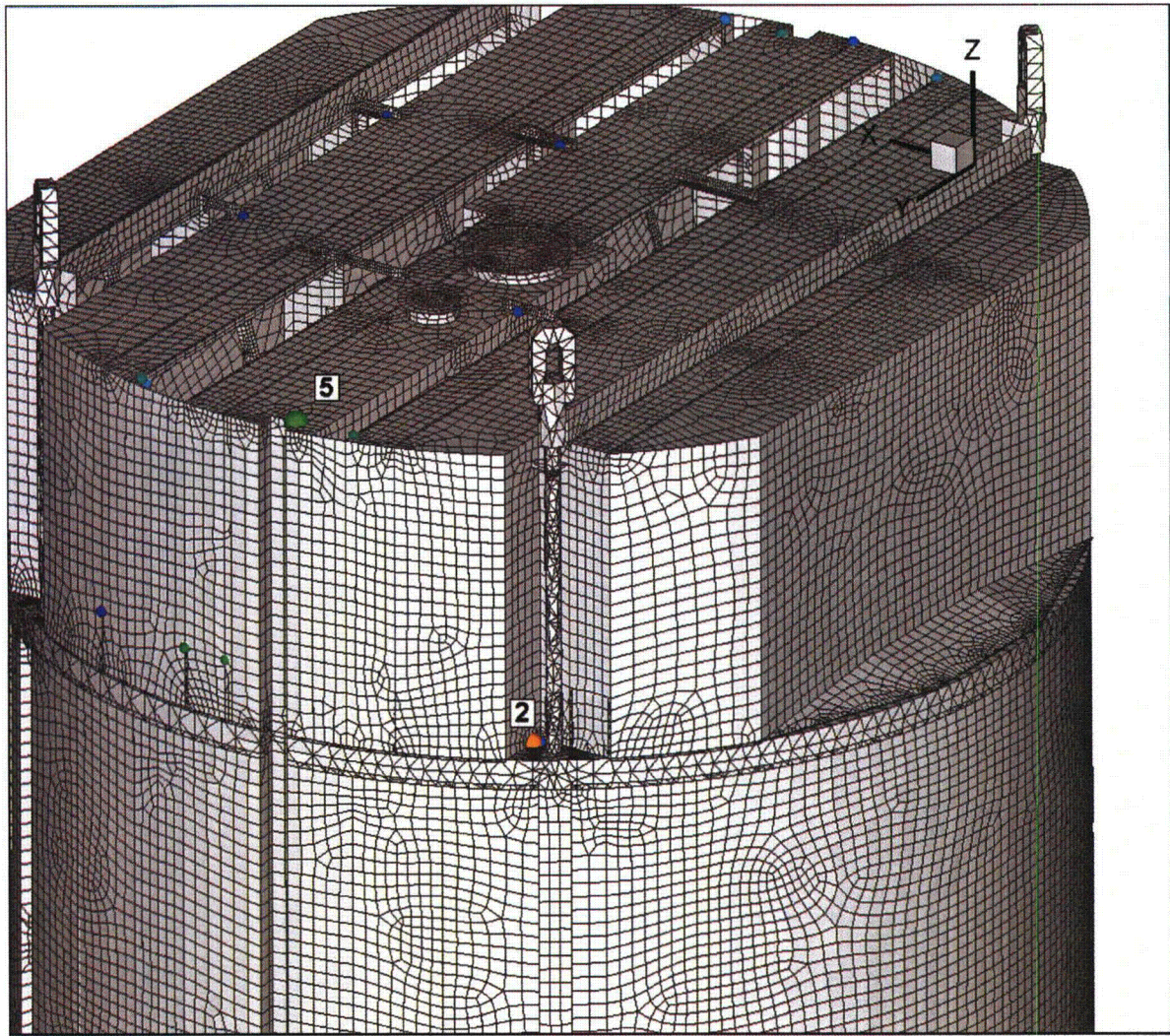


Figure 14b. Locations of minimum stress ratios, $SR-P \leq 5$, associated with maximum stress intensities at welds for CLTP operation with frequency shifts. The recorded stress ratio at a node is the minimum value taken over all frequency shifts. Numbers refer to the enumerated locations for SR-P values at welds in Table 8b. This view shows locations 2 and 5.

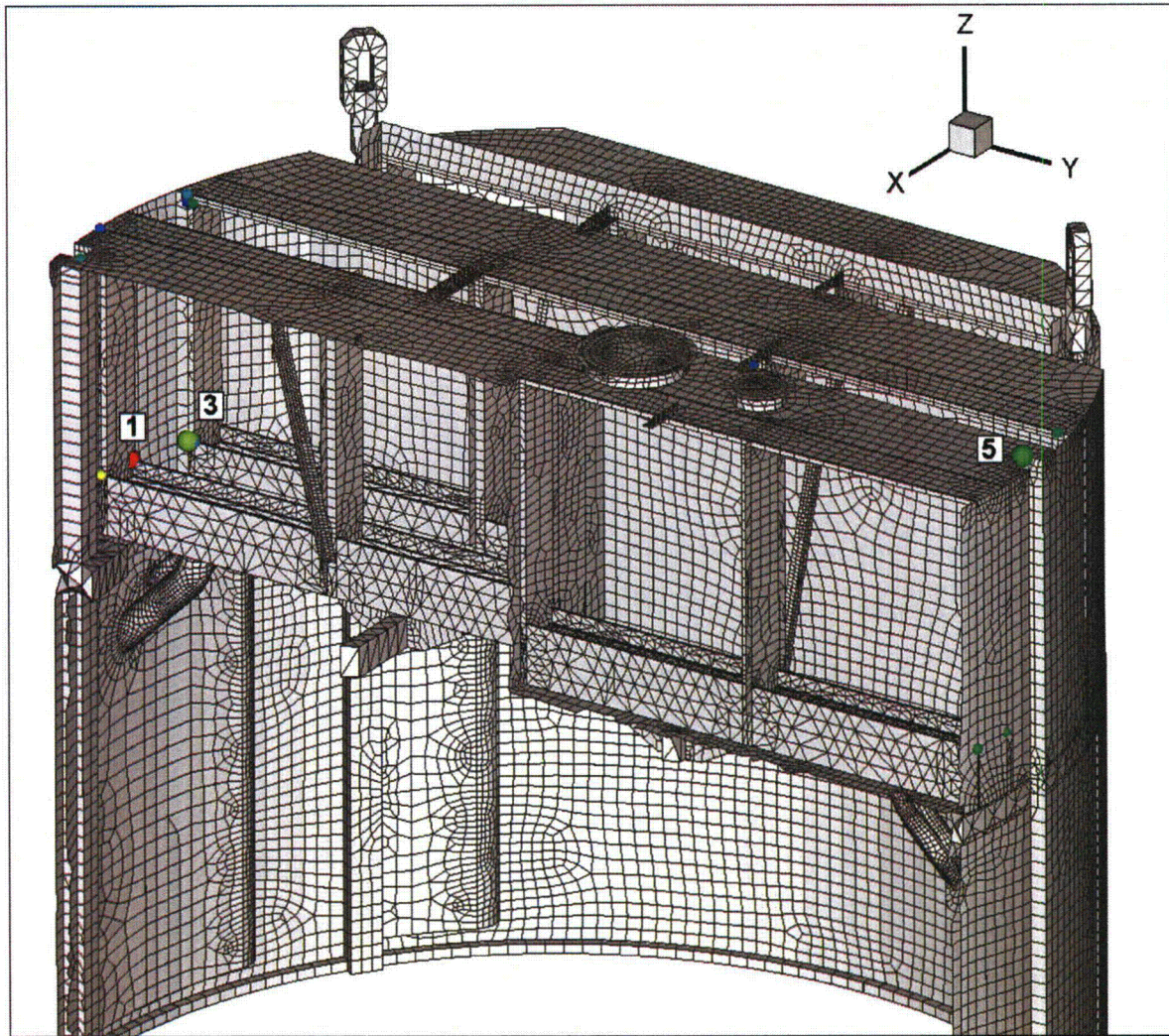


Figure 14c. Locations of minimum stress ratios, $SR-P \leq 5$, associated with maximum stress intensities at welds for CLTP operation with frequency shifts. The recorded stress ratio at a node is the minimum value taken over all frequency shifts. Numbers refer to the enumerated locations for SR-P values at welds in Table 8b. This view shows locations 1, 3 and 5.

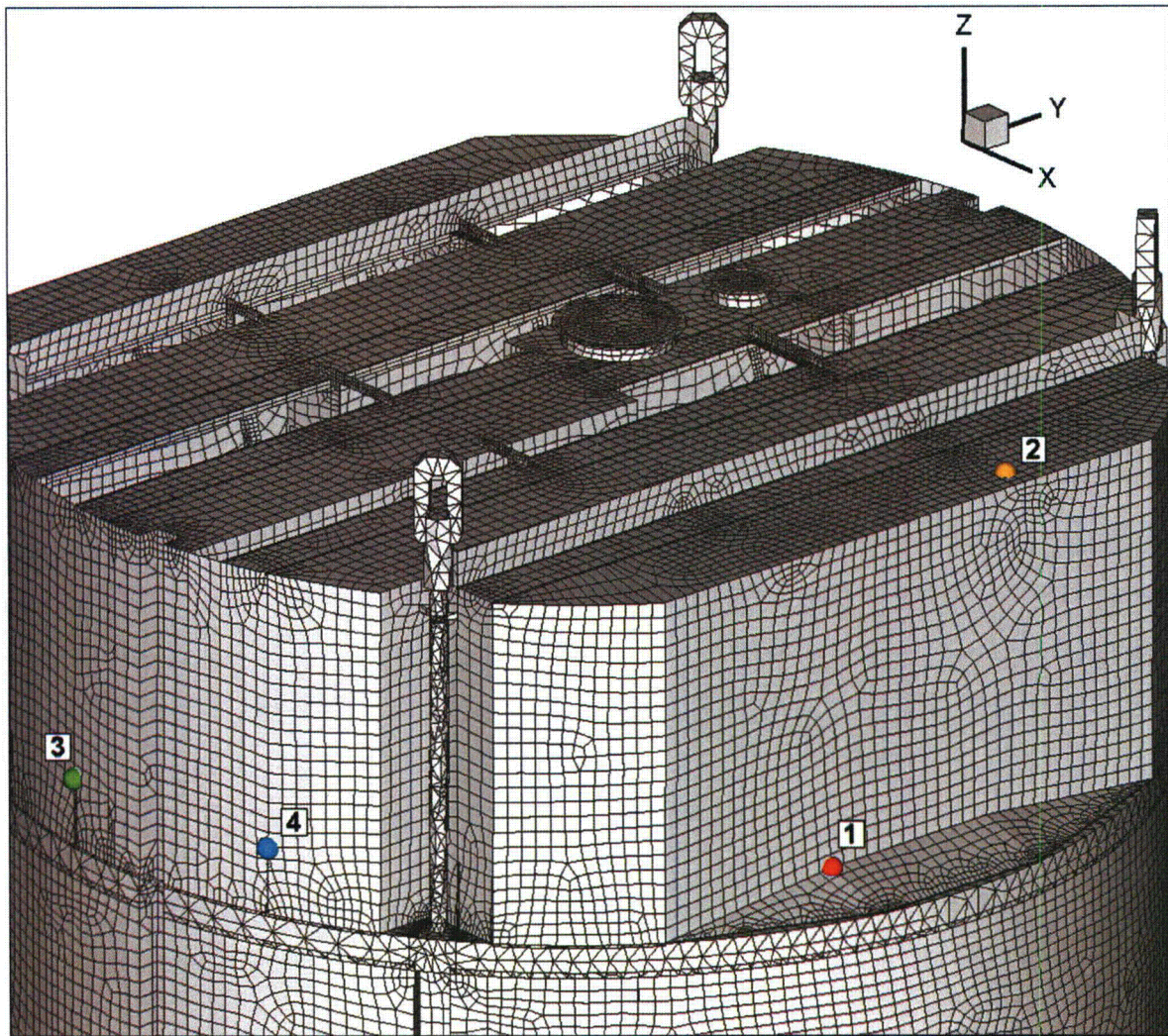


Figure 14d. Locations of minimum alternating stress ratios, $SR-a \leq 5$, at welds for CLTP operation with frequency shifts. The recorded stress ratio at a node is the minimum value taken over all frequency shifts. Numbers refer to the enumerated locations for $SR-a$ values at welds in Table 8b.

5.3 Frequency Content and Sensitivity to Frequency Shift of the Stress Signals

The stress signals contain a dominant 25-26 Hz component as well as components at 98.8 Hz and 149.6 Hz. This can be seen by examining the accumulative PSDs which are computed directly from the Fourier coefficients as

$$\Sigma(\omega_n) = \sqrt{\sum_{k=1}^n |\tilde{\sigma}(\omega_k)|^2}$$

where $\tilde{\sigma}(\omega_k)$ is the complex stress harmonic at frequency, ω_k . Accumulative PSD plots are useful for determining the frequency components and frequency ranges that make the largest contributions to the fluctuating stress. Unlike PSD plots, no “binning” or smoothing of frequency components is needed to obtain smooth curves. Steep step-like rises in $\Sigma(\omega)$ indicate the presence of a strong component at a discrete frequency whereas gradual increases in the curve imply significant content over a broader frequency range. From Parseval’s theorem, equality between $\Sigma(\omega_N)$ (where N is the total number of frequency components) and the RMS of the stress signal in the time domain is established.

Accumulative PSDs and PSD curves are plotted for the three nodes in Table 8b having the lowest alternating stress ratios. These are:

- Node 140583 – this node lies on the junction between the outer hood and the crease in the outer cover plate on the MSL AB side. The associated PSDs are shown in Figure 15a.
- Node 143720 – this node lies on junction of the vertical plate that lies at the end of one of the diagonal support braces and the outer hood top cover plate. The associated PSDs are shown in Figure 15b.
- Node 21519 – this node lies on an inner vane bank weld. The associated PSDs are shown in Figure 15c.

In each case, since there are six stress components and up to three different section locations for shells (the top, mid and bottom surfaces), there is a total of 18 stress histories per component. Moreover, at junctions there are at least two components that meet at the junction. The particular stress component that is plotted is chosen as follows. First, the component and section location (top/mid/bottom) is taken as the one that has the highest alternating stress. This narrows the selection to six components. Of these, the component having the highest Root Mean Square (RMS) is selected.

The accumulative PSD and the PSD are plotted at zero frequency shift and the frequency shift producing the highest alternating stress intensity. For the first two nodes, a large rise is observed over the 25-26 Hz frequency range (the peak in the PSD occurs at 25.7 Hz). Shifting the load frequencies from 0% to +10% does not significantly alter the response frequency. This means that essentially the same structural modes are being excited at this location. Moreover, it implies that the load spectrum is sufficiently broad about this frequency that significant excitation occurs at both the 0% and 10% shifts. For the second node, 143720, the plot differs

both in terms of the characteristic response frequency (approximately 108.7 Hz) and also the relative change in response amplitude between the 0% and +10% frequency shifts. Shifting the frequency to +10% gives rise to a dominant peak that is completely absent in the zero shift case. This is indicative of a narrow band or 'spike' in the load spectrum at about 98.5 Hz (this produces the 108.4 Hz peak after the +10% shift) that when appropriately shifted strongly couples to the structure and excites the observed structural response. Finally for the third node, 21519, the dominant response peak occurs at 149.7 Hz at the +10% shift, corresponding to a 136.1 Hz signal in the non-shifted case. As with the second node, frequency shifting produces a markedly different response spectrum about this frequency.

Further insight into the modal response can be obtained by examining how the maximum and alternating stress intensities of selected nodes vary with frequency shift. This evaluation is made in Figure 16 for the same three nodes having the lowest stress ratios. To generate these plots the frequency shifts are made in 0.5% increments thus achieving a finer resolution than for the 2.5% increments used to evaluate all the nodes. (This highlights another a useful advantage of the harmonic approach since, once the unit solution stresses are computed, the stress response at any shifted frequency can be easily and quickly evaluated thus allowing this higher resolution - in frequency shift - plot to be obtained in a few minutes. In a time-domain approach each frequency shift entails a complete finite element time simulation requiring days to weeks of computation time.)

These plots show that the highest alternating stress intensities, and therefore the lowest alternating stress ratio for these nodes all occur at the +10% shift. In each case the difference between the maximum and alternating stress intensities is representative of the static stress contribution. The variations in alternating stress intensity for the three nodes are 1039 psi (node 140583), 1164 psi (node 14370) and 1235 psi (node 21519). These are large variations. Though it is unlikely that the FEA modal frequency errors are this large (i.e., +10%), one is nevertheless forced to use the stress intensity values at this shift strongly suggesting that considerable conservatism is implicitly built into the frequency shifting approach.

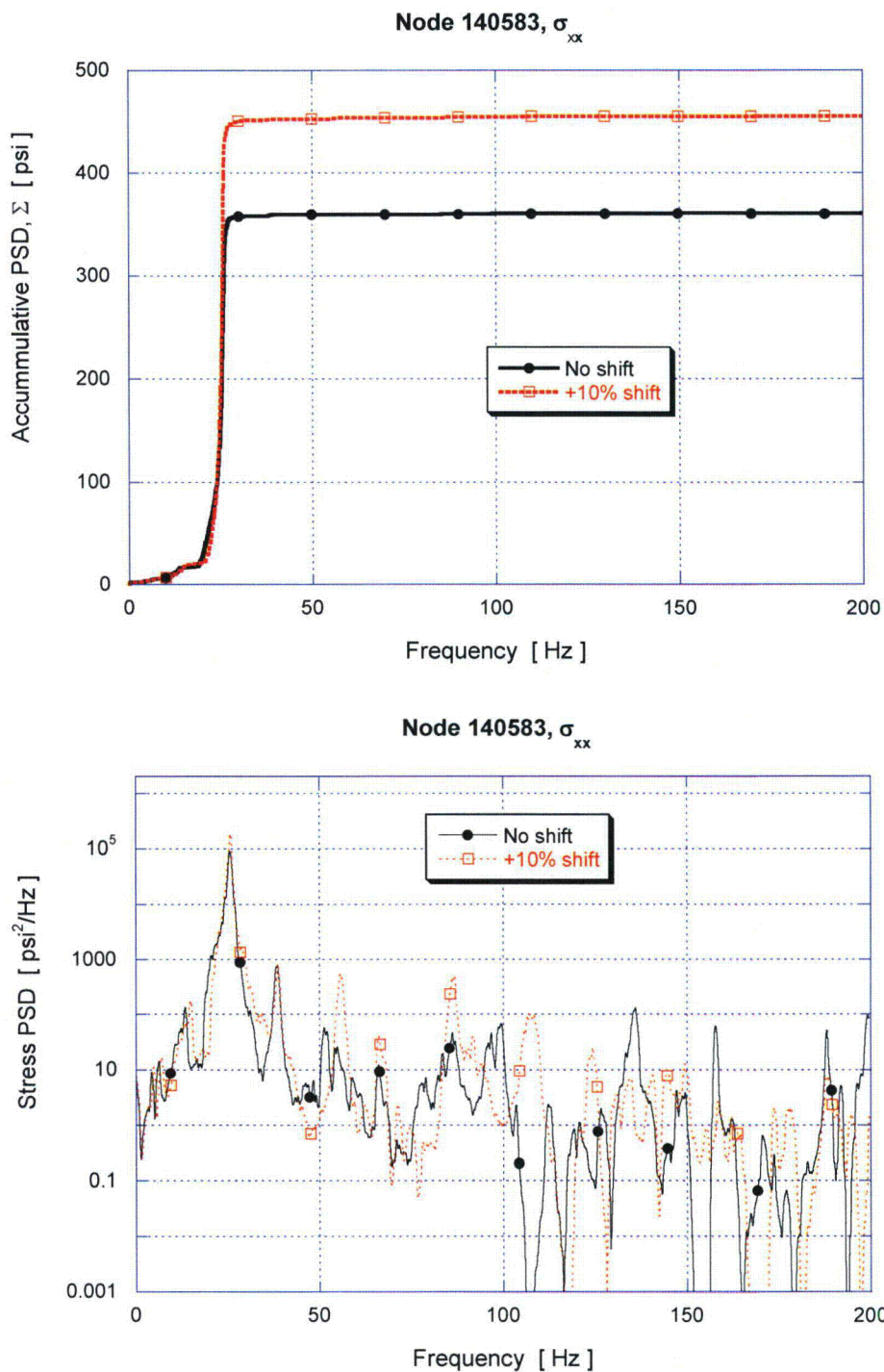


Figure 15a. Accumulative PSD and PSD of the σ_{xx} stress response at node 140583 for CLTP operation at zero and +10% frequency shifts.

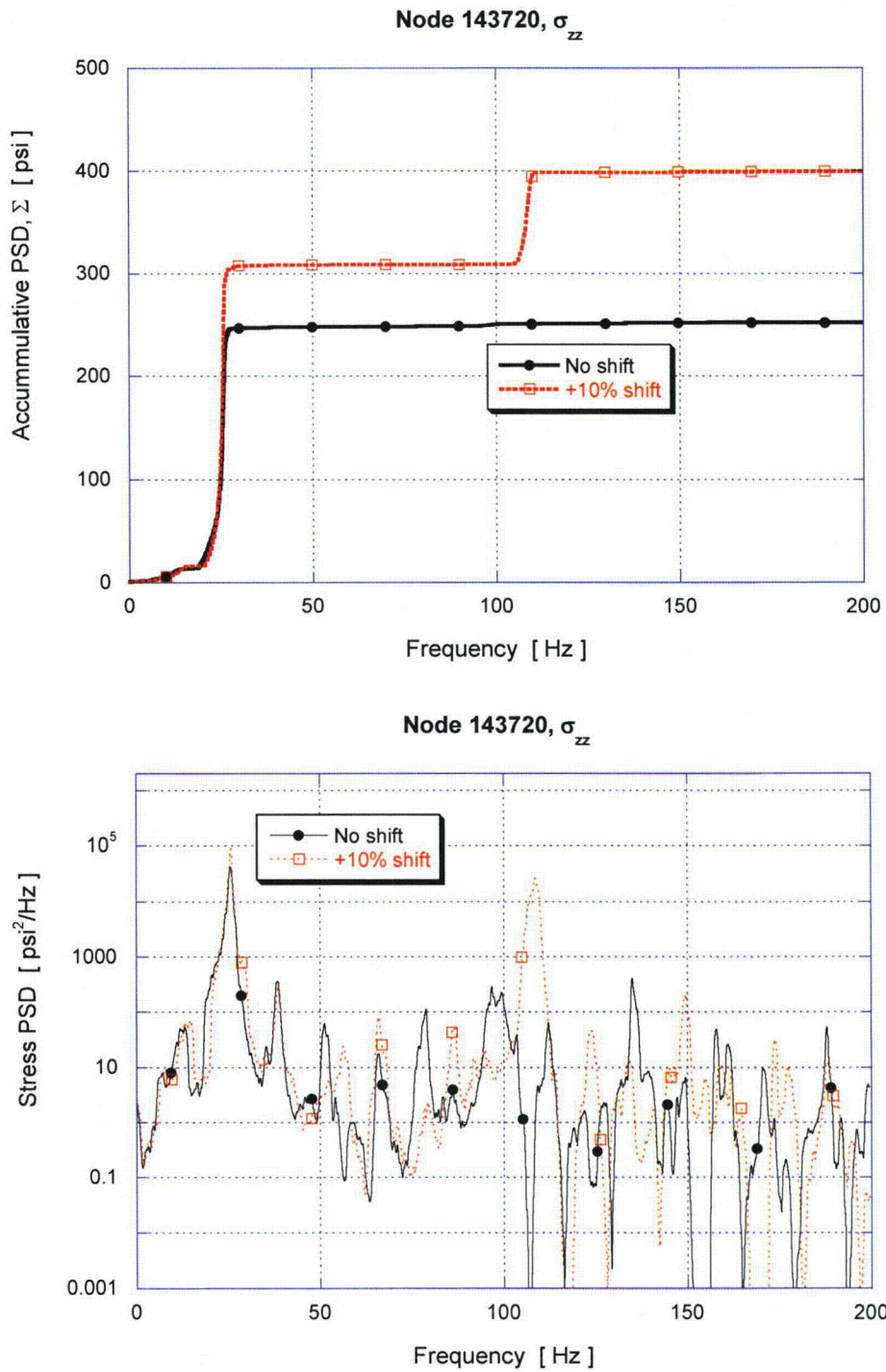


Figure 15b. Accumulative PSD and PSD of the σ_{zz} stress response at node 143720 for CLTP operation at zero and +10% frequency shifts.

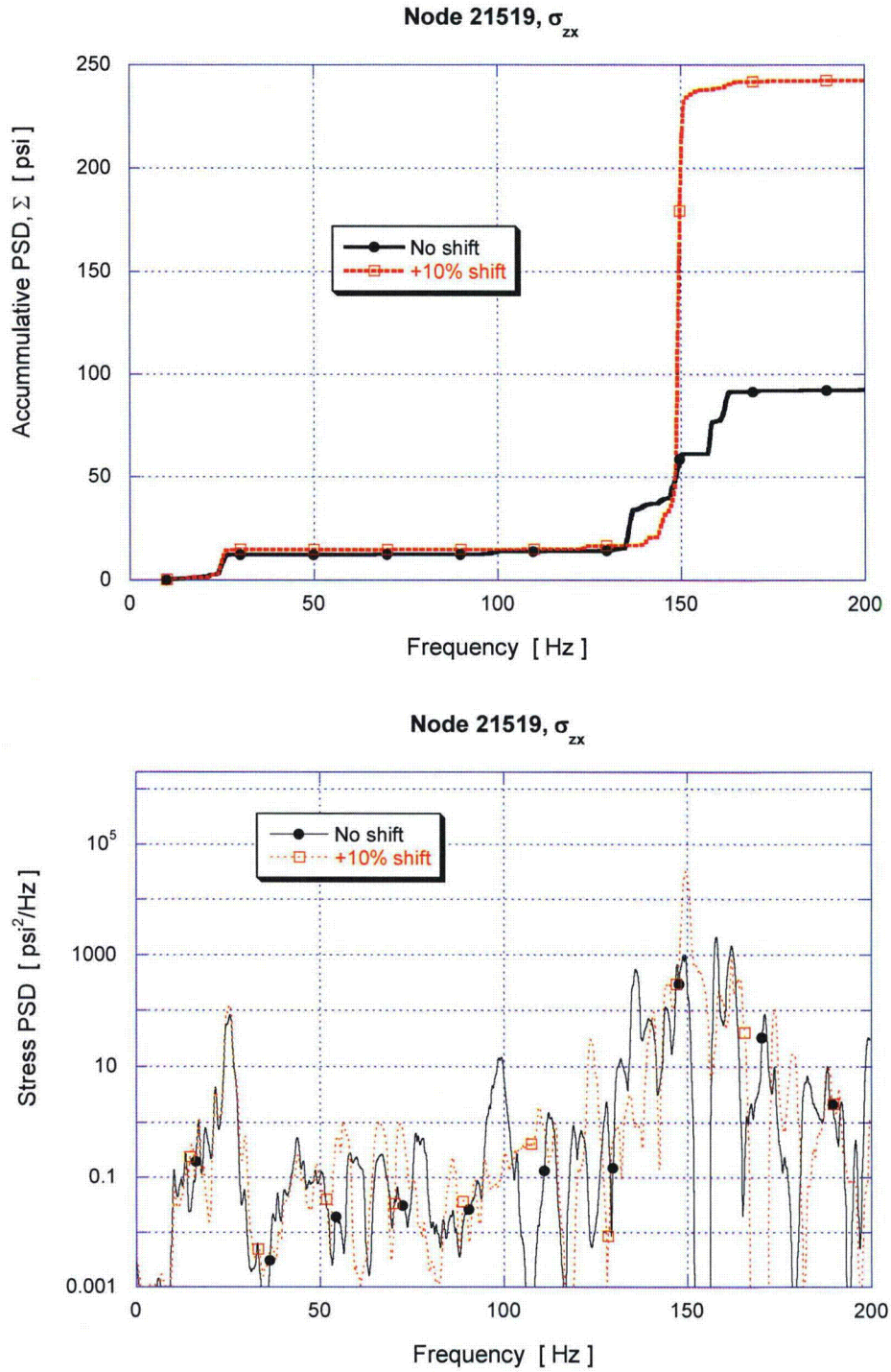


Figure 15c. Accumulative PSD and PSD of the σ_{zx} stress response at node 21519 for CLTP operation at zero and +10% frequency shifts.

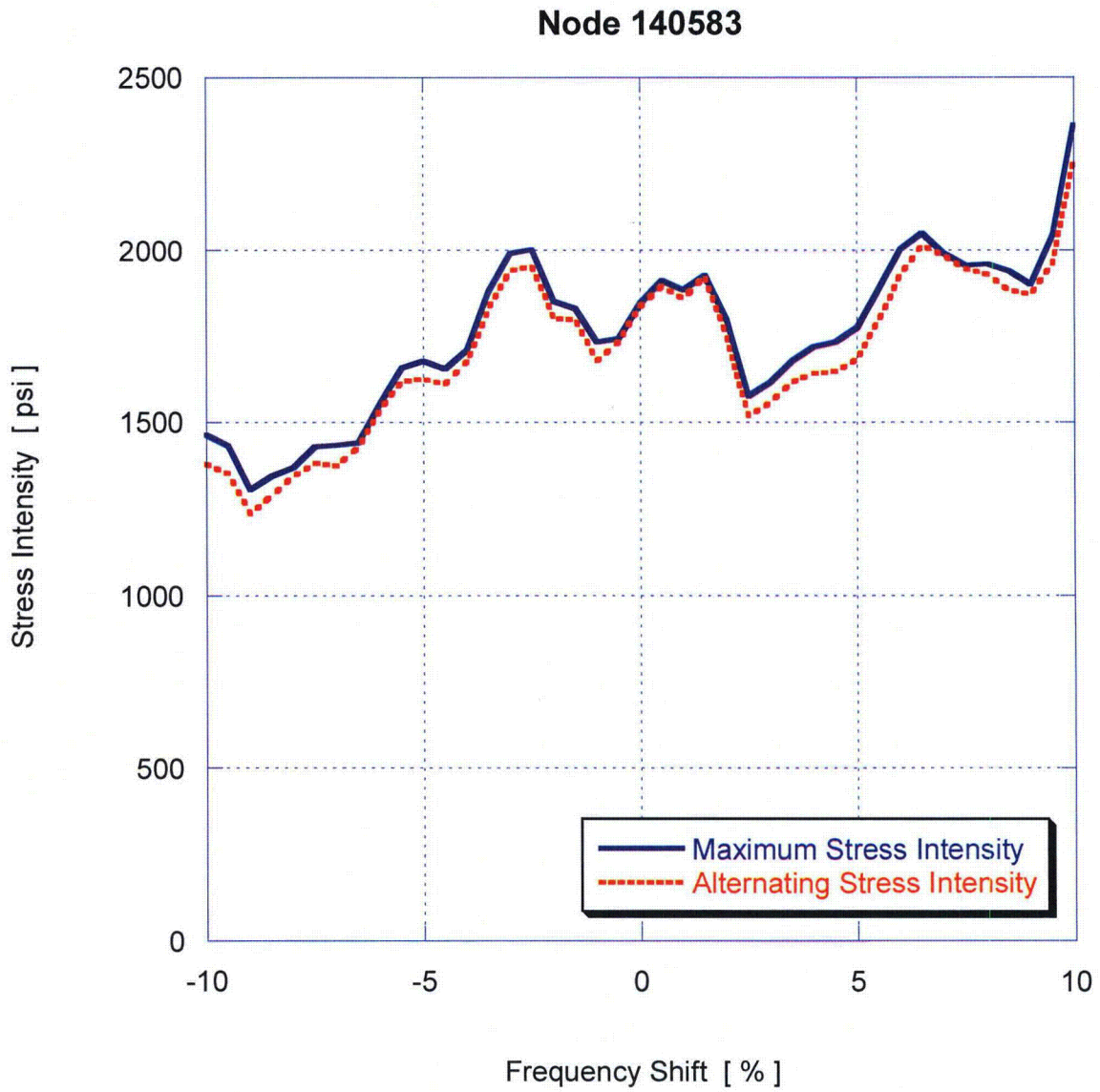


Figure 16a. Variation of maximum and alternating stress intensities with frequency shift for node 140583.

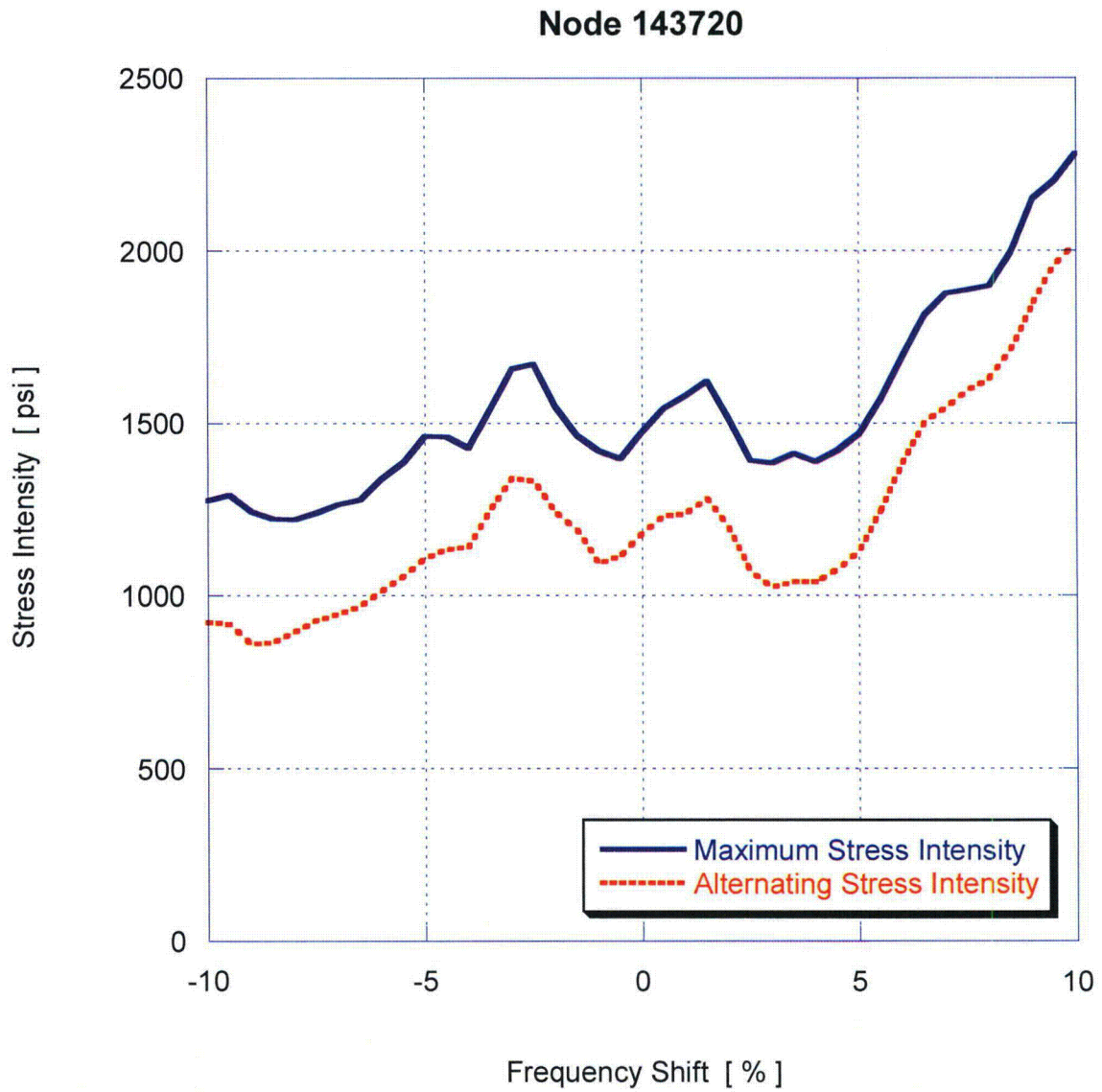


Figure 16b. Variation of maximum and alternating stress intensities with frequency shift for node 143720.

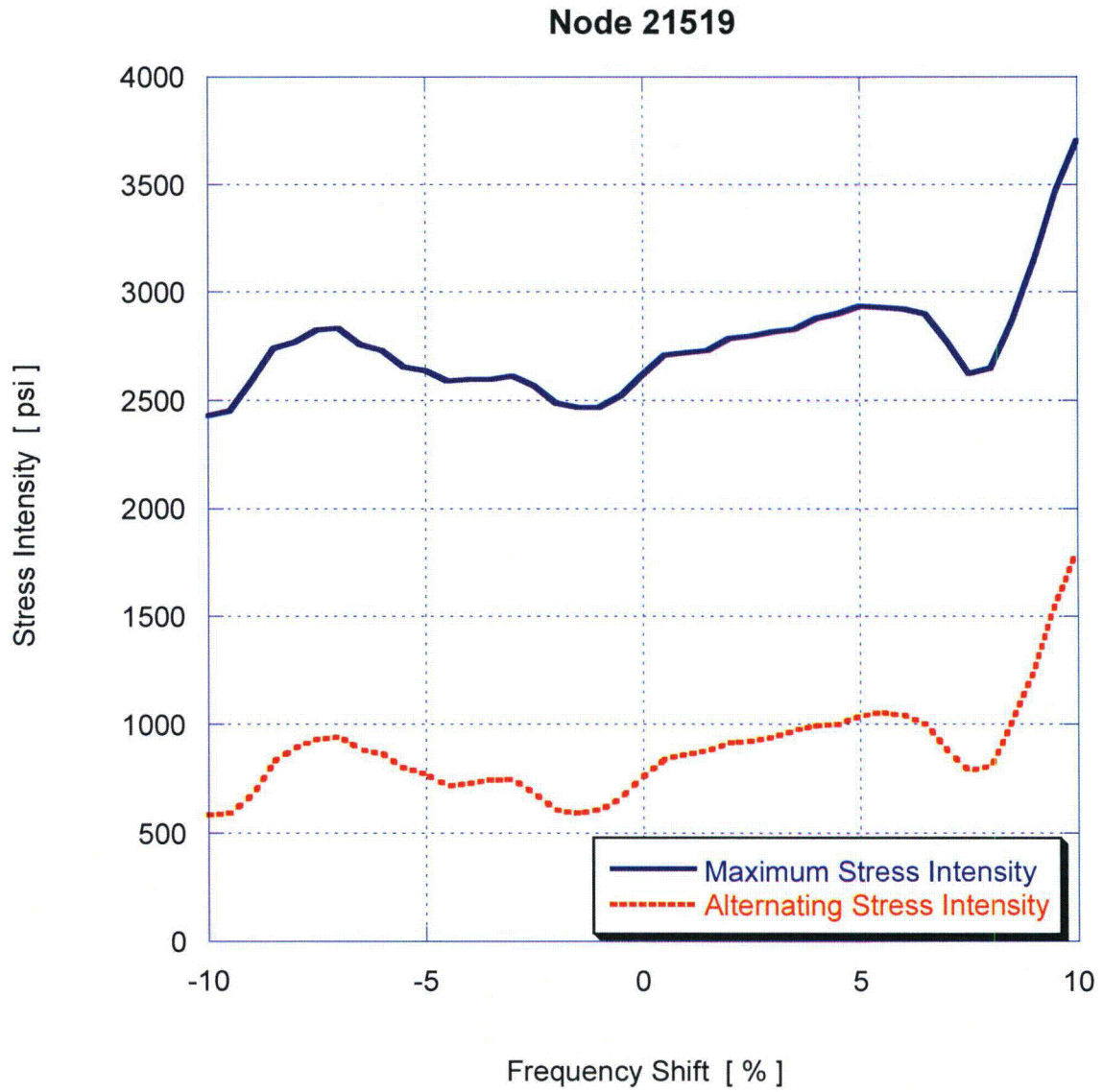


Figure 16c. Variation of maximum and alternating stress intensities with frequency shift for node 21519.

[[
[[⁽³⁾]]

⁽³⁾]]

[[

⁽³⁾]]

Table 10a. Locations with minimum stress ratios at no shift for EPU conditions with low flow load-based noise filtered. Stress ratios at every node are recorded as the lowest stress ratio identified during the frequency shifts. Stress ratios are grouped according to stress type (maximum – SR-P; or alternating – SR-a) and location (away from a weld or at a weld). Bold text indicates minimum stress ratio of any type on the structure.

Stress Ratio	Weld	Location	Location (in.)			node	Stress Intensity (psi)			Stress Ratio	
			x	y	z		Pm	Pm+Pb	S _{alt}	SR-P	SR-a
SR-P	No	NONE (All SR-P > 4)									
SR-a	No	NONE (All SR-a > 4)									
SR-P	Yes	1. Inner Vane Bank CD	-10.8	-99.7	12	21519	3385	3385	1496	2.75	4.59
"	"	2. Lifting Rod Support	-50.6	77.8	0	152128	3266	3266	>250	2.85	>20
"	"	3. Middle Vane Bank AB	32.2	-94.9	12	13858	2920	2920	1690	3.18	4.06
"	"	4. Inner Top Cover/Rail	-11.1	95.4	61.5	141731	1404	3989	492	3.5	13.96
"	"	5. Middle Plate/Inner Cover Plate AB	1.8	0	0	143461	1264	3491	274	3.99	25.08
"	"	6. Top Vane Bank Bar	23.2	94.9	61.5	6185	2212	2212	516	4.2	13.31
SR-a	Yes	1. Outer Hood CD/Outer Cover Plate AB	84.8	-17	3.6	140583	382	2449	2443	5.69	2.81
"	"	2. Middle Vane Bank AB	32.2	-94.9	12	13858	2920	2920	1690	3.18	4.06
"	"	3. Outer Top Cover AB/Vertical Plate Inside Hood	79.8	-25.6	61.5	140248	1049	2051	1683	6.8	4.08
"	"	4. Inner Vane Bank CD	-10.8	-99.7	12	21519	3385	3385	1496	2.75	4.59
"	"	5. Outer Hood AB/Outer Cover Plate AB	84.8	-6.5	3.6	140578	139	1506	1439	9.26	4.77

See Table 6a for coordinates description.

Table 10b. Locations with minimum stress ratios with frequency shifts for EPU conditions with low flow load-based noise filtered. Stress ratios at every node are recorded as the lowest stress ratio identified during the frequency shifts. Stress ratios are grouped according to stress type (maximum – SR-P; or alternating – SR-a) and location (away from a weld or at a weld). Bold text indicates minimum stress ratio of any type on the structure.

Stress Ratio	Weld	Location	% Freq. Shift	Location (in.)			node	Stress Intensity (psi)			Stress Ratio	
				x	y	z		Pm	Pm+Pb	S _{alt}	SR-P	SR-a
SR-P	No	NONE (All SR-P > 4)										
SR-a	No	NONE (All SR-P > 4)										
SR-P	Yes	1. Inner Vane Bank CD	-10.8	-99.7	12	21519	4570	4570	2674	2.03	2.57	10
"	"	2. Lifting Rod Support	-50.6	77.8	0	152128	3421	3421	334	2.72	20.58	10
"	"	3. Middle Vane Bank AB	32.2	-94.9	12	13858	3400	3400	2168	2.73	3.17	-10
"	"	4. Inner Top Cover/Rail	-11.1	95.4	61.5	141731	1420	4033	534	3.46	12.86	-2.5
"	"	5. Side Plate/Side Plate Turn	-23.2	-93.7	60	143143	2618	2929	1327	3.55	5.18	-7.5
"	"	6. Top Vane Bank Bar	-23.2	94.9	61.5	9031	2584	2584	1058	3.6	6.49	10
"	"	7. Diagonal Brace/Inner Cover Plate AB/Gusset	32.2	32.4	0	142843	1280	3843	1148	3.63	5.98	10
SR-a	Yes	1. Outer Hood/Outer Cover Plate AB	84.8	-17	3.6	140583	434	3117	3015	4.47	2.28	10
"	"	2. Outer Top Cover AB/Vertical Plate Inside Hood	79.8	-25.6	61.5	140248	1349	3134	2744	4.45	2.5	10
"	"	3. Inner Vane Bank CD	-10.8	-99.7	12	21519	4570	4570	2674	2.03	2.57	10
"	"	4. Middle Vane Bank AB	32.2	-94.9	12	13858	3400	3400	2168	2.73	3.17	-10
"	"	5. Middle Hood AB/Vertical Plate Inside Hood	50.8	32.4	54.5	140221	1007	2113	1835	6.6	3.74	10
"	"	6. Outer Hood AB/Outer Cover Plate A B	84.8	-1.3	3.6	140581	150	1907	1777	7.31	3.87	10
"	"	7. Vertical Angle/Diagonal Brace	68.2	-25.6	13.8	143500	1224	2267	1742	6.15	3.94	10

See Table 6a for coordinates description.

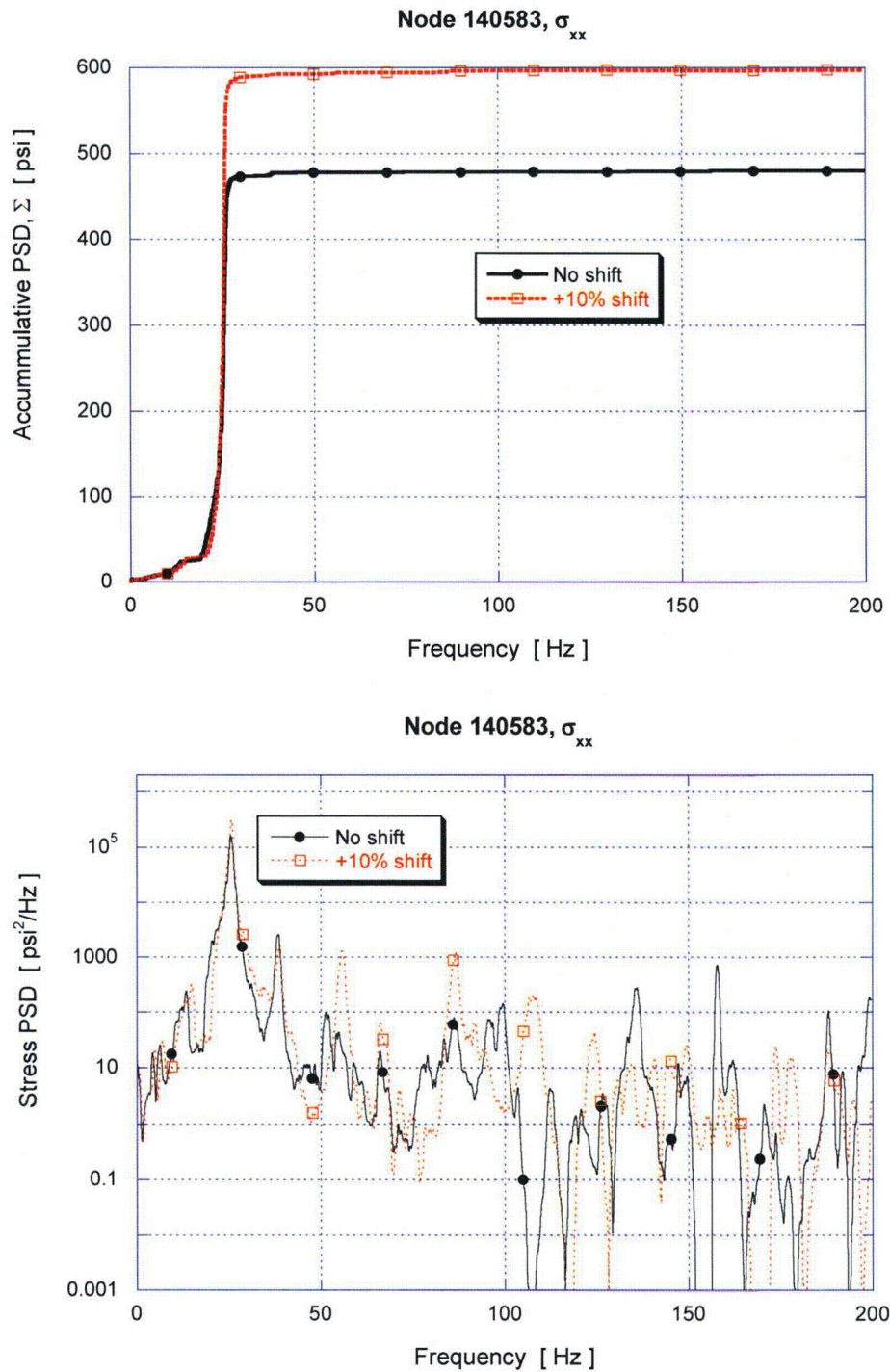


Figure 17a. Accumulative PSD and PSD of the σ_{xx} stress response at node 140583 for EPU operation at zero and +10% frequency shifts.

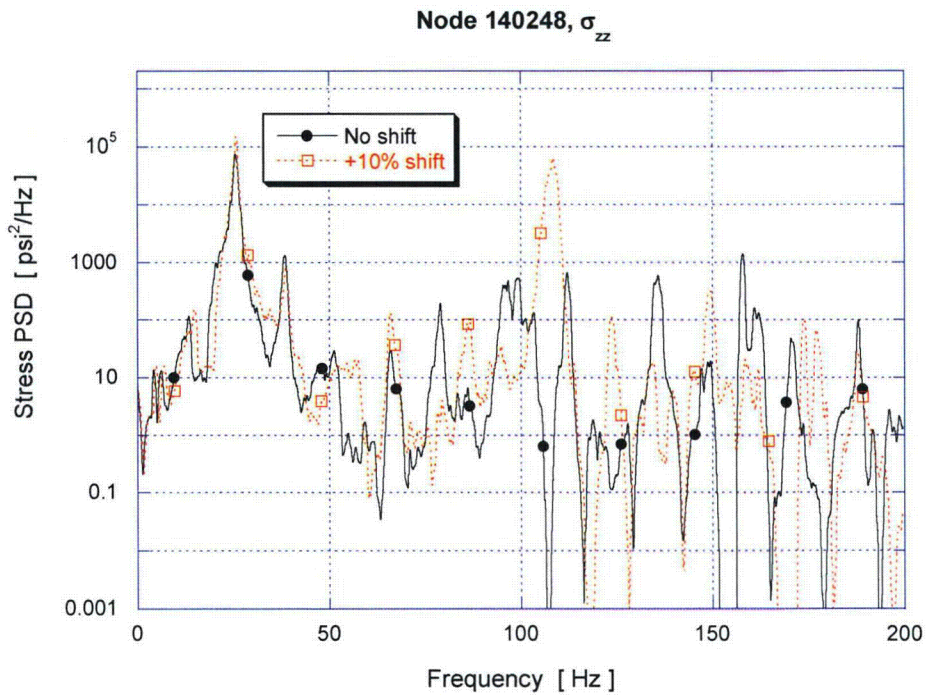
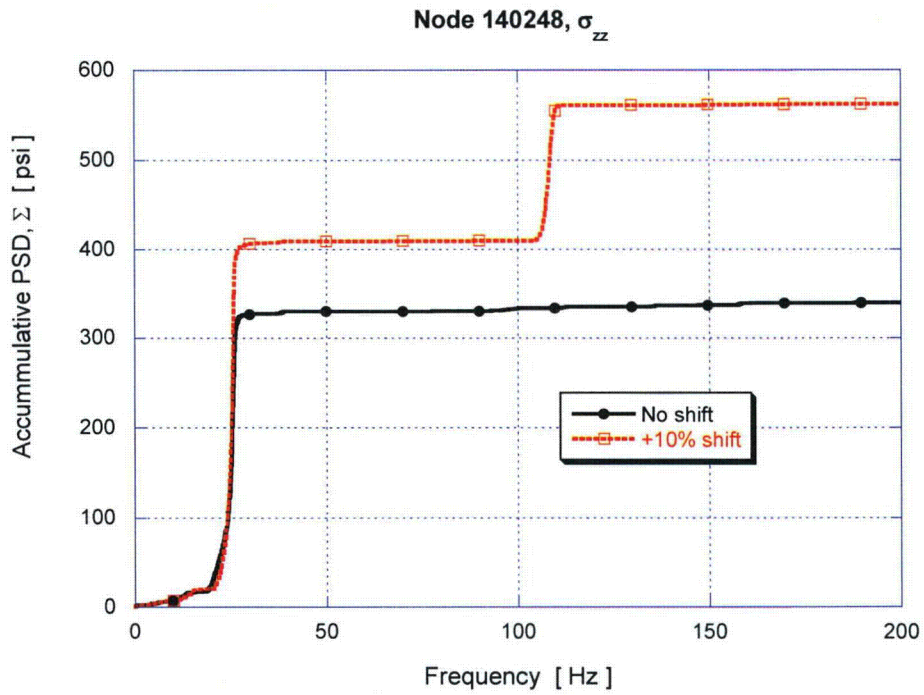


Figure 17b. Accumulative PSD and PSD of the σ_{zz} stress response at node 140248 for EPU operation at zero and +10% frequency shifts.

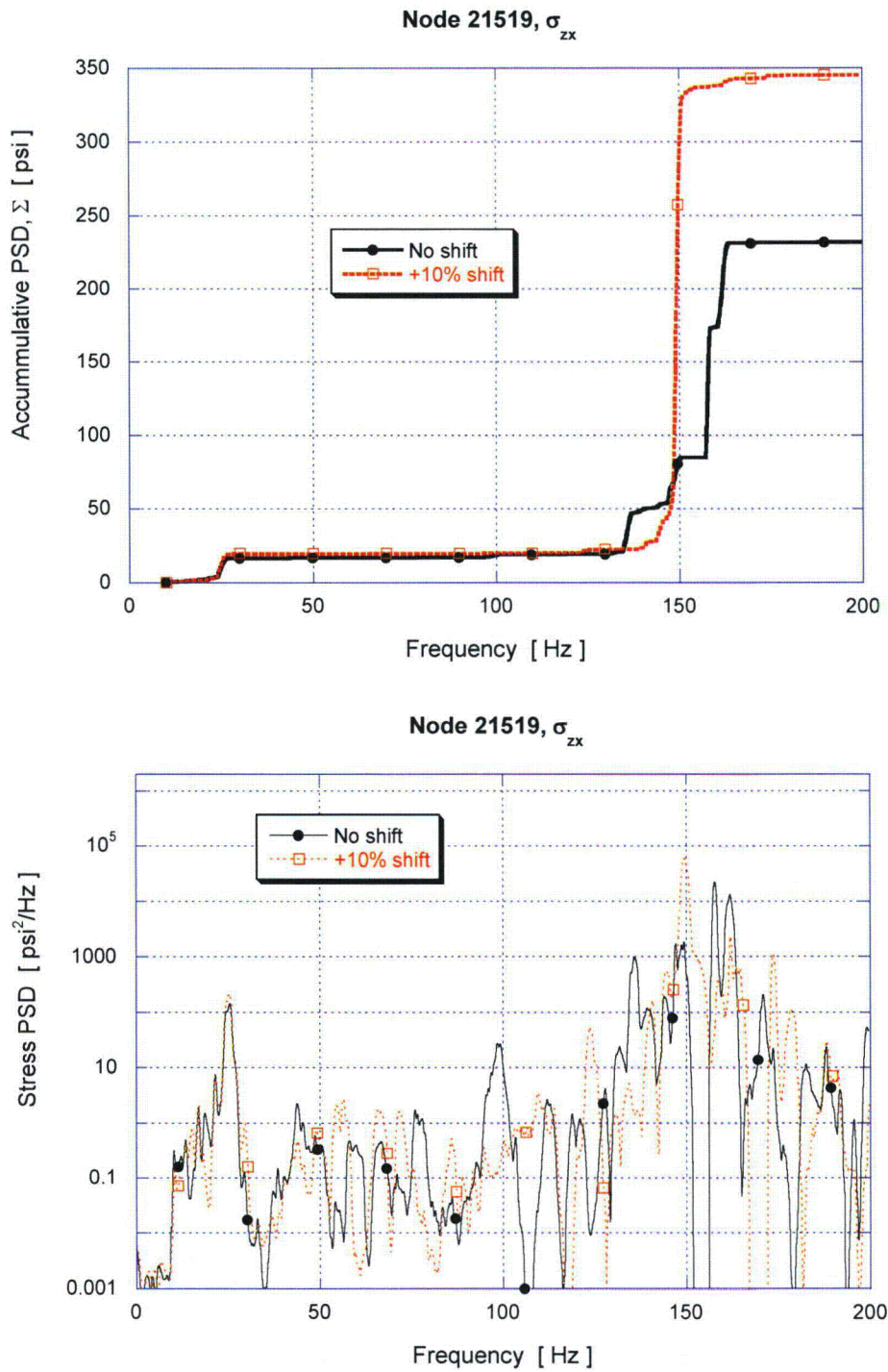


Figure 17c. Accumulative PSD and PSD of the σ_{zx} stress response at node 21519 for EPU operation at zero and +10% frequency shifts.

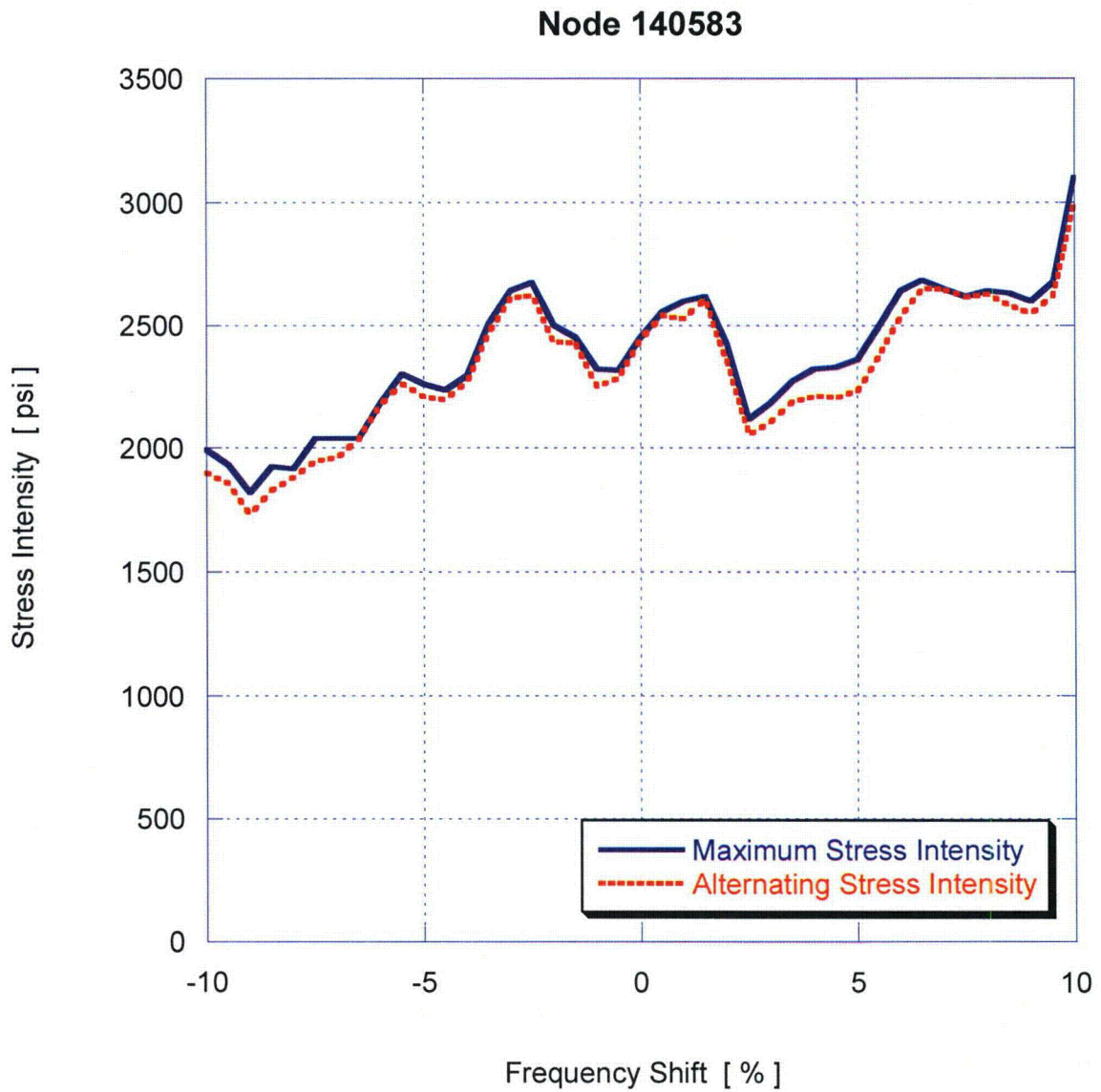


Figure 18a. Variation of maximum and alternating stress intensities with frequency shift for node 140583 at EPU operation.

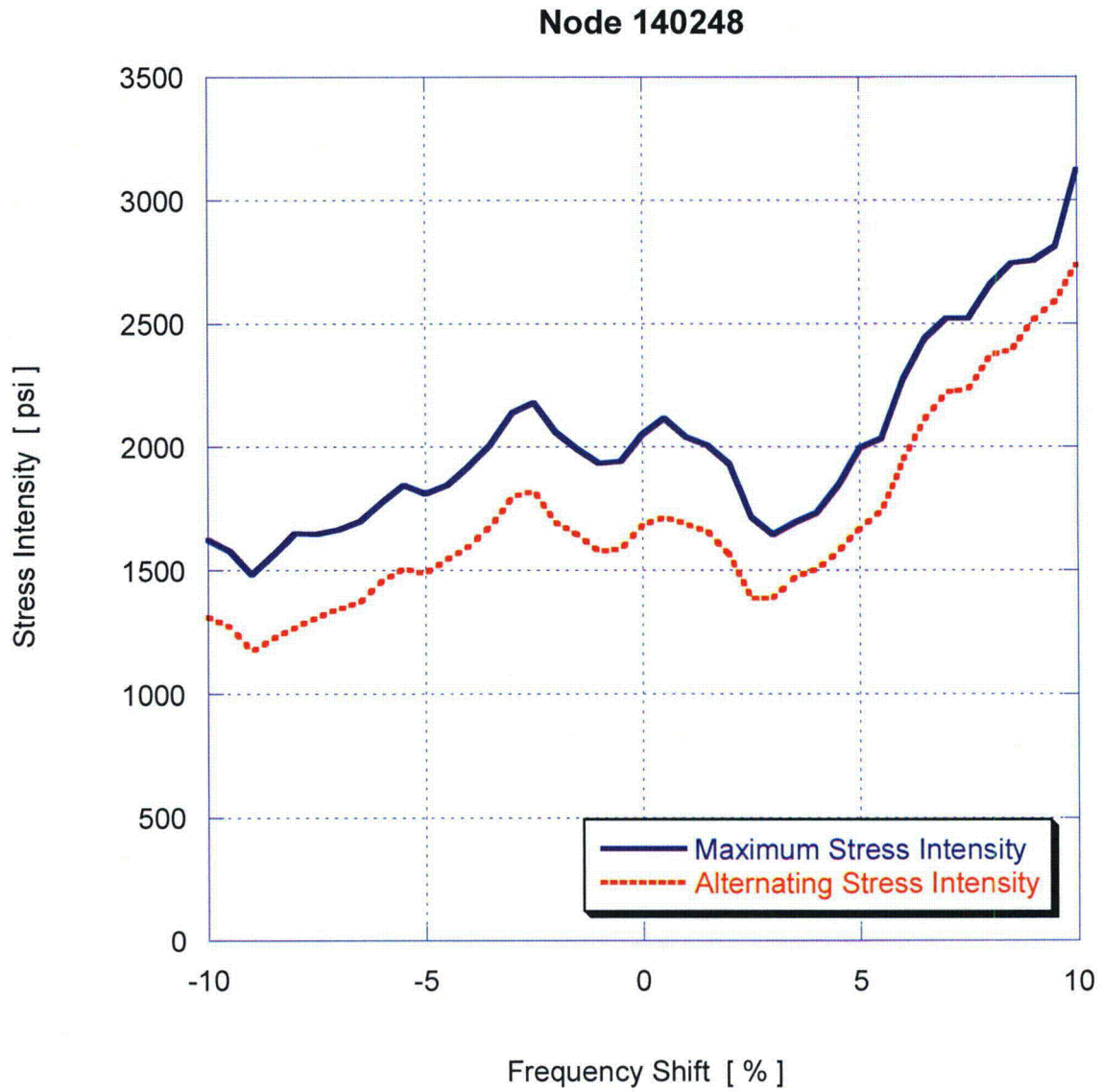


Figure 18b. Variation of maximum and alternating stress intensities with frequency shift for node 140248 at EPU operation.

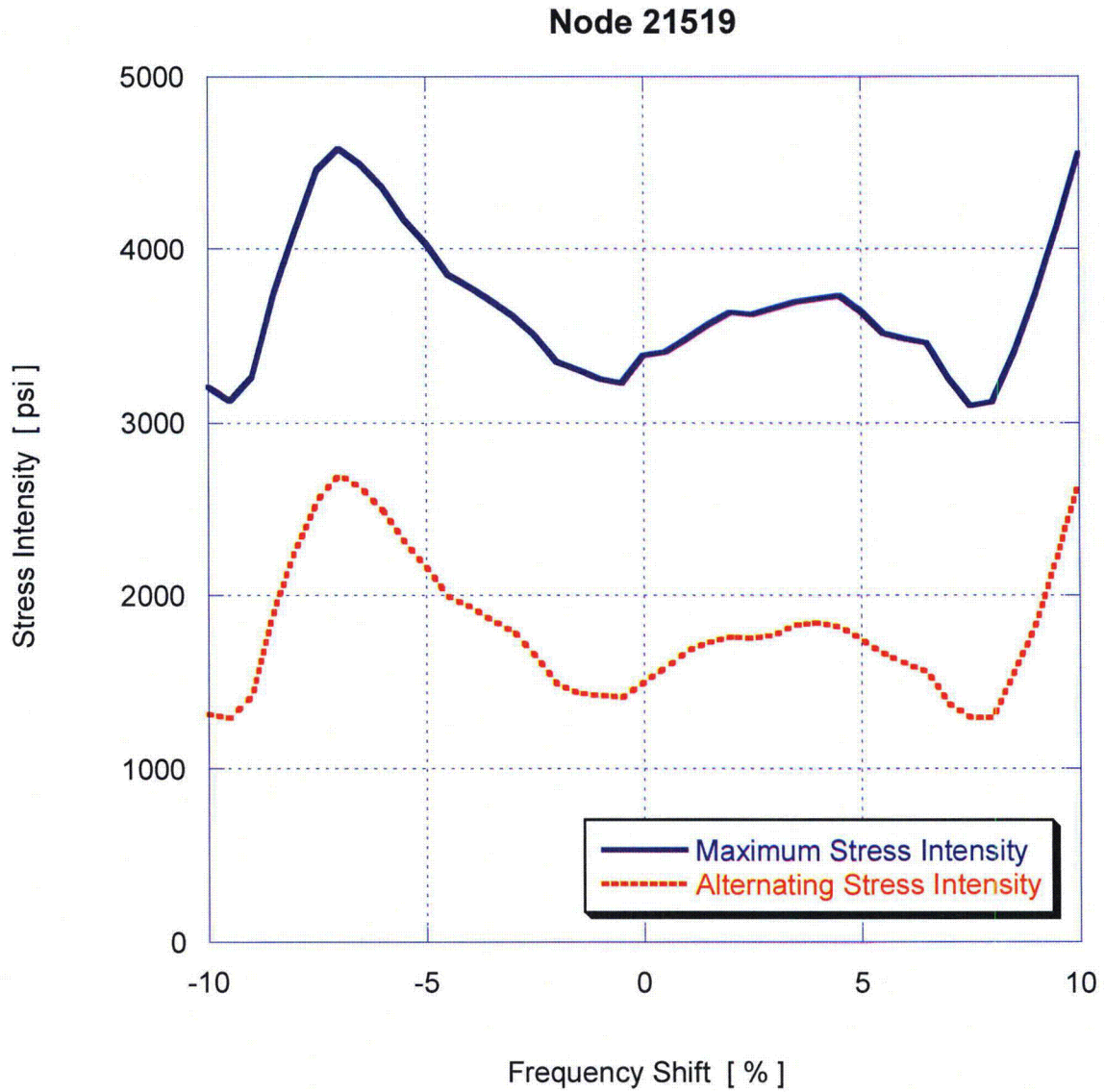


Figure 18c. Variation of maximum and alternating stress intensities with frequency shift for node 21519 at EPU operation.

6. Conclusions

A harmonic steam dryer stress analysis has been used to calculate high stress locations and calculated / allowable stress ratios for the Monticello steam dryer at both CLTP and EPU load conditions using plant measurement data. A detailed description of the harmonic methodology and the finite element model for the Monticello steam dryer is presented. The CLTP loads obtained in a separate acoustic circuit model [3], including end-to-end bias and uncertainty [3,4], were applied to a finite element model of the steam dryer consisting mainly of the ANSYS Shell 63 elements and brick continuum elements. The methods applied here follow those proposed in [4] which is under review by the NRC. The exception is that bump up factors are only applied over the 150-170 Hz range. Elsewhere the square of the EPU to CLTP velocity, 1.32, is employed as indicated in **Error! Reference source not found..**

The resulting stress histories were analyzed to obtain maximum and alternating stresses at all nodes for comparison against allowable levels. These results are tabulated in Table 8 of this report. At CLTP, the minimum alternating stress ratio at nominal operation is 3.74 and the minimum alternating stress ratio taken over all frequency shifts is 3.02. In both cases the minimum stress ratio corresponds to an alternating stress. Examination of the spectral content in the stresses reflects a significant 25-26 Hz signal that is the dominant contributor to the lowest stress ratios.

At estimated EPU conditions, the limiting alternating stress ratio without frequency shifting is $SR-a=2.81$. When frequency shifting is included the alternating stress ratio reduces to 2.28. The limiting maximum stress intensity at any frequency shift for EPU is $SR-P=2.03$.

On the basis of these CLTP plant loads, the dynamic analysis of the steam dryer shows that the combined acoustic, hydrodynamic, and gravity loads produce the minimum stress ratios in the Table below. These stress ratios qualify the steam dryer with substantial margin for EPU conditions.

Frequency Shift	Minimum Stress Ratio at CLTP		Minimum Stress Ratio at EPU	
	Max. Stress, SR-P	Alternating Stress, SR-a	Max. Stress, SR-P	Alternating Stress, SR-a
0% (nominal)	2.89	3.74	2.75	2.81
-10%	2.81	4.89	2.73	3.17
-7.5%	2.86	4.95	2.08	2.70
-5%	2.88	4.23	2.31	3.11
-2.5%	2.87	3.47	2.65	2.59
+2.5%	2.87	4.4	2.57	3.06
+5%	2.85	4.06	2.55	3.04
+7.5%	2.83	3.43	2.76	2.59
+10%	2.50	3.02	2.03	2.28
All shifts	2.50 - 2.89	3.02 - 4.95	2.03 - 2.75	2.28 - 3.17
Limiting Value	2.50	3.02	2.03	2.28

7. References

1. Continuum Dynamics, Inc. (2005). "Methodology to Determine Unsteady Pressure Loading on Components in Reactor Steam Domes (Rev. 6)." C.D.I. Report No. 04-09 (Proprietary).
2. ASME (2007). ASME Boiler & Pressure Vessel Code, 2007 edition, Section III, Division 1.
3. Continuum Dynamics, Inc. (2007). "Acoustic and Low Frequency Hydrodynamic Loads at CLTP Power Level on Monticello Steam Dryer to 200 Hz, Revision 2" C.D.I. Report No. 07-25P (Proprietary).
4. EPRI Report (2008), "BWRVIP-194: BWR Vessel and Internals Project. Methodologies for Demonstrating Steam Dryer Integrity for Power Uprate," Report No. 1016578.
5. Continuum Dynamics, Inc. (2007). "Flow-Induced Vibration in the Main Steam Lines at Monticello and Resulting Steam Dryer Loads, Rev. 0," C.D.I. Report No. 07-23P (Proprietary)
6. Continuum Dynamics, Inc. (2007). "Methodology to Predict Full Scale Steam Dryer Loads from In-Plant Measurements, with the Inclusion of a Low Frequency Hydrodynamic Contribution (Rev. 1)" C.D.I. Report No. 07-09P (Proprietary).
7. Structural Integrity Associates, Inc. (2007). "Monticello Main Steam Line 100% CLTP Strain Data Submission. SIA Letter Report No. KKF-07-013 with Inclusion of Channel 29"
8. ANSYS Release 10.0. URL <http://www.ansys.com>. Documentation: ANSYS 10.0 Complete User's Manual Set
9. Press, W. H., S. A. Teukolsky, et al. (1992). *Numerical Recipes*, Cambridge University Press.
10. Continuum Dynamics, Inc. (2008). "Stress Assessment of Browns Ferry Nuclear Unit 1 Steam Dryer, Rev. 1," C.D.I. Report No. 08-06P (Proprietary).
11. Continuum Dynamics, Inc. (2007). Response to NRC Request for Additional Information on the Hope Creek Generating Station, Extended Power Uprate, RAI No. 14.110
12. ASME (1983). ASME Boiler & Pressure Vessel Code, 1983 edition, Section III, Appendix I
13. Baumeier, T., Avallon, E.A. and Baumeister III, T. (eds.) (1978). Marks' Handbook for Mechanical Engineers, 8th Edition, McGraw-Hill Book Co.
14. U.S. Nuclear Regulatory Commission, (2007). Regulatory Guide 1.20 "Comprehensive Vibration Assessment Program for Reactor Internals During Preoperational and Initial Startup Testing," March 2007.

This Document Does Not Contain Continuum Dynamics, Inc. Proprietary Information

15. Tecplot 10 (2004). URL: <http://www.tecplot.com>. Documentation: *Tecplot* User's Manual Version 10 Tecplot, Inc. Bellevue, Washington October.
16. SI Calculation No. 0801040.301, Revision 0, dated 10/31/08, "Steam Dryer Outer Hood Submodel Analysis," Prepared by Minghao Qin; Checked by Soo Bee Kok; Approved by Karen K. Fujikawa

**Attachment IV to
Enclosure 13 to L-MT-08-052**

C.D.I. Technical Note No. 08-12NP:

Limit Curve Analysis with ACM Rev. 4
for Power Ascension at Monticello, Revision 2

November 2008

(Non-Proprietary)

Limit Curve Analysis with ACM Rev. 4 for
Power Ascension at Monticello

Revision 2

Prepared by

Continuum Dynamics, Inc.
34 Lexington Avenue
Ewing, NJ 08618

Prepared under Purchase Order No. 00013758 for

Northern States Power Company, a Minnesota Corporation (NSPM)
Monticello Nuclear Generating Plant
2807 W County Road 75
Monticello, MN 55362

Approved by



Alan J. Bilanin

Prepared by



Milton E. Teske

November 2008

Table of Contents

Section	Page
Table of Contents.....	i
1. Introduction	1
2. Approach.....	2
3. Limit Curves	4
4. References.....	9

1. Introduction

During power ascension of Monticello Nuclear Generating Plant (MNGP), from Current Licensed Thermal Power (CLTP) to Extended Power Uprate (EPU), Northern States Power Company, a Minnesota Corporation (NSPM), is required to monitor the dryer stresses at plant power levels that have not yet been achieved. Limit curves provide an upper bound safeguard against the potential for dryer stresses becoming higher than allowable, by estimating the not-to-be-exceeded main steam line pressure levels. In the case of MNGP, in-plant main steam line data have been analyzed at CLTP conditions to provide steam dryer hydrodynamic loads [1]. EPU is 120% of Original Licensed Thermal Power (OLTP); CLTP is 106.3% of OLTP. A finite element model stress analysis has been undertaken on the CLTP loads [2]. These loads provide the basis for generation of the limit curves to be used during MNGP power ascension.

Continuum Dynamics, Inc. (C.D.I.) has developed an acoustic circuit methodology (ACM) that determines the relationship between main steam line data and pressure on the steam dryer [3]. This methodology and the use of a finite element model analysis provide the computational algorithm from which dryer stresses at distinct steam dryer locations can be tracked through power ascension. Limit curves allow NSPM to limit dryer stress levels, by comparing the main steam line pressure readings – represented in Power Spectral Density (PSD) format – with the upper bound PSD derived from existing in-plant data.

This technical note summarizes the proposed approach that will be used to track the anticipated stress levels in the MNGP steam dryer during power ascension, utilizing Rev. 4 of the ACM [4], and the options available to NSPM should a limit curve be reached.

2. Approach

The limit curve analysis for MNGP, to be used during power ascension, is patterned after the approach followed by Entergy Vermont Yankee (VY) in its power uprate [5]. In the VY analysis, two levels of steam dryer performance criteria were described: (1) a Level 1 pressure level based on maintaining the ASME allowable alternating stress value on the dryer, and (2) a Level 2 pressure level based on maintaining 80% of the allowable alternating stress value on the dryer. The VY approach is summarized in [6].

To develop the limit curves for MNGP, the stress levels in the dryer were calculated for the current plant acoustic signature, at CLTP conditions, and then used to determine how much the acoustic signature could be increased while maintaining stress levels below the stress fatigue limit. During power ascension, strain gage data will be converted to pressure in PSD format at each of the eight main steam line locations, for comparison with the limit curves. The strain gage data will be monitored throughout power ascension to observe the onset of discrete peaks, if they occur.

The finite element analysis of in-plant CLTP data found a lowest alternating stress ratio of 3.02 [2] as summarized in Table 1. The minimum stress ratios include the model bias and uncertainties for specific frequency ranges as suggested by the NRC [7]. The results of the ACM Rev. 4 analysis (based on Quad Cities Unit 2, or QC2, in-plant data) are summarized in Table 2 (a negative bias is conservative). The standpipe excitation frequency of the main steam safety relief valves in MNGP is anticipated to be 160 Hz [8], and thus the uncertainty determined around the QC2 Electromatic excitation frequency of 135 Hz has been applied to the 158 to 162 Hz frequency interval [9]. The additional bias and uncertainties, as identified in [10], [11], [12], [13], [14], and [15], are shown in Table 3. SRSS of the uncertainties, added to the ACM bias, results in the total uncertainties shown in Table 4. These uncertainties were applied to the finite element analysis, resulting in the minimum stress ratio of 3.02 for ASME Level A load combinations.

Table 1. Peak Stress Limit Summary for ACM Rev. 4

Peak Stress Limit	13,600 psi (Level 1)	10,880 psi (Level 2)
Minimum Stress Ratio	3.02	2.42

Table 2. Bias and uncertainty for ACM Rev. 4

[[

(3)]]

Table 3. MNGP additional uncertainties (with references cited)

[[

(3)]]

Table 4. MNGP total uncertainty

[[

(3)]]

3. Limit Curves

Limit curves were generated from the in-plant CLTP strain gage data reported in [1]. These data were filtered across the frequency ranges shown in Table 5 to remove noise and extraneous signal content, as suggested in [16, 17]. The resulting PSD curves for each of the eight strain gage locations were used to develop the limit curves, shown in Figures 1 to 4. Level 1 limit curves are found by multiplying the main steam line pressure PSD base traces by the square of the corrected limiting stress ratio ($3.02^2 = 9.12$), while the Level 2 limit curves are found by multiplying the PSD base traces by 0.64 of the square of the corrected limiting stress ratio (recovering 80% of the limiting stress ratio, or $0.80^2 \times 3.02^2 = 0.64 \times 9.12 = 5.84$), as PSD is related to the square of the pressure.

Table 5. Exclusion frequencies for MNGP at CLTP conditions
(Recirc = recirculation pumps)

Frequency Range (Hz)	Exclusion Cause
0.0 – 2.0	Mean
58.5 – 61.5	Line Noise
119.7 – 120.3	Line Noise
179.6 – 180.4	Line Noise
51.2 – 52.3	Recirc Pump B Electrical Single Phase
128.6 – 130.2	Recirc Pump B Speed (5x)
133.8 – 134.2	Recirc Pump A Speed (5x)
154.9 – 155.4	Recirc Pump B Electrical Three Phase
14.0 – 34.0	Pipe Vibration

[[

Figure 1. Level 1 (black) and Level 2 (red) limit curves for main steam line A, compared ⁽³⁾ against the base curves (blue) over the frequency range of interest: A upper strain gage location (top); A lower strain gage location (bottom).

[[

Figure 2. Level 1 (black) and Level 2 (red) limit curves for main steam line B, compared ⁽³⁾]] against the base curves (blue) over the frequency range of interest: B upper strain gage location (top); B lower strain gage location (bottom).

[[

Figure 3. Level 1 (black) and Level 2 (red) limit curves for main steam line C, compared against the base curves (blue) over the frequency range of interest: C upper strain gage location (top); C lower strain gage location (bottom).⁽³⁾]]

[[

Figure 4. Level 1 (black) and Level 2 (red) limit curves for main steam line D, compared against the base curves (blue) over the frequency range of interest: D upper strain gage location (top); D lower strain gage location (bottom).⁽³⁾]]

4. References

1. Continuum Dynamics, Inc. 2008. Acoustic and Low Frequency Hydrodynamic Loads at CLTP Power Level on Monticello Steam Dryer to 200 Hz (Rev. 2). C.D.I. Report No. 07-25 (Proprietary).
2. Continuum Dynamics, Inc. 2008. Stress Assessment of Monticello Steam Dryer (Rev. 1). C.D.I. Report No. 07-26 (Proprietary).
3. Continuum Dynamics, Inc. 2005. Methodology to Determine Unsteady Pressure Loading on Components in Reactor Steam Domes (Rev. 6). C.D.I. Report No. 04-09 (Proprietary).
4. Continuum Dynamics, Inc. 2007. Methodology to Predict Full Scale Steam Dryer Loads from In-Plant Measurements, with the Inclusion of a Low Frequency Hydrodynamic Contribution (Rev. 1). C.D.I. Report No. 07-09 (Proprietary).
5. Entergy Nuclear Northeast. 2006. Entergy Vermont Yankee Steam Dryer Monitoring Plan (Rev. 4). Docket 50-271. No. BVY 06-056. Dated 29 June 2006.
6. State of Vermont Public Service Board. 2006. Petition of Vermont Department of Public Service for an Investigation into the Reliability of the Steam Dryer and Resulting Performance of the Vermont Yankee Nuclear Power Station under Uprate Conditions. Docket No. 7195. Hearings held 17-18 August 2006.
7. NRC Request for Additional Information on the Hope Creek Generating Station, Extended Power Uprate. 2007. RAI No. 14.67.
8. Continuum Dynamics, Inc. 2008. Flow-Induced Vibration in the Main Steam Lines at Monticello and Resulting Steam Dryer Loads (Rev. 0). C.D.I. Report No. 07-23 (Proprietary).
9. BWRVIP-194: BWR Vessel and Internals Project, Methodologies for Demonstrating Steam Dryer Integrity for Power Uprate. EPRI, Palo Alto, CA, and Continuum Dynamics, Inc., Ewing, NJ: 2008. 1016578.
10. Structural Integrity Associates, Inc. 2007. Evaluation of Monticello Strain Gage Uncertainty and Pressure Conversion (Rev. 0). SIA Calculation Package No. MONT-11Q-302.
11. Continuum Dynamics, Inc. 2005. Vermont Yankee Instrument Position Uncertainty. Letter Report Dated 01 August 2005.
12. Exelon Nuclear Generating LLC. 2005. An Assessment of the Effects of Uncertainty in the Application of Acoustic Circuit Model Predictions to the Calculation of Stresses in the Replacement Quad Cities Units 1 and 2 Steam Dryers (Rev. 0). Document No. AM-21005-008.

This Document Does Not Contain Continuum Dynamics, Inc. Proprietary Information

13. Continuum Dynamics, Inc. 2007. Finite Element Modeling Bias and Uncertainty Estimates Derived from the Hope Creek Unit 2 Dryer Shaker Test (Rev. 0). C.D.I. Report No. 07-27 (Proprietary).
14. NRC Request for Additional Information on the Hope Creek Generating Station, Extended Power Uprate. 2007. RAI No. 14.79.
15. NRC Request for Additional Information on the Hope Creek Generating Station, Extended Power Uprate. 2007. RAI No. 14.110.
16. Structural Integrity Associates, Inc. 2007. Monticello Main Steam Line 100% CLTP Strain Data Transmission. SIA Letter Report No. KKF-07-013 with inclusion of Channel 29.
17. J. Ferrante Email Correspondence: "Logic for Declaring Piping Vibrations." 02 February 2008.

Enclosure 14 to L-MT-08-052

**Midwest Independent System Operator
(MISO) Grid Stability Study Summary**

ENCLOSURE 14

Introduction

Two System Impact Studies (SIS) (References 1 & 2) were performed by the Midwest Independent System Operator, Inc (MISO) to evaluate the impact of the Monticello Nuclear Generating Plant (MNGP) Extended Power Uprate (EPU) operation on transmission system reliability. The Reference 1 study analyzed an Interconnection Request for 13 MWe to support an EPU Phase I power increase following the 2009 refuel outage. The Reference 2 study analyzed an Interconnection Request for 60.8 MWe to support an EPU Phase II power increase following the 2011 refuel outage. A summary and results of both these studies is provided herein.

Design Basis

The design basis for the electrical power system is defined in the MNGP Updated Safety Analysis Report (USAR) Sections 1.2.6 and 8.1:

“Sufficient normal and standby auxiliary sources of electrical power are provided to attain prompt shutdown and continued maintenance of the plant in a safe condition under all credible circumstances. The capacity of the power sources is adequate to accomplish all required engineered safeguards functions under all postulated design basis accident conditions.”

“The plant electrical power system is designed to provide a diversity of dependable power sources which are physically isolated so that any one failure affecting one source of supply will not propagate to alternate sources. The plant auxiliary electrical power systems are designed to provide electrical and physical independence and adequate power supplies for startup, operation, shutdown, and for other plant requirements which are important to safety.”

The Nuclear Management Company, LLC (NMC) provided MNGP’s docketed position on 10 CFR 50 Appendix A, General Design Criteria (GDC) 17 compliance in a letter (Reference 3) dated July 21, 2006, “Response to Generic Letter 2006-02, ‘Grid Reliability and the Impact on Plant Risk and the Operability of Offsite Power.’” The following is an excerpt from this letter:

“Generally, the NMC-operated plants were licensed to comply with the Atomic Energy Commission General Design Criteria as proposed on July 10, 1967 (AEC GDC) as described in the plant Final (Updated) Safety Analysis Report. AEC GDC proposed Criterion 39, which provides guidance applicable to the design of the AC electrical power system supplies to the engineered safety features, states:

“Alternate power systems shall be provided and designed with adequate independency, redundancy, capacity, and testability to permit the functioning required of the engineered safety features. As a minimum, the onsite power system and the offsite power system shall each, independently, provide this capacity assuming a failure of a single active component in each power system.

ENCLOSURE 14

“Thus, many of the provisions of GDC Criterion 17 are not applicable to the NMC operated plants, the responses to the questions reflect that the plants are not committed to GDC Criterion 17, and the responses do not in any manner commit to or imply compliance with GDC Criterion 17 for the NMC-operated plants.”

Offsite Power System General Description

Transmission Interconnections

The plant electrical output is connected to the grid via an on-site switchyard. Existing transmission outlet facilities consist of two 345 KV, two 230 KV, and three 115 KV transmission lines as shown in USAR Section 15, Drawing NH-178635.

The 345 KV portion of the switchyard has positions for connecting the generator output, two transmission lines, a 345-230-13.8 KV autotransformer, a 345-13.8 KV transformer, a 345-34.5 KV transformer, and a 345-115-13.8 KV autotransformer. The 345 KV bus and circuit breaker arrangement is based on ultimate development into a breaker-and-one-half system. The present installation is a ring bus configuration. One 345 KV transmission line is routed to connect into the 345 KV loop around the Twin Cities Metropolitan Area at the Elm Creek Substation. The other line connects to the 345 KV transmission system at the Sherburne County Substation.

The 230 KV portion of the switchyard is provided to establish an interconnection with the transmission system of Great River Energy. An autotransformer connects the 345 KV and 230 KV busses.

The 115 KV portion of the switchyard is connected to the 345 KV bus through an autotransformer. The 115 KV bus is arranged in a ring bus configuration. In addition to the autotransformer connection to the 115 KV bus, there are three transmission line connections. One of the three transmission lines connects into the 115 KV transmission system at Lake Pulaski and at Dickinson Substation. The second line connects at Hassan Substation. The third 115 KV line connects to the Sherburne County substation.

The 13.8 KV portion of the switchyard is provided to establish reliable power sources to various plant equipment. These include the plant auxiliary reserve transformer (1AR); discharge structure transformers (X7, X8); cooling tower fan transformers (X50, X60, X70, X80); transformer XP91, which powers the hydrogen water chemistry cryogenic system panel, and an alternate feed (through transformer 6) to the training center.

Plant Auxiliary Power Supplies

Three transformers are provided to supply the plant with offsite power from the substation. All three sources can independently provide adequate power for the plant's safety-related loads. These transformers and their interconnections to the substation are as follows:

ENCLOSURE 14

The primary station auxiliary transformer, 2R, is fed from 345 KV Bus No. 1 via 345 KV to 34.5 KV transformer 2RS, a current limiting reactor and fuse assembly, and underground cabling from the substation to the area northwest of the turbine building where 2R transformer is located. The 2R transformer is of adequate size to provide the plant's full auxiliary load requirements.

The reserve transformer, 1R, is fed from the 115 KV substation via an overhead line from the substation to the area northwest of the turbine building where 1R transformer is located. The 1R transformer is of adequate size to provide the plant's full auxiliary load requirements.

The reserve auxiliary transformer, 1AR, is located southwest of the reactor building and may be fed from two separate 13.8 KV sources in the substation. One method of supplying the 1AR transformer is from the tertiary winding of the 10 transformer, the auto-transformer that interconnects the 345 KV and 115 KV systems. Power is routed from the tertiary winding of 10 transformer to 1AR via circuit breaker 1N2 and underground cabling from the substation to 1AR transformer. The alternate method of feeding 1AR is from 345 KV Bus No. 1 via 345 KV to 13.8 KV transformer 1ARS, circuit breaker 1N6, and underground cabling from the substation to 1AR. Circuit breakers 1N2 and 1N6 are interlocked to prevent having both breakers simultaneously in the closed position. The 1AR transformer is sized to provide only the plant's essential 4160 Volt buses and connected loads.

Transformers 2R and 1AR are considered as a single offsite source when 1AR is supplied from 345 KV Bus No. 1 as numerous common mode failures exist which could cause simultaneous deenergization of both transformers. To minimize the potential for common mode failure, the normal alignment of off-site sources to the plant is 2R transformer supplying plant load, 1R transformer energized in reserve, and 1AR transformer energized from 10 transformer as a third distinct off-site source to the essential buses.

Transmission Line Reliability

The five (345 KV and 115 KV) transmission line connections to the switchyard are all connected into the Xcel Energy interconnected transmission grid. The points of connection to the grid are arranged by routes and intra-right-of-way spacing to minimize multiple line outages while performing the requirement of delivering power to locations which best satisfy system growth needs. The 345 KV and 115 KV lines, as well as the lines to which they interconnect, are designed and built to exceed the requirements of the National Electric Safety Code for heavy loading districts, Grade B construction. Lightning performance design of the transmission lines is based on less than one outage per 100 miles per year.

The five Xcel Energy transmission lines leave the Monticello substation through three separate rights-of-way: Sherburne County line corridor; St. Cloud line corridor; and a common corridor for the Elm Creek, Dickinson-Lake Pulaski, and Hassan lines. These rights-of-way are considered independent as they are greater than 1/4 mile apart at a distance of one mile from the plant.

ENCLOSURE 14

Analysis

The power increase related to the EPU project is planned in two phases: one increase following the 2009 refueling outage and the remaining increase following the 2011 refueling outage. A request for interconnection rights of an additional 13 MWe was identified by MISO as Project G725. The 13 MWe is an increase above the current interconnection rights of 607.2 MWe and was requested to accommodate the first phase power increase following the 2009 refuel outage. A request for interconnection rights of an additional 60.8 MWe was identified by MISO as Project G929. The 60.8 MWe request will accommodate the electrical output expected at EPU reactor thermal power of 2004 MWth.

A summary of each study is provided below.

Project G725, 13 MWe Increase Request:

Study Methodology and Assumptions:

A benchmark case computer model was developed for the study from the MAPP 2005 series models. This model was used for steady state power flow analysis focused on thermal loadings under both normal and N-1 contingency conditions. The model included transmission system updates and prior-queued generation projects in the region that could have an impact on the MNGP generation increase. Monticello output was set at 607 MWe net and additional generation near the Monticello unit that was not at maximum output or in service was set at maximum and put into service. This represents a summer peak condition

expected at the time of the MNGP output increase. A subsequent study case model was developed incorporating the MNGP requested 13 MWe increase in electrical output. The analysis was done for station load supplied from both the 345 KV substation and the 115 KV substation.

For the transient stability analysis, a computer model called the Northern MAPP stability package was used. Again, benchmark case and study case models were developed. This is a summer off-peak model. Regional generation was added and adjusted for peak output. Corresponding load sinks were adjusted as appropriate. The stability of the grid was then analyzed for regional single-line ground faults with breaker failure and 3-phase faults without breaker failure.

The Interconnection Request for this project asked that the total MNGP electrical output be classified as Network Resource Interconnection Service (NRIS). In order to be classified as NRIS, the project request must pass a generator deliverability study. This study was included in the SIS.

ENCLOSURE 14

A short circuit analysis was completed that calculates the fault currents available with the increased generation and verifies that these values are within the interrupting capacity of the existing MNGP substation breakers.

The stability study examined the effects of the more limiting reactive capability of the existing generator due to the MW increase.

Study Results:

For steady state conditions the study concluded there are no system intact, injection constraints or voltage violations associated with the increase in the MNGP electrical output. This was verified for both the cases where house loads are supplied from the 345 KV substation or the 115 KV substation.

For transient conditions, no violations of stability criteria were identified. Voltage control was acceptable with the existing generator reactive capability.

The deliverability analysis concluded that the full electrical output of 620.2 MW from the MNGP can be classified as NRIS.

The short circuit analysis concluded the interrupting capability of the existing substation breakers is adequate for the 13 MWe increase in generator output.

The 345 KV and 115 KV bus voltages were shown to remain within acceptable limits. Specifically, the following voltage limits are needed to adequately supply the in-house safety and non-safety loads as defined by the plant AC Load Study:

- Acceptable 345 KV grid voltage range = 342-362 KV
- Acceptable 115 KV grid voltage range = 116-121 KV

The above limits were found to be maintained for the following regional contingencies:

- (1) Loss of the Monticello nuclear power generating unit
- (2) Loss of Xcel's largest generating unit
- (3) Loss of the largest transmission circuit or intertie
- (4) Loss of largest system load

Project G929, 60.8 MWe Increase Request:

Study Methodology and Assumptions:

A benchmark case computer model was developed using the G725 study model. This model was used for steady state power flow analysis focused on voltage and thermal loadings under both normal and N-1 contingency conditions. The model used in the G725 study included the addition of prior-queued regional projects that would likely be operating

ENCLOSURE 14

by the requested in-service date of June of 2009. MISO determined that no other prior queued generator projects would need to be added to the G929 model based on the requested in-service date of June 2011. There were some changes made to the D curve, constants and inertia of the MNGP generator expected due to the generator upgrade. Also, the station load was increased by 3 MW expected due to increased pumping power at EPU conditions. With the increase in electrical output, the reactive capability of the Monticello generator falls short of the 0.95 lead/lag power factor (pf) required by the MISO interconnection tariff. To compensate, the addition of two 60 MVAR capacitor banks connected to the MNGP 115 kV bus were included in the model. Monticello output was set at 641.9 MWe (gross) and additional generation near the Monticello unit was set at summer peak conditions. A subsequent study case model was developed incorporating the MNGP requested 60.8 MW increase. The analysis was done for station load supplied from both the 345 kV substation and the 115 kV substation.

For the transient stability analysis, a computer model called the Northern MAPP stability package was used. This is a summer off-peak model. Again, the G725 model was used as the benchmark case. The MNGP output and regional generation was added and adjusted for peak output and corresponding load sinks were adjusted as appropriate. The stability of the grid was then analyzed for regional single-line ground faults with breaker failure and 3-phase faults without breaker failure. In addition to the regional faults normally assessed, MISO was asked to specifically analyze the following cases (per IEEE Std. 765) using the reactive capability of the generator:

1. Loss of the Monticello generating unit
2. Loss of NSP's largest generating unit (Sherco Unit 3)
3. Loss of the largest transmission circuit or intertie (from Load Flow)
4. Loss of the largest system load (Fifth Street = 150 MW)

The Interconnection Request for project G929 asked that the total MNGP electrical output be classified as Network Resource Interconnection Service (NRIS). In order to be classified as NRIS, the project request must pass a generator deliverability study. This study was included in the SIS.

A short circuit analysis was completed that calculates the fault currents available with the increased generation and verifies that these values are within existing NSP substation breakers at Monticello and adjacent substations.

The steady state and stability studies examined the effects of the more limiting reactive capability of the generator due to the MW increase by running cases with and without the two 60 MVAR capacitor banks in service.

Results:

For steady state conditions the study concluded there are no injection constraints or voltage violations associated with the increase in the MNGP electrical output. This was

ENCLOSURE 14

verified for both the cases where house loads are supplied from the 345 kV bus or the 115 kV bus. Screening results using only the reactive capability of the generator showed no change to the conclusions.

For transient conditions no violations of stability criteria were identified. The 345 kV & 115 kV substation bus voltages remain within acceptable values with and without additional reactive capability.

The deliverability analysis concluded that the full electrical output of the MNGP can be classified as NRIS; therefore non-injection constraints identified in the steady state analysis do not need to be mitigated under this project.

The short circuit analysis concluded the interrupting capability of NSP 345 kV, 230 kV and 115 kV substation breakers at Monticello and adjacent substations are adequate for the increased generator output.

Conclusions

The results of both these System Impact Studies indicate that the MNGP electrical output can be increased to 705.7 MW (gross) without compromising the off-site power grid or its capability to supply in-plant loads.

ENCLOSURE 14

References

1. Midwest ISO "System Impact Study for Generation Interconnection" Midwest ISO Project G725, Queue # 39099-01" dated May 22, 2008. This study is supported by accompanying reports:
 - "Deliverability Study for Generation Interconnection" Midwest ISO Project G725, Queue # 39099-01, dated March 4, 2008.
 - "Short Circuit Study for Generation Interconnection", Midwest ISO Project G725, Queue # 39099-01, dated June 2, 2008.
 - "G725 Transient Stability Study MISO Queue # 39099-01" dated February 15, 2008
 - "G725 Transient Stability Study MISO Queue # 39099-01 Addendum" dated May 29, 2008.

2. Midwest ISO "G929 System Impact Study for Generation Interconnection" dated October 6, 2008. This study is supported by accompanying reports:
 - "Deliverability Study for Generation Interconnection" Project G929, Queue #39426-02, dated 9/09/2008.
 - " Short Circuit Study for Generation Interconnection" Project G929, Queue # 39426-02, dated 10/13/2008
 - "G929 Transient Stability Study" dated 9/12/2008.

3. Letter from NMC, LLC (Edward J, Weinkam) to US NRC Document Control Desk, Response to Generic Letter 2006-02, "Grid Reliability and the Impact on Plant Risk and the Operability of Offsite Power," dated July 21, 2006.